MODELING AND ANALYSIS OF ORTHOTROPIC PLATE WITH CIRCULAR CUTOUT AND ADHESIVE BONDED PATCH

THESIS

Mark W. Hunter, Captain, USAF

AFIT/GAE/ENY/90D-11

AFIT/GAE/ENY/90D-11

MODELING AND ANALYSIS OF ORTHOTROPIC PLATE WITH CIRCULAR CUTOUT AND ADHESIVE BONDED PATCH

THESIS

Presented to the Faculty of the School of Engineering
of the Air Force Institute of Technology
Air University
In Partial Fulfillment of the
Requirements for the Degree of
Master of Science in Aeronautical Engineering

Mark W. Hunter, B.S.
Captain, USAF

December 1990

Preface

The purpose of this study was to investigate a modeling technique to simply and adequately model an adhesive bonded patch on an orthotropic plate. No previous models have been found which used the following method: three-dimensional spring elements to model the bond.

This report is limited to linear material behavior. While this does not technically tell the entire story behind the behavior of the patched plate, I believe that it provides a complete picture of the modeling process for, and applicability to, actual composite repairs. This thesis is also the basis for further work into the nonlinear material range and three-dimensional stress states.

I would like to thank my faculty advisor, Capt H. Gans who gave timely guidance essential to the completion of this study. Deep gratitude is also expressed to Dr. Venkayya of the Flight Dynamics Laboratory and T. Reinhart of the Wright Research and Development Center, otherwise known as the Materials Laboratory. I also wish to thank the men and women of the Materials Laboratory who made things and made things happen; Jim, Brian, Mac, Jack, John, and the others who made it all possible.

And finally, I wish to acknowledge my gratitude to my wife, Toni, for her understanding and patience though our first eighteen months of marriage.

In memory of Wayne Wilsdon, Capt, USAF, GAE-90D.

Mark W. Hunter

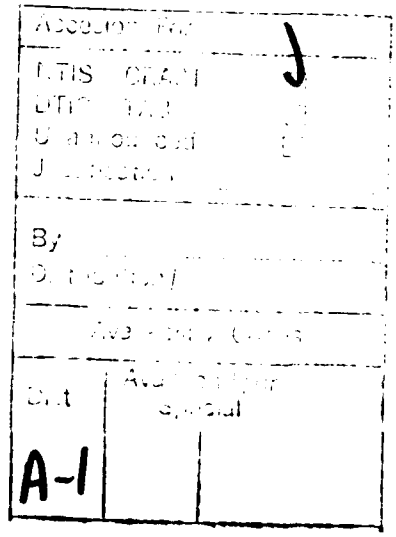

Table of Contents

List of Figures

List of Tables

Abstract

To further advance aerospace battle damage repair techniques for composite repairs, a finite element model of an orthotropic plate with a hole and patch was constructed to investigate the accuracy of such a model. The fundamental problem in this model is the development of a simple and accurate method of modeling the bond between patch and plate. MSC/NASTRAN spring elements were used to this end. The spring elements provided an elastic method of load transfer between the plate and the patch. MSC/Nastran was used for model solution while SDRC I-DEAS was used for Pre- and Post-Processing of the finite element model. Two-dimensional CQUAD4 elements were used to model the plate and patch. Physical test specimens were constructed to validate the model. The plate considered was a 16 ply AS4/3501-6 graphite/epoxy composite with dimensions 30" x 10" x 0.0832" with a five inch diameter hole centered in the plate. Three different patch concepts were modeled. The strain correlation between the finite element model and the test specimens was excellent for points far away from the hole and centered on the patch. Areas near the edge of the patch and hole were not as successful, probably due to the rapidly changing strain fields near these areas.

MODELING AND ANALYSIS OF ORTHOTROPIC PLATE WITH CIRCULAR CUTOUT AND ADHESIVE BONDED PATCH

I. Introduction

Purpose. Today's modern military aircraft, such as the ATF, AV-8B, B-2, and ATA, are designed to very tight weight tolerances. The structure weight-to-gross weight ratio is constantly decreasing as aircraft design advances. These advances are possible through the use of lightweight laminated composite materials in primary and secondary load bearing structures. The orthotropic materials allow structure material properties to be oriented favorably with the load and load path the structure will be required to withstand. Presently, this is usually accomplished with graphite/epoxy (gr/ep) structure, where the lay-up of the gr/ep is tailored to meet the load requirements.

These advances in design and manufacturing have markedly increased the performance of military aircraft and at the same time left the armed services with a gap in their battle damage repair concepts. The aircraft battle damage repair (ABDR) concept stresses metallic repairs for all structural damage incurred on aircraft (1:2-3). This concept was viable in the era of all, or mostly, metallic aircraft. Battle damage to

today's and tomorrow's aircraft may require more than just aluminum and rivets to adequately repair.

Objective. This thesis is primarily an investigation of modeling techniques applicable to damaged composite panels with adhesively bonded "scab" patches. Noted below are several goals which, if accomplished, could lead to advances in battle damage repair of composite structures. The following goals of this thesis, in order of importance, are as follows:

1. Develop an accurate and workable finite element model (FEM) of an adhesively bonded patch and plate.

2. Characterize and evaluate potential ABDR class materials needed to accomplish the modeled repairs.

3. Evaluate potential ABDR class hardware required to accomplish the modeled repairs.

Procedure. The FEM will be "constructed" using Structural Dynamics Research Corporation's (SDRC) Integrated Design Engineering Analysis Software (I-DEAS) on a Digital Equipment Corporation (DEC) VAX 11/785 running the VMS operating system. Within this environment, the FEM of the plate, patch, and bond will be defined along with the loads, restraints, and constraints of the model. Model solution will be accomplished outside of I-DEAS. I-DEAS will be used to write a MacNeal-Schwendler Corporation (MSC)/NASTRAN data deck. The data deck will then be transferred to a SUN 4 Workstation running under the Unix operating system. The SUN will actually solve the model using MSC/NASTRAN. Once the solution is complete, the

post-processing will take place inside I-DEAS. The required hard copy output is then generated.

The physical model will be manufactured from gr/ep and configured to match the FEM. Nine base panels will be manufactured. Eight will have centrally located holes matching the FEM's. The panels are repaired, or left as is, and then strain gages are attached at specific locations. The panels are then tested in tension and the strain gage data recorded.

The final phase of the procedure involves reducing the strain gage data and comparing it to the data generated using the FEM.

II. Background

ABDR. According to T O 1-1H-39, General Technical Manual, Aircraft Battle Damage Repair:

> The primary purpose of ABDR is to restore sufficient strength and serviceability to permit damaged aircraft to fly additional operational sorties, of at least partial mission capability, within time to contribute to the outcome of the on-going battle. (1:vii)

This manual is dedicated almost entirely to metallic structural repairs, and the portions dealing with damaged composite structures treat those structures as basically metallic in nature, (i.e. they use the same type of repairs as for the metallic structures).

There are on-going efforts to determine the most efficient method of field level composite damage repair. Hinkle and Van Es (2:11) recently completed a contract with USAF, in which they demonstrated the accuracy and viability of the McDonnell Douglas CREPAIR; a computer based repair design and analysis tool. This effort was dedicated entirely to bolted repairs of composite panels using metallic patches. Most accepted repair methods to date still revolve around metallic patches fastened with mechanical bolts. Adhesively bonded repairs are being investigated on the national and international level as well (3:6-1 to 6-21).

There are many factors to be considered when preparing to explore the patch-bonded-on-orthotropic-plate concept:

1. Material analysis of the orthotropic plate.
2. Material analysis of the adhesive.
3. Material analysis of the patch.
4. Surface preparation of patch and plate.
5. Bonding environment requirements.
6. Loads analysis of the plate with adhered patch.
7. ABDR requirements.

In the past decade considerable work has been accomplished in many of these areas.

Materials. The development of the constitutive matrices for a composite laminate are well understood (4:147-237). The fundamental building block for an accurate composite material analysis is the individual ply properties that make up the laminate. Ply properties of given materials are available through various sources (5:335).

Many small, and even large, software packages have been developed to quickly analyze laminates and compute their constitutive matrices (6). Using the constitutive matrix, the theory of elasticity can be used to analyze relatively simple structural configurations. However, an FEM is needed for structures with either complex geometry, boundary conditions, or loads.

Information on the material properties of adhesives in various environments with different forms of surface preparation are available from many sources, governmental as well as private (7). Typical relevant information on adhesives documents the shear modulus, shear strength, and expected bond line thickness.

Modeling. The analysis of the completed plate with bonded patch is relatively complex and has been treated little in the past. In fact, the bond line and the load transfer through the bond line is a major modeling problem. The thesis completed by Smith (8:35-39) attempted to model a gr/ep patch on a damaged aluminum plate. His model was fundamentally simplified as noted below:

> Inherent within both of these repair models is buried the assumption that a perfect bond exists between the aluminum and the repair patch. Without this assumption the model would become significantly more complex.

Other sources have also modeled the patch-to-panel interface as a perfect bond (2:6-1 to 6-21). In using the perfect bond model, the section of the plate that is overlapped by the patch is treated as a single piece of material and not as two separate entities. The material characteristics of both are superimposed to form a third, hybrid material.

The modeling of the bond line is of fundamental importance to this current thesis. An FEM of the adhesive is necessary to adequately predict the load transfer between the patch and the plate as well as the failure load of the bonded system. Once an adequate FEM has been constructed and verified, various bonded repair concepts can be evaluated using ABDR criteria.

III. Theory

Orthotropic Material Analysis. Before an FEA can proceed, the material characteristics of the elements must be defined. An orthotropic material, which is what the individual plys of a composite structure are assumed to be, has a constitutive matrix which relates the six stresses to the six strains in the material axis system. The six stresses are the three normal stresses and three shear stresses; likewise, the six strains are three normal strains and three shear strains. An orthotropic constitutive matrix contains nine independent material constants which define the behavior of the material.

$$\sigma_{ij} = Q_{ij}\,\varepsilon_{ij} \tag{1}$$

σ_{ij} - Stresses

ϵ_{ij} - Strains

Q_{ij} - Reduced Stiffnesses

The reduced stiffness matrix simply relates lamina stresses and strains and is comprised of the engineering constants, i.e. Young's modulus, Poisson's ratio, and shear modulus. The reduced stiffness matrix is defined for a particular lamina assuming the principal material directions coincide with the coordinate system for the structure. For a generally oriented lamina, the transformed reduced stiffness matrix must be used. This involves a simple coordinate transformation to the chosen axis system. Q-bar$_{ij}$ designates the transformed matrix. The

next step involves combining laminae to form a laminate stiffness matrix.

For a general laminate under plane stress, using the Kirchhoff hypothesis for plates, and accounting for out of plane displacements and curvatures, the stress-strain relationship for the kth lamina in a laminate can be defined as:

$$\{\sigma\}_k = [\bar{Q}]_k \{\{\varepsilon^0\} + z\{\kappa\}\} \tag{2}$$

$\{\varepsilon^0\}$ - Laminate Middle Surface Strains

$\{\kappa\}$ - Laminate Middle Surface Curvatures

The resultant forces and moments acting on a laminate are obtained by integration of the stresses in each lamina through the thickness of the laminate.

$$\{N\} = \int_{-t/2}^{t/2} \{\sigma\}\, dz = \sum_{k=1}^{N} \int_{z_{k-1}}^{z_k} \{\sigma\}_k\, dz \tag{3}$$

$$\{M\} = \int_{-t/2}^{t/2} \{\sigma\}\, z\, dz = \sum_{k=1}^{N} \int_{z_{k-1}}^{z_k} \{\sigma\}_k\, z\, dz \tag{4}$$

{N} - Resultant Laminate Forces

{M} - Resultant Laminate Moments

t - Laminate Thickness

z_k - Distance From Midsurface to Bottom of kth Lamina

After integrating and partitioning, the stiffness equations may be represented as follows:

$$\begin{Bmatrix} N \\ M \end{Bmatrix} = \begin{bmatrix} A & B \\ B & D \end{bmatrix} \begin{Bmatrix} \varepsilon^0 \\ \kappa \end{Bmatrix} \tag{5}$$

where

$$A_{ij} = \sum_{k=1}^{N} (\bar{Q}_{ij})_k (z_k - z_{k-1}) \tag{6}$$

$$B_{ij} = \frac{1}{2} \sum_{k=1}^{N} (\bar{Q}_{ij})_k (z_k^2 - z_{k-1}^2) \tag{7}$$

$$D_{ij} = \frac{1}{3} \sum_{k=1}^{N} (\bar{Q}_{ij})_k (z_k^3 - z_{k-1}^3) \tag{8}$$

A_{ij} - Extensional Stiffnesses

B_{ij} - Coupling Stiffnesses

D_{ij} - Bending Stiffnesses

The presence of the B_{ij} term implies coupling between bending and extension of a laminate. A symmetric laminate, with respect to lamina orientation about the midsurface, will result in all coupling stiffnesses being zero. This is the configuration chosen for the composite panel in this thesis.

Finite Element Analysis. The use of finite element theory is necessary in order to analyze structures too complex to be solved by classical analytical methods. The complexities can arise from several sources:

1. Complex geometry.
2. Complex loads.

3. Complex boundary conditions.

Finite element modeling, as applied here, basically involves the discretization of real complex structures into a number of smaller parts or regions called elements. Each element is connected to its surrounding elements at a number of finite points, called nodes. The only interaction of the elements is through the forces they apply at the nodes. Depending on the problem being modeled and the elements used, the nodes may have from one to six degrees of freedom (DOF). The assumption of small displacements and small rotations, and linear material behavior lead to a linearized formulation and a solution through linear algebra.

Cook breaks down the finite element analysis (FEA) into seven parts:

1. Divide the structure into finite elements.

2. Formulate the properties of each element. This means determining nodal loads associated with all element deformation states that are allowed.

3. Assemble elements to obtain the finite element of the structure.

4. Apply the known loads: nodal forces and/or moments.

5. Specify how the structure is supported. This step involves setting several nodal displacements to known values.

6. Solve the simultaneous linear algebraic equations to determine nodal DOF (nodal displacements in stress analysis)

7. In stress analysis, calculate element strains from the nodal DOF and the element displacement field interpolation, and finally calculate stresses from strains. (9:4)

In a FEA, solutions are calculated for the nodal displacements and rotations in all the elements making up the structure, for a given loading. The elements making up the model must satisfy the conditions of equilibrium and compatibility. That is to say, the summation of forces at any node must be zero and the displacements of the nodes must be such that voids or displacement discontinuities do not occur.

As referred to above, each type of element has its own elemental stiffness matrix. This matrix relates displacements for the given DOF of the element to the force required to achieve that displacement. Once an element has been chosen that best models the physical situation at hand, the "stiffness matrix" for that element can be derived by a number of methods. Some common methods are direct stiffness, virtual work, and isoparametric. The matrix equation relating structure stiffness , nodal displacement, and nodal loads is shown below:

$$[K]\{D\} = \{R\} \tag{9}$$

[K] - Structure Stiffness Matrix

{D} - Nodal DOF Displacement Vector

{R} - Applied and Reaction Nodal Loads

The physical meaning of [K], as well as a procedure for formulating [K], is described in the following statement:

> The jth column of [K] is the vector of loads that must be applied to the nodal DOF in order to maintain the deformation state associated with the unit value of DOF j while all other nodal DOF are zero. (9:34)

The above description for evaluating [K] is the direct stiffness approach. This approach is useful for developing an intuitive understanding of [K] and evaluating simple structures. Note that [K] is singular in its original form. In order to solve for unknown reactions and displacements Equation 9 must be partitioned. After known nodal DOF displacements and loads are identified, Equation 9 is partitioned according to the known and unknown portions of the nodal displacements and forces:

$$\begin{bmatrix} K_{11} & K_{12} \\ K_{21} & K_{22} \end{bmatrix} \begin{Bmatrix} D_x \\ D_c \end{Bmatrix} = \begin{Bmatrix} R_c \\ R_x \end{Bmatrix} \tag{10}$$

$\{D_C\}$ - Known Nodal Displacements

$\{R_C\}$ - Applied Nodal Forces

$\{D_X\}$ - Unknown Nodal Displacements

$\{R_X\}$ - Nodal Reaction Forces

The above equation can be successfully solved provided that there are sufficient boundary conditions to prevent rigid body motion of the modeled structure; i.e. $\{D_C\}$ determines if a solution is possible. Now, solutions are calculated for the unknown displacements:

$$\{D_x\} = [K_{11}]^{-1} (\{R_c\} - [K_{12}]\{D_c\}) \tag{11}$$

And similarly, the nodal reaction forces are calculated:

$$\{R_x\} = [K_{21}]\{D_x\} + [K_{22}]\{D_c\} \tag{12}$$

Generalized Stiffness Matrix. Deriving the elemental stiffness matrix for a given element type is the fundamental theoretical procedure behind a FEA. Actual computer program equations start with the elemental stiffness matrix as a known, dependent only on the type of element modeled. The potential energy form of solution is a classical method.

$$\pi_p = U + \Omega \tag{13}$$

π_p - Potential Energy on an Elastic Body

U - Strain Energy

Ω - Potential of Loads

For linearly elastic body under conservative loads, with volume V and surface area S:

$$\pi_p = \int_V \frac{1}{2}\{\varepsilon\}^T[E]\{\varepsilon\}\,dV - \int_V \{u\}^T\{F\}\,dV - \int_S \{u\}^T\{\Phi\}\,dS - \{D\}^T\{P\} \tag{14}$$

[E] - Constitutive Matrix

$\{\epsilon\}$ - Strain Field Vector

{F} - Vector of Body Forces

$\{\Phi\}$ - Vector of Surface Tractions

{P} - Vector of Loads Applied to DOF

{u} - Displacement Field Vector

NOTE: The above equation neglects initial strains and stresses.

The principle of stationary potential energy states that equilibrium prevails when $\delta\pi_p=0$ for any small admissible variation of the original structure. π_p is a function of the displacement DOF defined by the structure. Applying the principle of stationary potential energy:

$$\delta\pi_p=\frac{\partial\pi_p}{\partial D_i}=0 \qquad i=1,2,\ldots,n \tag{15}$$

D_i - ith Structure Displacement DOF

If D_i is a nodal displacement (or rotation), the above equation is a nodal equilibrium equation stating that forces (or moments) applied at the node sum to zero in the direction D_i. The potential energy equation components, for a single element, can also be expressed as:

$$U=\frac{1}{2}\{D\}^T[K]\{D\}; \qquad \Omega=-\{D\}^T\{R\} \tag{16}$$

This leads to the equation for [K], in terms of D_i:

$$K_{ij}=\frac{\partial^2\pi_p}{\partial D_i\partial D_j} \tag{17}$$

This provides the basis for generating the stiffness matrix for a generalized element. Typically though, the finite element form of the Rayleigh-Ritz method uses generalized coordinates which provide for a simpler mathematical evaluation of the stiffness matrix:

$$u=\sum_{i=1}^{l} a_i f_i \qquad v=\sum_{i=l+1}^{m} a_i f_i \qquad w=\sum_{i=m+1}^{n} a_i f_i \tag{18}$$

u, v, and w - Displacement Components of a Point

a_i - Generalized Coordinates

$f_i = f_i(x,y,z)$

Each of the functions f_i must be admissible, i.e. each must satisfy compatibility and essential boundary conditions. Usually the f_i are polynomials. Now π_p becomes a function of DOF a_i and the equilibrium equation is defined by n algebraic equations:

$$\frac{\partial \pi_p}{\partial a_i} = 0 \quad for \quad i=1,2,3,\ldots,n \tag{19}$$

A Rayleigh-Ritz solution is usually approximate because the functions f_i are usually incapable of exactly representing the actual displacements. Additional sources of information on FEA are available (9, 10).

IV. Modeling

In order to adequately design and test the bonded patch repair concept, an analytical model must be developed. An FEM which can model the plate, patch, and the bond joining them both is necessary. The model must be relatively simple (capable of being formulated and solved in a reasonable amount of time with computers at hand) and still achieve reasonable accuracy compared to the physical situation. The results of the model solution will be verified through testing of physical specimens.

Physical Model. The plate configuration (Figure 1) was chosen for ease of manufacturing and testing, for both the analytical and physical models, as well as being relevant to the discussion of ABDR of composite structures. The dimensions of the composite panel reflect the current limitations of approved ABDR composite repair procedures. The circular cutout is five inches in diameter and centered on the panel. A three-to-one ratio of length-to-width of the panel is considered fairly standard in order to limit end effects from the gripped end. The extra 10 inches in panel length is taken up in the grips.

The material composition of the panel is representative of current composite structures; Hercules AS4/3501-6 is a very common prepreg used in manufacturing composite components.

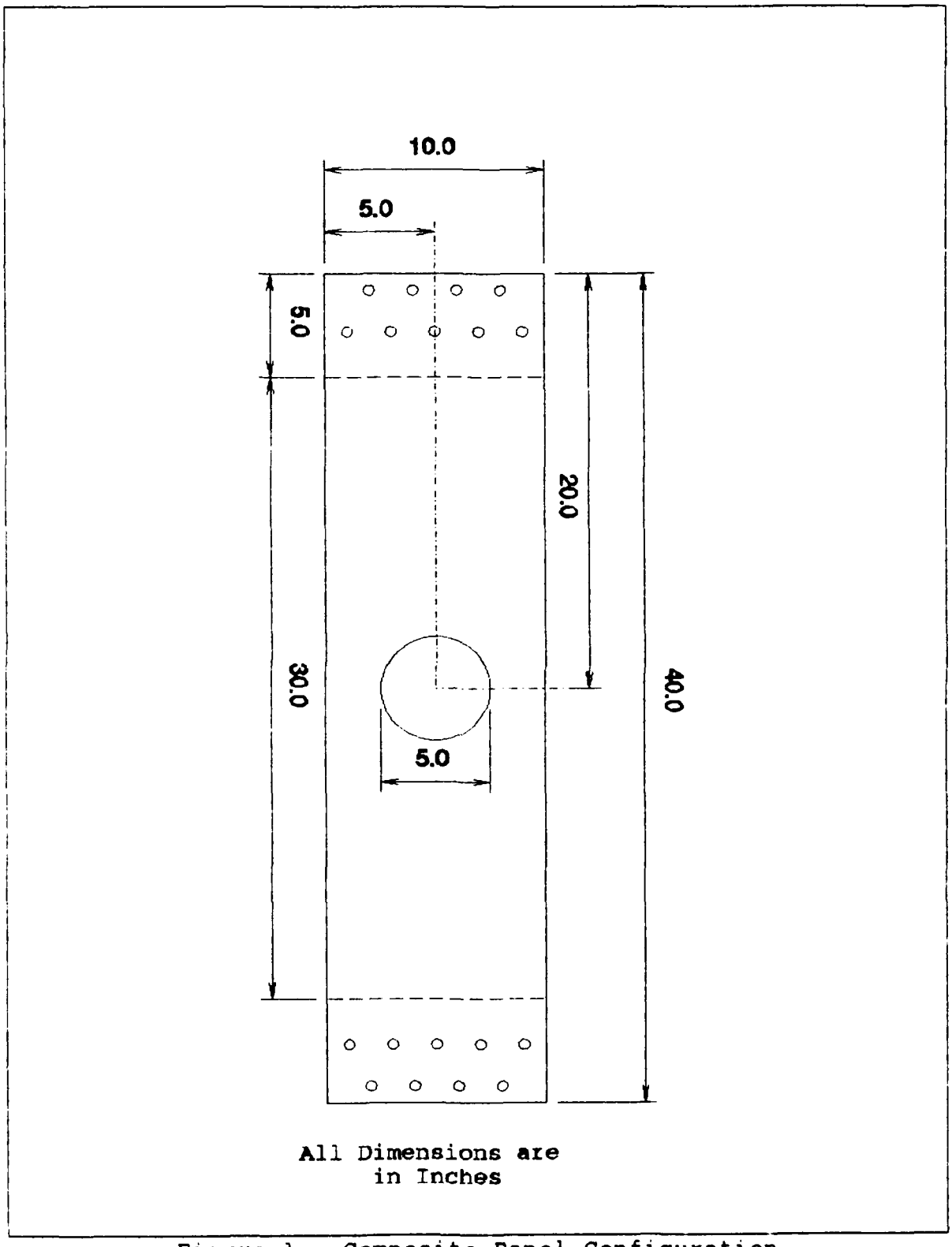

Figure 1. Composite Panel Configuration

The ply lay-up of the panels is $(\pm 45, 0_2, 90, 0_2, 90)_s$ (Figure 2), simulating a strength critical composite panel. Nine panels were cured according to the manufacturers specifications (5).

The test matrix for the panels is noted in Table 1. The undamaged panel and the two panels without repairs are used to verify the analytical model before the patch and bondline elements are added. If the FEM does not accurately predict the strain fields of these relatively simple cases, then the FEM with the patch and the bondline included could not be expected to accurately model the physical specimen.

Number of Panels	Repair Concept
1	Undamaged
2	No Repair
2	4-Ply Patch, 7" Dia
2	6-Ply Patch, 7" Dia
2	8-Ply Patch, 9" Dia

Table 1. Number and Type of Test Panels

Originally, the patch material was to be fabricated from 3M's SP 377 CU1, a low energy cure unidirectional gr/ep prepreg tape (7). This material is a possible ABDR candidate composite repair material due to its relatively low temperature requirements for cure. Not only can the material be fully cured at 205 °F for two hours, but it has a room temperature storable life of one year. The adhesive used to bond the patch and panel was also from this family of low

AS4/3501-6 TEST LAMINATE

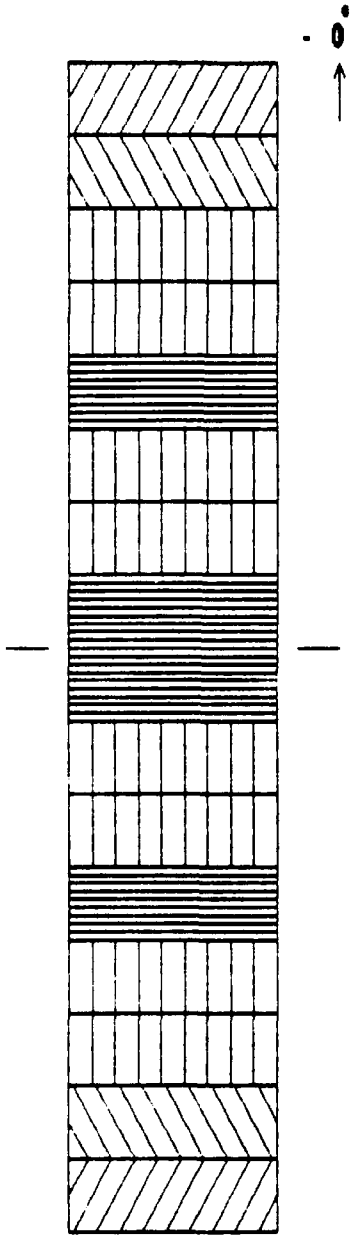

A - Matrix (Membrane)

1.03314E+06	1.22804E+05	0.00105590
1.22804E+05	6.27324E+05	0.0179341
0.00105590	0.0179341	1.73371E+05

B - Matrix (Membrane - Bending)

0.0	0.0	0.0
0.0	0.0	0.0
0.0	0.0	0.0

D - Matrix (Bending)

538.672	139.110	19.2031
139.110	282.630	19.2031
19.2031	19.2031	168.280

S - Matrix (Transverse Shear)

0.0	0.0
0.0	0.0

Laminate thickness = 0.0832 in

Figure 2. Composite Panel Properties

energy cure prepregs. The adhesive, AF 377, is an epoxy film which is also cured at 205 °F for two hours. The film incorporates an extremely light weight scrim cloth to hold the uncured epoxy together. The scrim cloth also has a secondary function of controlling the bondline thickness of the cured adhesive.

The patch laminates are $(0)_X$, where X indicates the number of lamina in the patch (Figures 3,4, and 5). The patches are intended to bring back the stiffness in the longitudinal direction only. Also, the patches are produced such that all the lamina of the patch are the same size, i.e. no taper of the patch. The patches are centered on the "damaged" area.

The methodology of the "repair" is as follows:

1. The panel has a five inch circular cutout centered on it. The cutout was made first with a hole-saw and taken to the final dimensions with a router.

2 The patch plys are cut from the patch material, SP 377 CU1.

3. The plys are stacked as required and cured under vacuum, 27 inches of Mercury, and heat. The process is controlled by a prototype hot-bonder. This foot-locker sized machine controls the vacuum and heat applied to the patch to match a pre-programmed cycle (Figure 6).

4. The panel is cleaned and abraded around the cutout in preparation for bonding the patch.

5. The adhesive film is cut from a roll of AF 377 and temporarily spot bonded to the patch.

6. The patch and adhesive film is positioned on the panel and taped in place. A filler material is positioned in the cutout to prevent the patch from being pushed down into the hole once the vacuum is applied.

PATCH 4-PLY

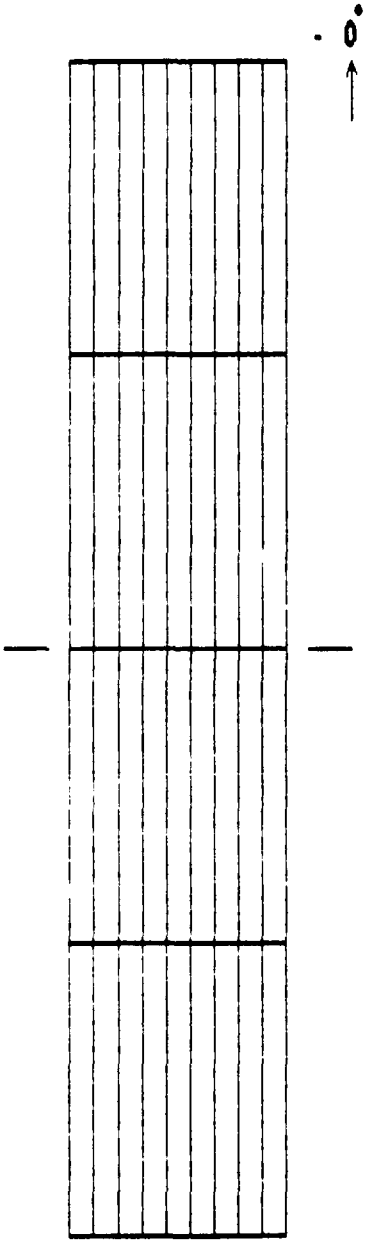

A - Matrix (Membrane)

4.33007E+05	8158.11	0.0
8158.11	27193.7	0.0
0.0	0.0	20800.0

B - Matrix (Membrane - Bending)

0.0	0.0	0.0
0.0	0.0	0.0
0.0	0.0	0.0

D - Matrix (Bending)

15.6114	0.294127	0.0
0.294127	0.980424	0.0
0.0	0.0	0.749909

S - Matrix (Transverse Shear)

17333.3	0.0
0.0	17333.3

Laminate thickness = 0.0208 in

Figure 3. Patch Properties 4-Ply

PATCH 6-PLY

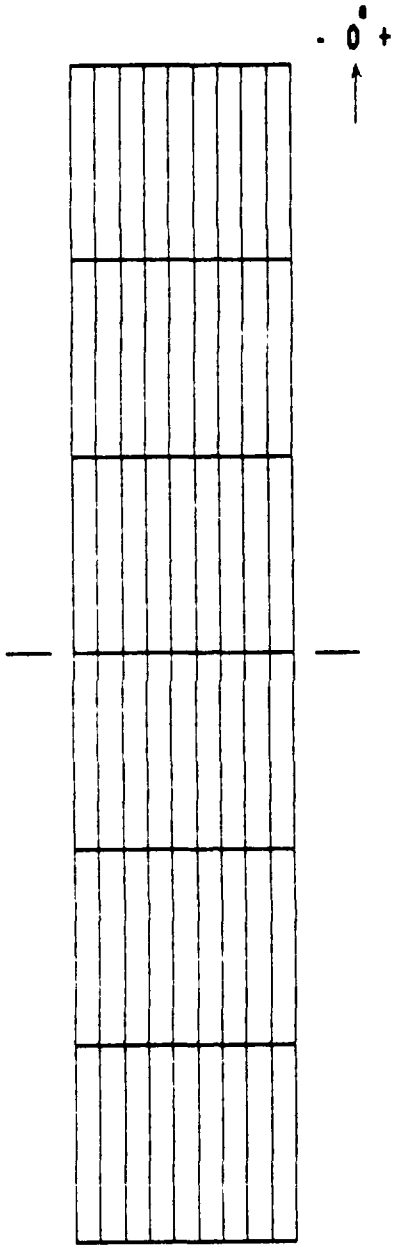

A - Matrix (Membrane)

6.49511E+05	12237.2	0.0
12237.2	40790.6	0.0
0.0	0.0	31200.0

B - Matrix (Membrane - Bending)

0.0	0.0	0.0
0.0	0.0	0.0
0.0	0.0	0.0

D - Matrix (Bending)

52.6884	0.992679	0.0
0.992679	3.30893	0.0
0.0	0.0	2.53094

S - Matrix (Transverse Shear)

26000.0	0.0
0.0	26000.0

Laminate thickness = 0.0312 in

Figure 4. Patch Properties 6-Ply

PATCH 8-PLY

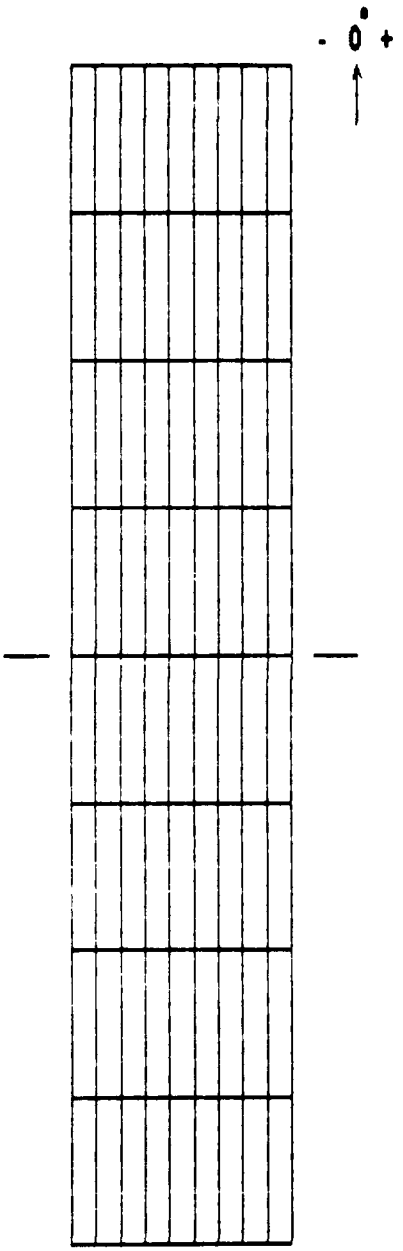

A - Matrix (Membrane)

8.66015E+05	16316.2	0.0
16316.2	54387.4	0.0
0.0	0.0	41600.0

B - Matrix (Membrane - Bending)

0.0	0.0	0.0
0.0	0.0	0.0
0.0	0.0	0.0

D - Matrix (Bending)

124.891	2.35302	0.0
2.35302	7.84339	0.0
0.0	0.0	5.99928

S - Matrix (Transverse Shear)

34666.7	0.0
0.0	34666.7

Laminate thickness = 0.0416 in

Figure 5. Patch Properties, 8-Ply

7. The secondary adhesive bonding is accomplished in the same manner as the cure of the patch.

Once the patch is bonded to the panel, the conglomeration is ready for instrumentation and testing.

The above sequence of events was the original plan, using actual ABDR capable material and equipment in fabricating the composite "repair." Unfortunately this plan went awry. After several patches were cured, they were inspected by ultrasonic C-scan, using a SRL Model 1750 Mini-C, in a water immersion test. The C-scan showed regular areas (dark areas) of high void content in all of the patches (Figure 7). An inspection of cross-sections of one of the patches revealed that the prepreg material itself was resin starved. The cross-sectioned patch delaminated within one of the plys and not at a ply interface (Figure 8). The SP 377 CU1 prepreg, which had been delivered from the manufacturer about three weeks prior to this finding, had visible (once we knew what to look for) areas of resin starvation all along the roll of material. This problem made the material useless for this project.

Due to time constraints, the patch material used in all the patches was of the same material as the original panels, AS4/3501-6. The configuration of the patches did not change. Although the material used in adhering the patch to the panel was still AF 377, the method of bonding changed. Instead of the hot-bonder, a hot press was used for the bonding process (Figure 9). This was due to time constraints and probability of success.

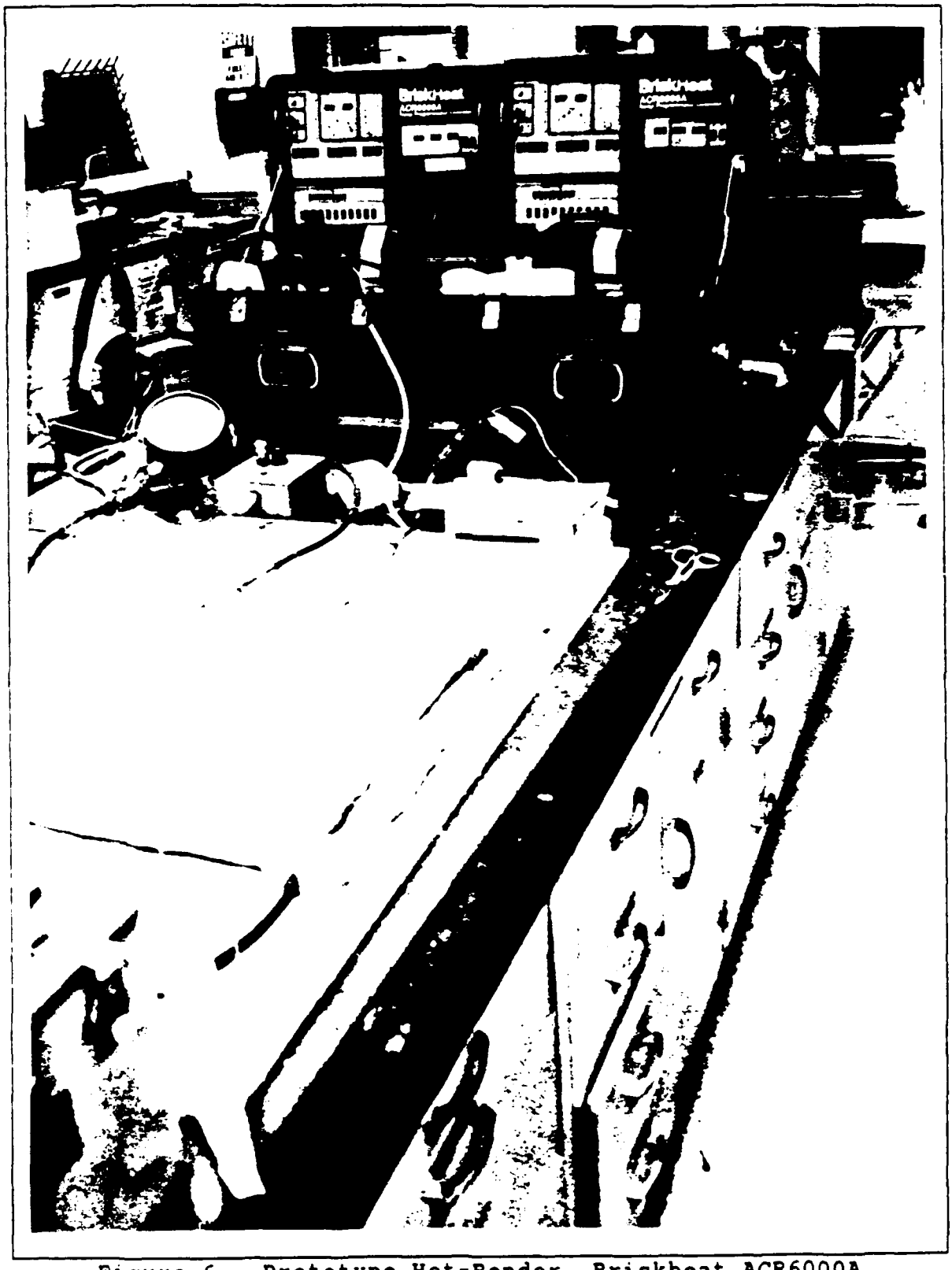

Figure 6. Prototype Hot-Bonder, Briskheat ACR6000A

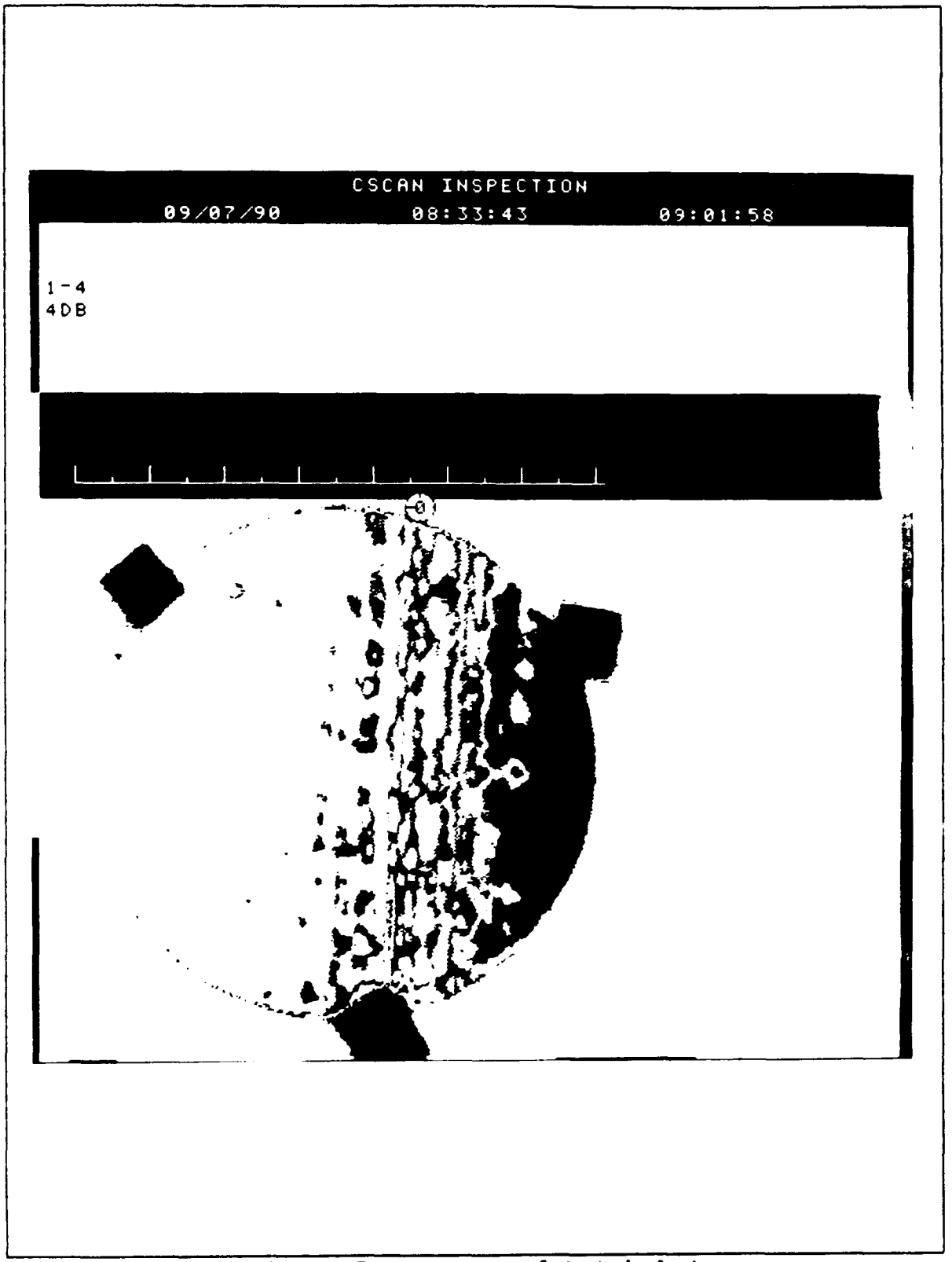

Figure 7. C-Scan of Patch 1-4

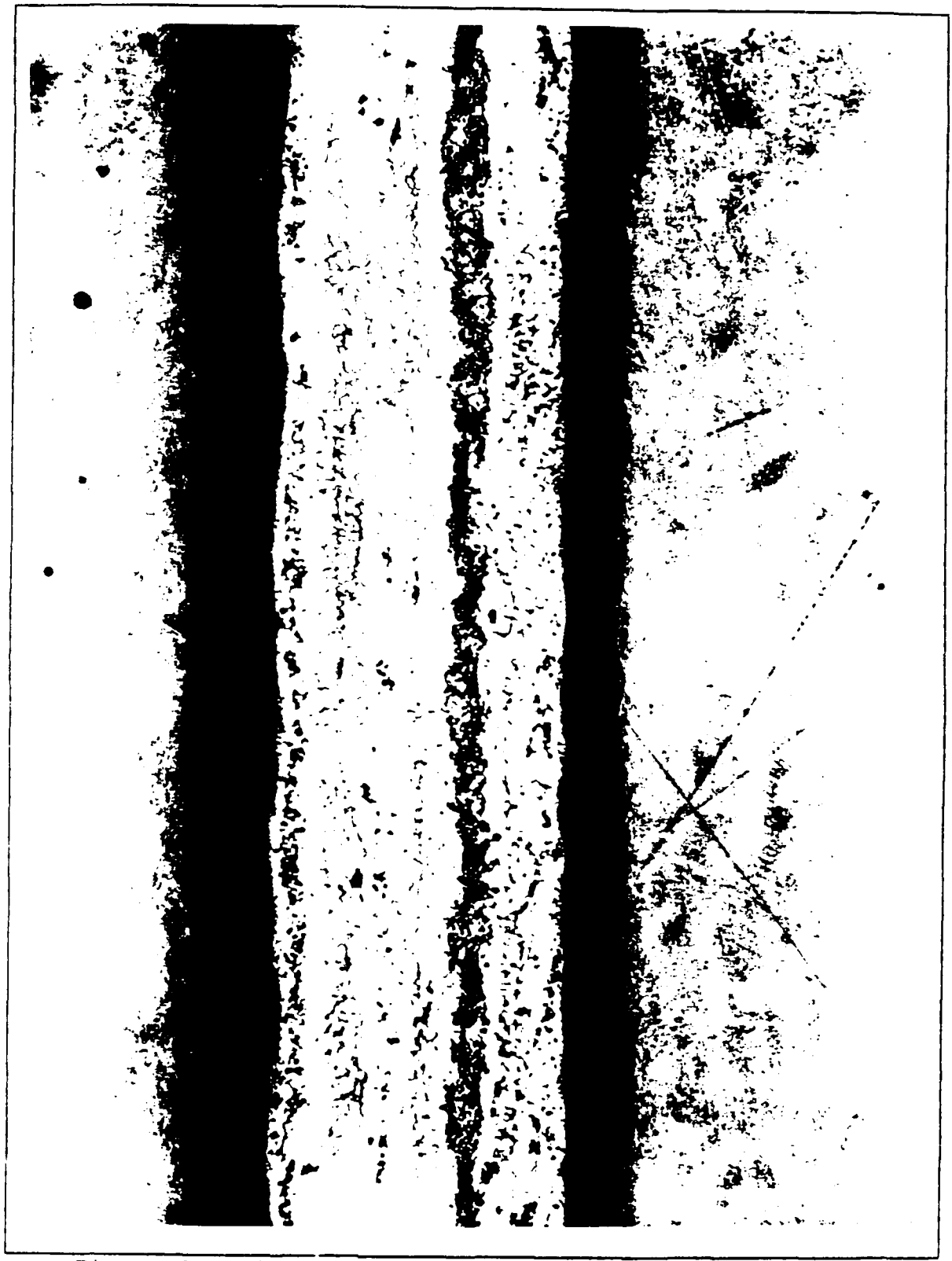

Figure 8. Micrograph of Cross-Section of 4-Ply Patch

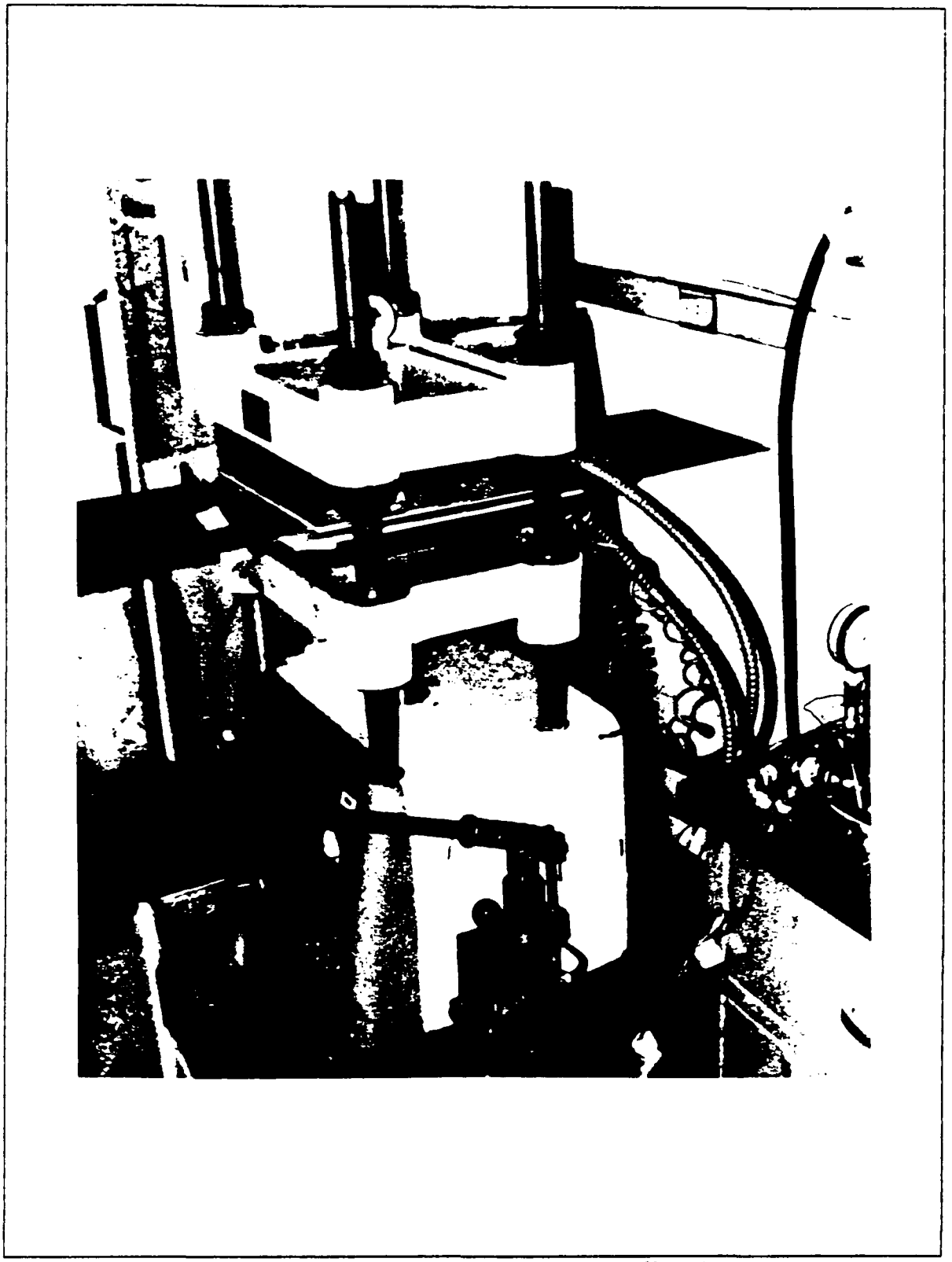

Figure 9. Hot Press Curing Adhesive

The material properties of AS4/3501-6, as obtained through Mall (11), are listed in Table 2. His data is used rather than the manufacturers data on the basis of conservatism and completeness.

Modulus of Elasticity E_1	20.7E06 psi
Modulus of Elasticity E_2 and E_3*	1.3E06 psi
Possion's Ratio ν_{12}, ν_{23}*, and ν_{13}*	0.3
Shear Modulus G_{12}, G_{23}*, and G_{13}*	1.0E06 psi

Table 2. Ply Properties of AS4/3601-6
* - Assumed Property

Analytical Model. The analytical model is constructed with the use of SDRC I-DEAS. This software package enables pre- and post-processing of the analytical model in a graphical environment. I-DEAS is used to generate the Bulk Data Deck and Case Control Deck of a MSC/NASTRAN FEM. The user supplies the Executive Control Deck. The solution is returned to I-DEAS for post-processing and evaluation.

MSC/NASTRAN Version 65 was used instead of Version 66 as the latter version, apparently, cannot solve for the inter-laminar stresses or strains of a laminate material. A data

deck submitted under Version 65, using Alter 79 for Rigid Format 24, produces the required results; while, the same data deck submitted under Version 66 will not successfully finish.

The first step in the analytical modeling process is the definition of the panel. Due to the loading and physical symmetry, only a quarter of the panel must be modeled. This saves modeling and computation time. The correct geometry of the quarter panel is described as a surface. This surface is subdivided into the many finite elements that will model the panel (Figure 10). If bending moments had been applied, the argument of symmetry would not be valid due to the ±45 plys in the panel.

Once the base panel is meshed, the element type to be used must be defined. The element used in the model of the panel is the MSC/NASTRAN CQUAD4 element. The CQUAD4 is an isoparametric membrane-bending element. The forces, stresses, and the associated coordinate system supported by this element are illustrated in Figure 11 (12:7-9). In this model the membrane and bending properties are not coupled. This is basically a two-dimensional element. This model is designed to keep all relevant DOF in-plane, i.e. bending is not present.

The material properties associated with the CQUAD4 elements are defined using the material properties of one ply of AS4/3501-6. I-DEAS uses the data on one ply of material as the building block for the material property of an entire

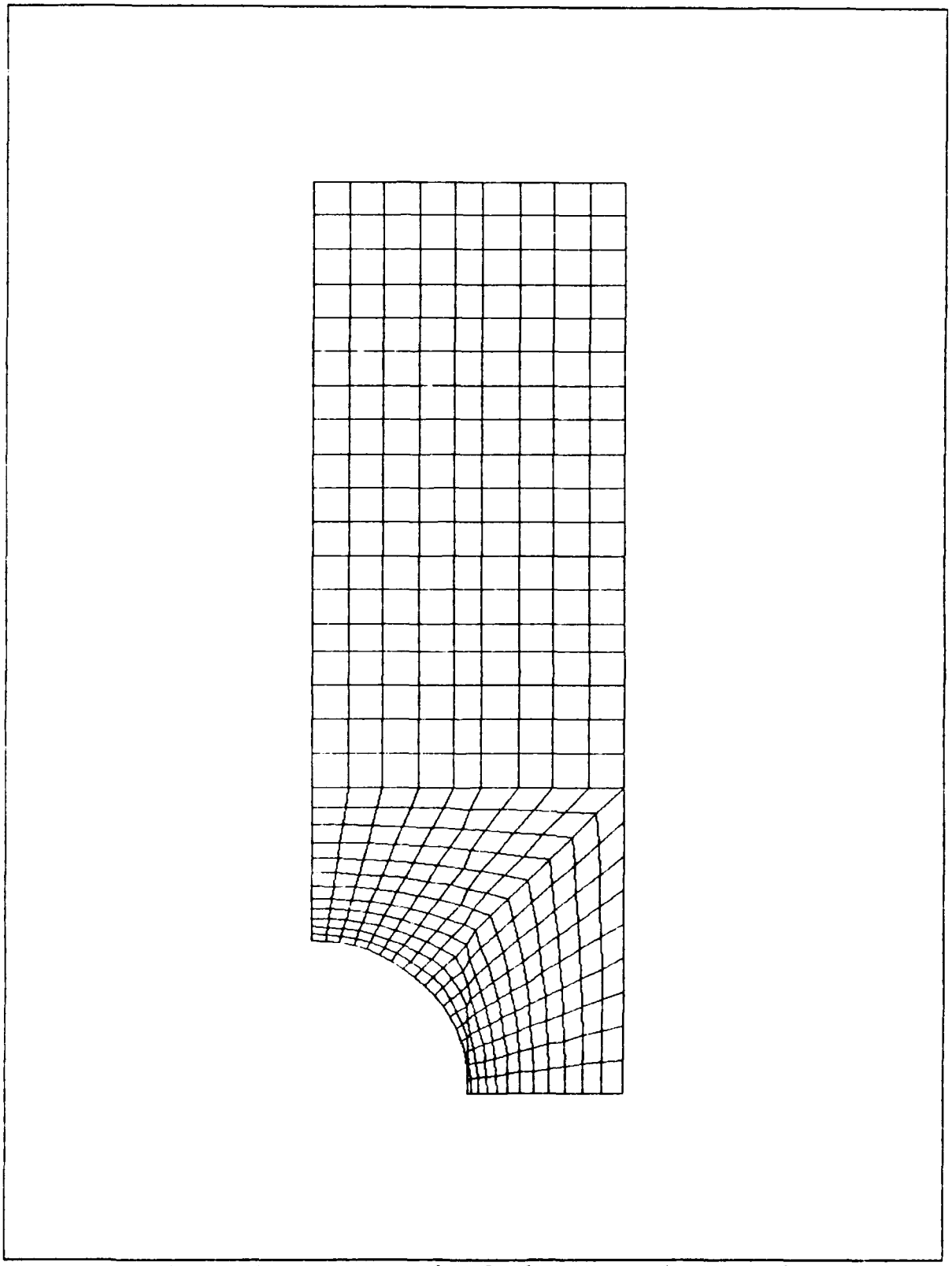

Figure 10. FEM Mesh of the Composite Panel

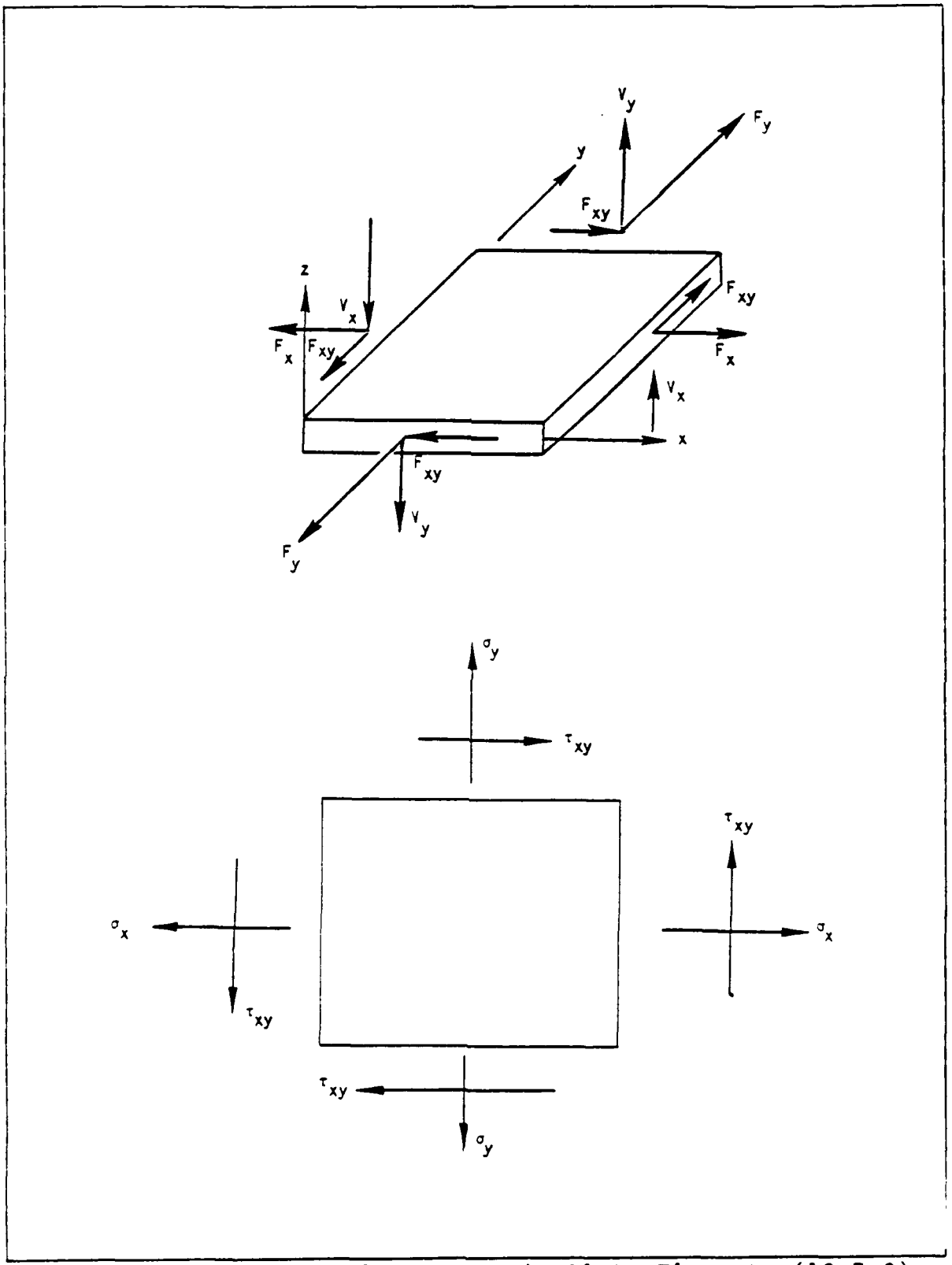

Figure 11. Forces and Stresses in Plate Elements (12:7-9)

laminate. The laminate is defined by the number of plys, orientation of the plys, and stacking sequence.

After the elements forming the panel have been described, the restraints on the model must be applied. The restraints are imposed along the two lines of symmetry. They keep the model from displacing in a rigid-body fashion and force the symmetry that would exist in a model of the whole panel (Figure 12).

The loads are applied in a consistent nodal approach that accurately reproduces the distributed load of a grip (on the physical specimen) onto the boundary nodes of the model. The loads are shown in Figure 13. The nodal loads modeled represent an equivalent end loading, for an entire panel, of 1800 pounds.

Once the restraints and loads have been applied, constraints must be defined. If no constraints are applied, the deformed model will have an elongated central portion at the end of the panel due to the nodal loads. This obviously is not what happens in the actual panel and the constraints simply force the end of the model to behave in the same manner as the physical panel. Thus the end of the panel remains square after loading (Figure 14). The encircled "MP" identifies the illustrated constraint as an MSC/NASTRAN multipoint constraint.

I-DEAS is then used to produce the MSC/NASTRAN Data Deck and the solution is accomplished on a SUN 4 Workstation. The

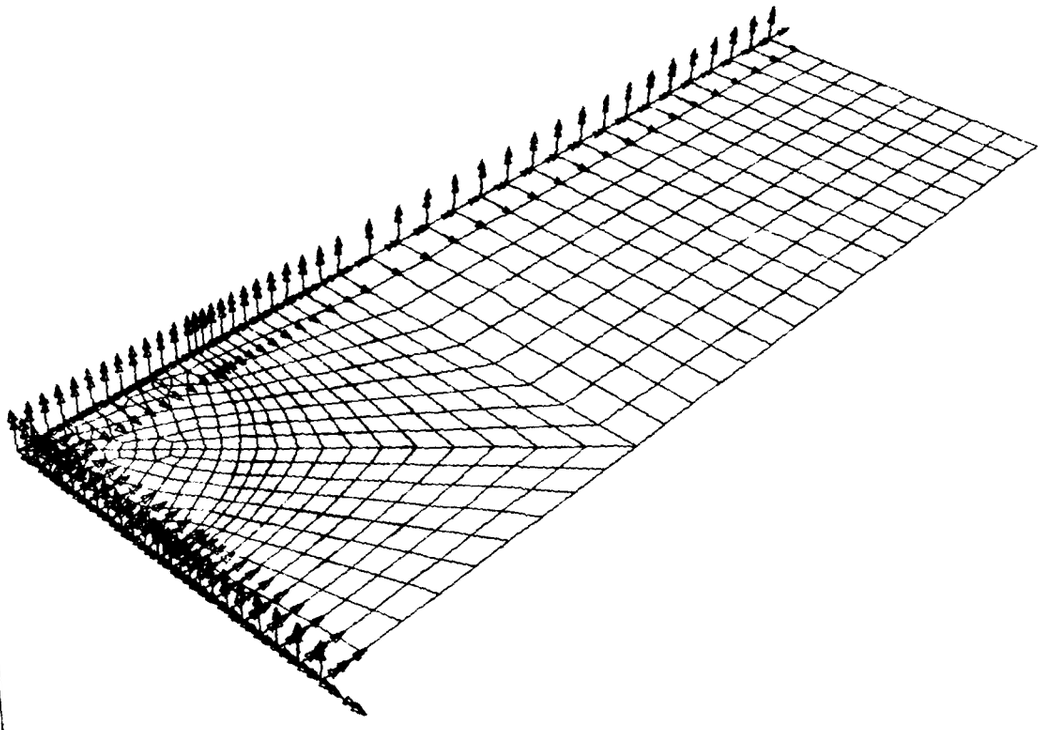

Figure 12. Quarter-Panel Restraints

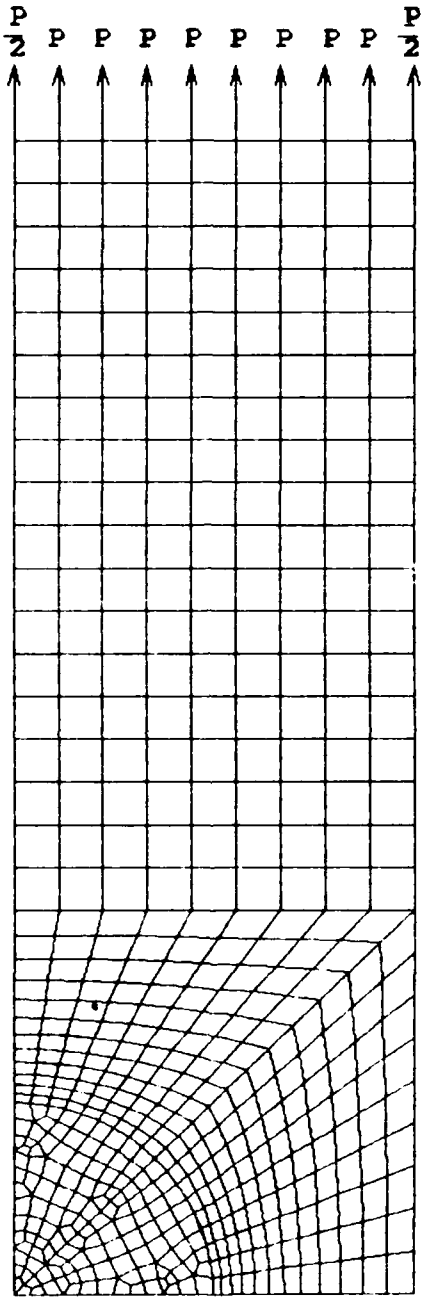

Figure 13. Nodal Loads of the Panel

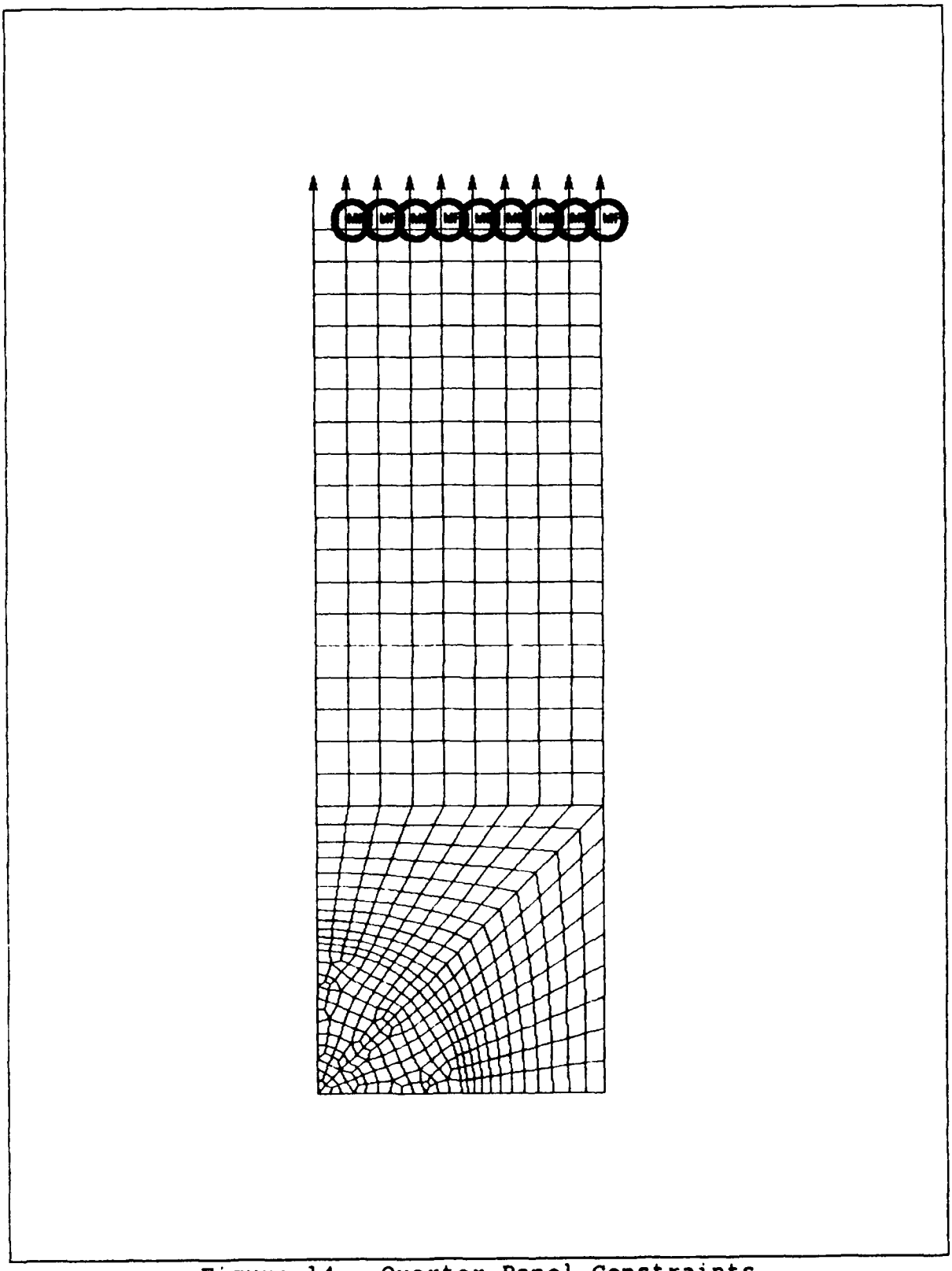

Figure 14. Quarter-Panel Constraints

workstation was used for the MSC/NASTRAN solution instead of the VAX as the VAX is fairly slow to solve the computational problems due to the number of users, and various demands on the system. Afterwards, data-loader software is used to reformat the MSC/NASTRAN solution into the I-DEAS universal file format. The solution universal file is then read into I-DEAS for the post-processing phase.

Before proceeding further, the model must be tested for convergence and accuracy. The theoretical value for the maximum stress of a plate with hole under axial loading is available for homogenous materials (13:81). The material properties for the plate are temporarily redefined for those of aluminum. The solution of the maximum stress on the homogenous plate is compared to the theoretical value. The FEM solution obtains a value of maximum stress within six percent of the theoretical value. Next, the model is tested for convergence; that is, with a finer grid and more elements will the solution converge toward the correct answer. Figure 15 is the refined model. The maximum stress value for this model was within three percent of the theoretical value.

The FEM of the patch is accomplished in the same manner as the panel. The patch FEM approximates a quarter circle as much as the elements will allow; Figure 16 represents the seven inch diameter patch. The patch is offset above the plane of the panel by a distance equivalent to the adhesive thickness, 0.004 inches. This is not actually necessary, but

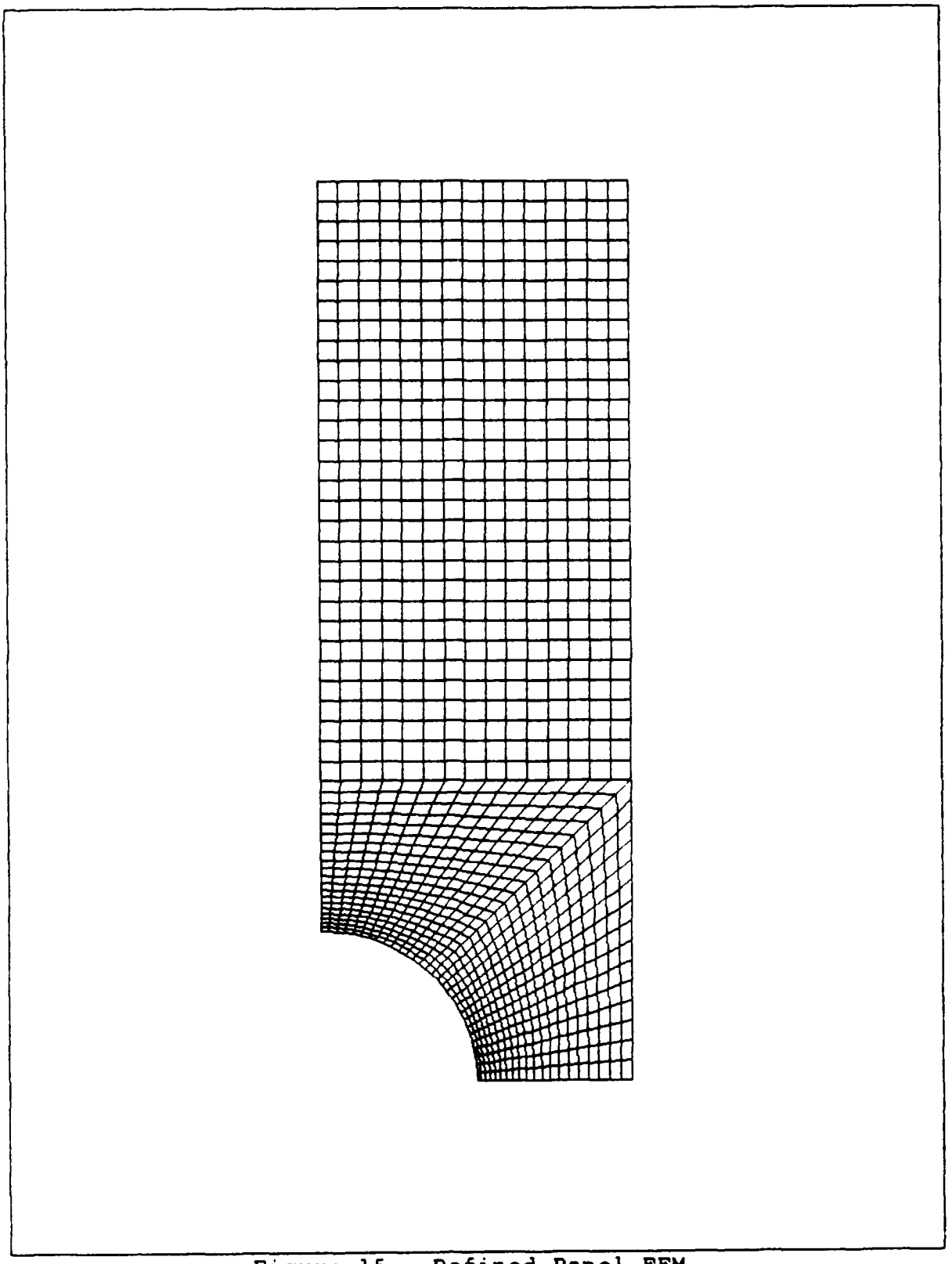

Figure 15. Refined Panel FEM

it eases the modeling and interpretation of the results in a graphical environment. The elements and nodes of the patch FEM are modeled to match the panel FEM elements and nodes. Nodes of the patch lie directly above nodes of the panel (Figure 17). The model is now ready for the adhesive elements.

Modeling the Adhesive. The adhesive is modeled with the MSC/NASTRAN CELAS2 scalar spring element. This element was chosen as it can be used as the basic building block for an elastic material characterization FEM. The basic nature of the spring element, and its parameters, allows fine control over the FEM incorporating it.

The element functions as a linear spring associated with two discrete points (nodes). Any CELAS2 element can act along any one of the six DOF available to the nodes. That is, a CELAS2 element can be defined (between two nodes) to function only in the x-axis direction; any relative movement between the two nodes in the y- and z-axis directions will not generate any reactions due to that movement. Therefore, three displacement, CELAS2 elements can be associated with a pair of nodes. Each of the three elements acts along a different axis, and the stiffness of any element is independent of the other two (Figure 18). The "spring" between two nodes can thus be tailored to fit the behavior desired.

The underlying assumption in using the CELAS2 elements is that the adhesive stiffness is constant. This limits the use

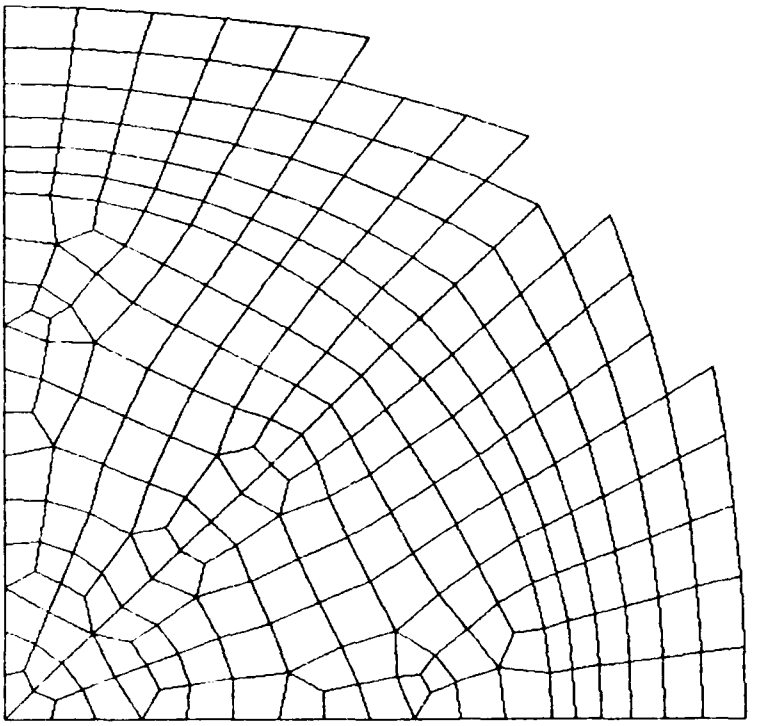

Figure 16. FEM of the Patch, Approximating a Circular Patch

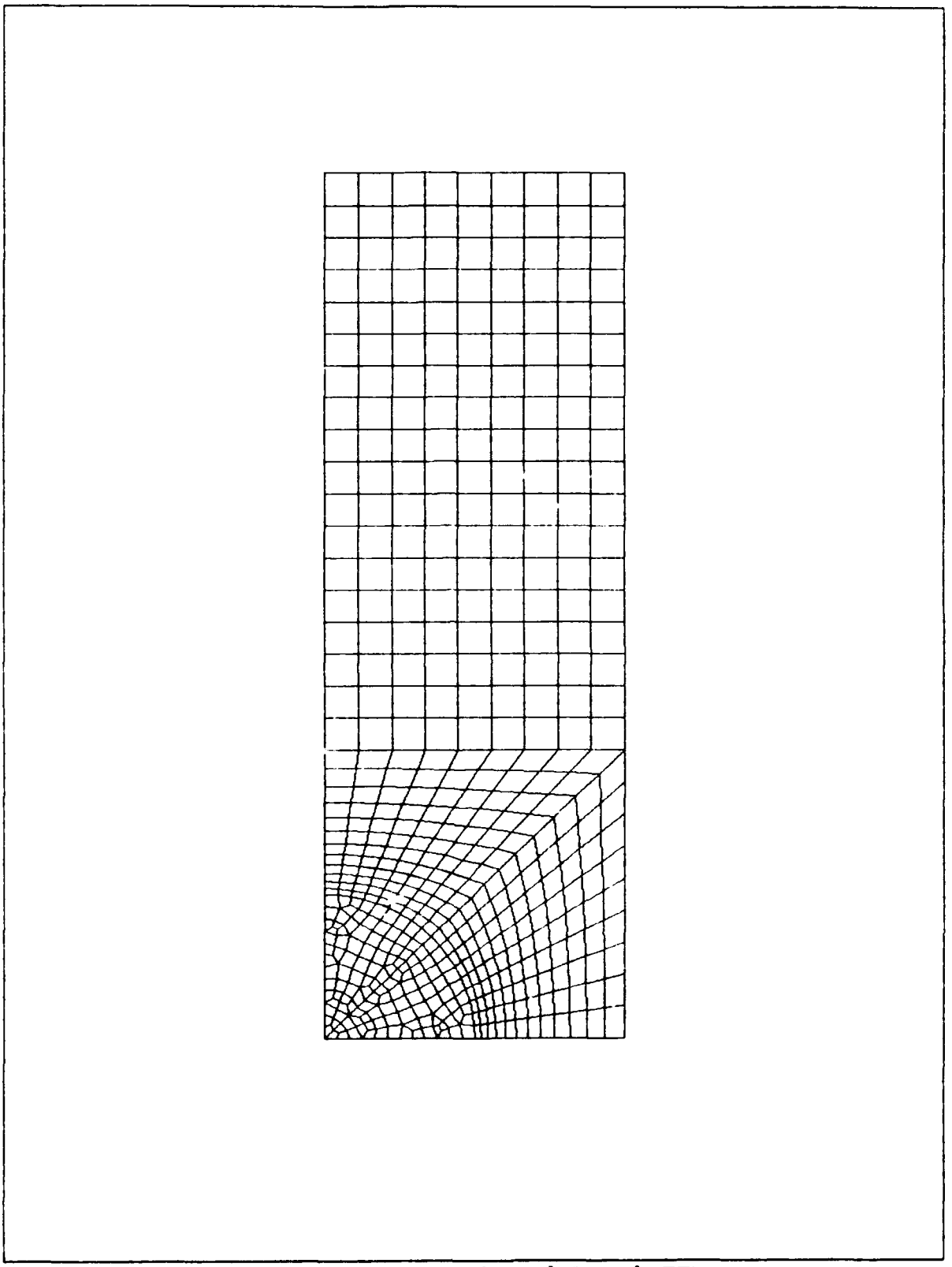

Figure 17. Patch and Panel FEM

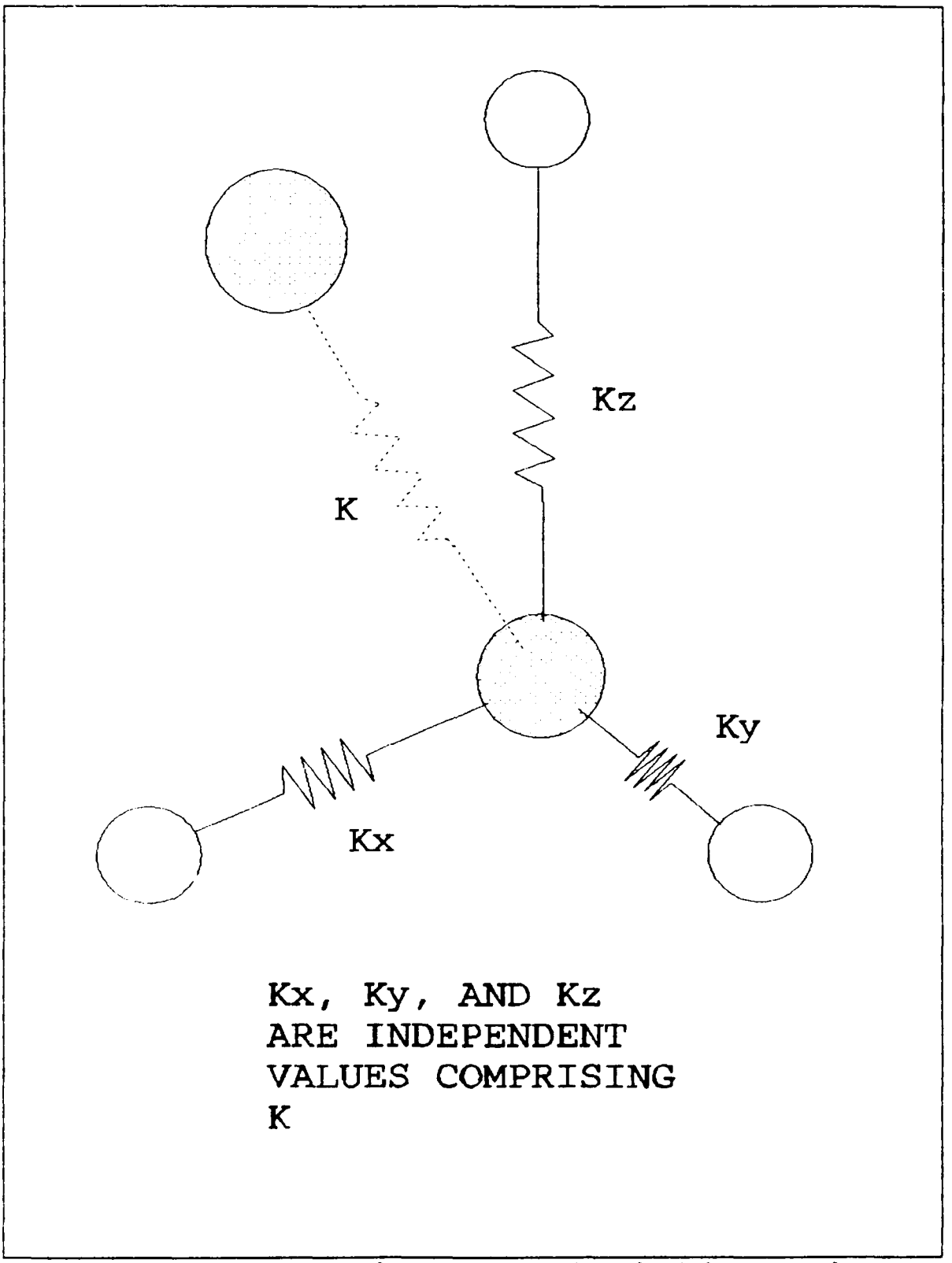

Figure 18. CELAS2 Elements Associated With Two Nodes

of this method to relatively linearly elastic adhesives below the yield point. To complete the model, scalar values of stiffness associated with the spring elements must be determined. Both these concerns will be addressed with a standardized adhesive test.

Calibration Test. Testing of bulk adhesives is relatively straightforward, with results for many adhesives available (5). At the time of this thesis no neat resin data was available for 3M's AF 377. If it had been, it would have been of marginal use. According to Hughes, et al.:

> Neat specimens are fabricated in the typical "dog-bone" shape used for metallic materials. They are tested in uniaxial tension at several strain rates and temperatures. This information, however, is not directly applicable to bonded joint analysis. The constraint that the adherend applies to the adhesive as it is strained prevents the normal Poisson effect from taking place. (14:141-175)

Since no adhesive shear data is available, at the time of this thesis, the only way to gather the necessary information for assigning values to the spring elements is through actual shear tests.

In order to "calibrate" the springs, an FEM of a ANSI/ASTM D 3528-76 test is created using the same methodology as the patch and panel before. This test is the "Standard Test Method for Strength Properties of Double Lap Shear Adhesive Joints by Tension Loading" (15:331-336). Figure 19 represents the specimen used in this test. The FEM analog is shown in Figures 20, 21, and 22. The FEM of the double lap shear specimen is such that all the elements have the same

area (this simplifies the calibration effort). The nodes of the FEM are defined such that linked pairs have the same x and y coordinate but are separated in the z (thickness) direction by the thickness of the bond, as is the patch and panel. Each pair of corresponding nodes, of the thick and thin adherends, are "connected" by three linear spring elements, as described previously, though only one of the three is represented in Figure 22.

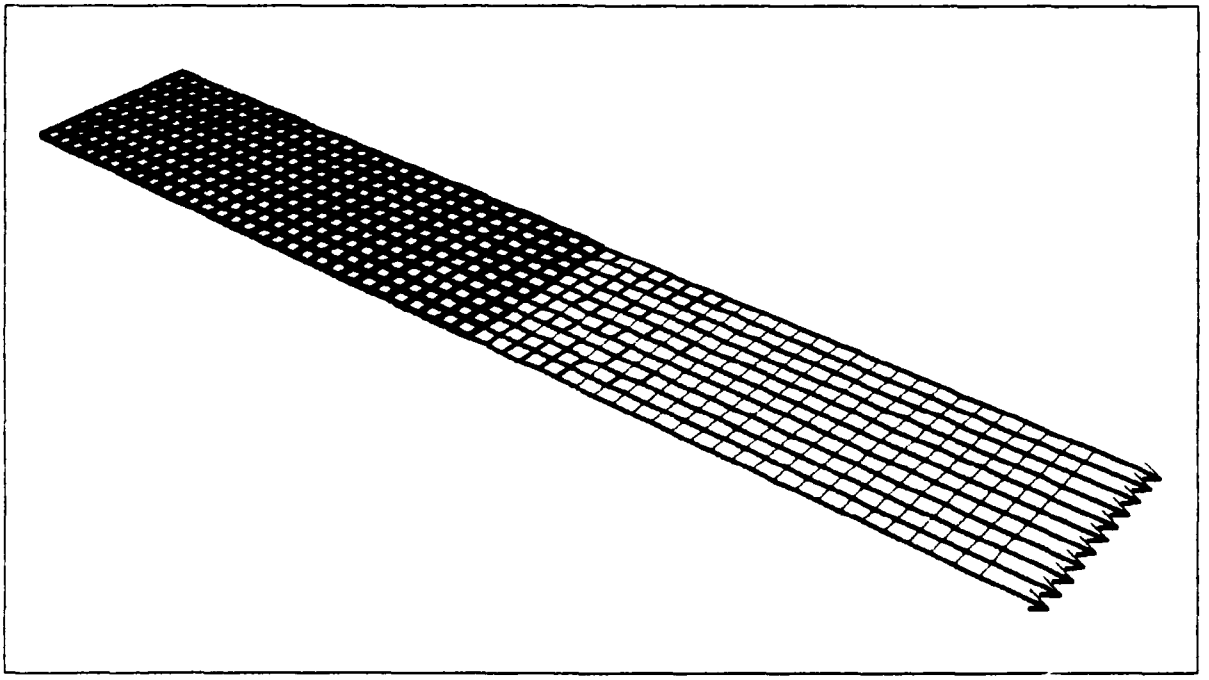

Figure 20. FEM of Double Lap Shear Specimen and Loads

Considering the adhesive thickness, the equivalent spring out-of-plane stiffness for a film adhesive is on the order of 60% of the equivalent spring in-plane stiffness (16:160). Both in-plane springs have the same value of stiffness, since the adhesive behaves similarly in both in-plane directions. The FEM spring values are assigned according to the bond area

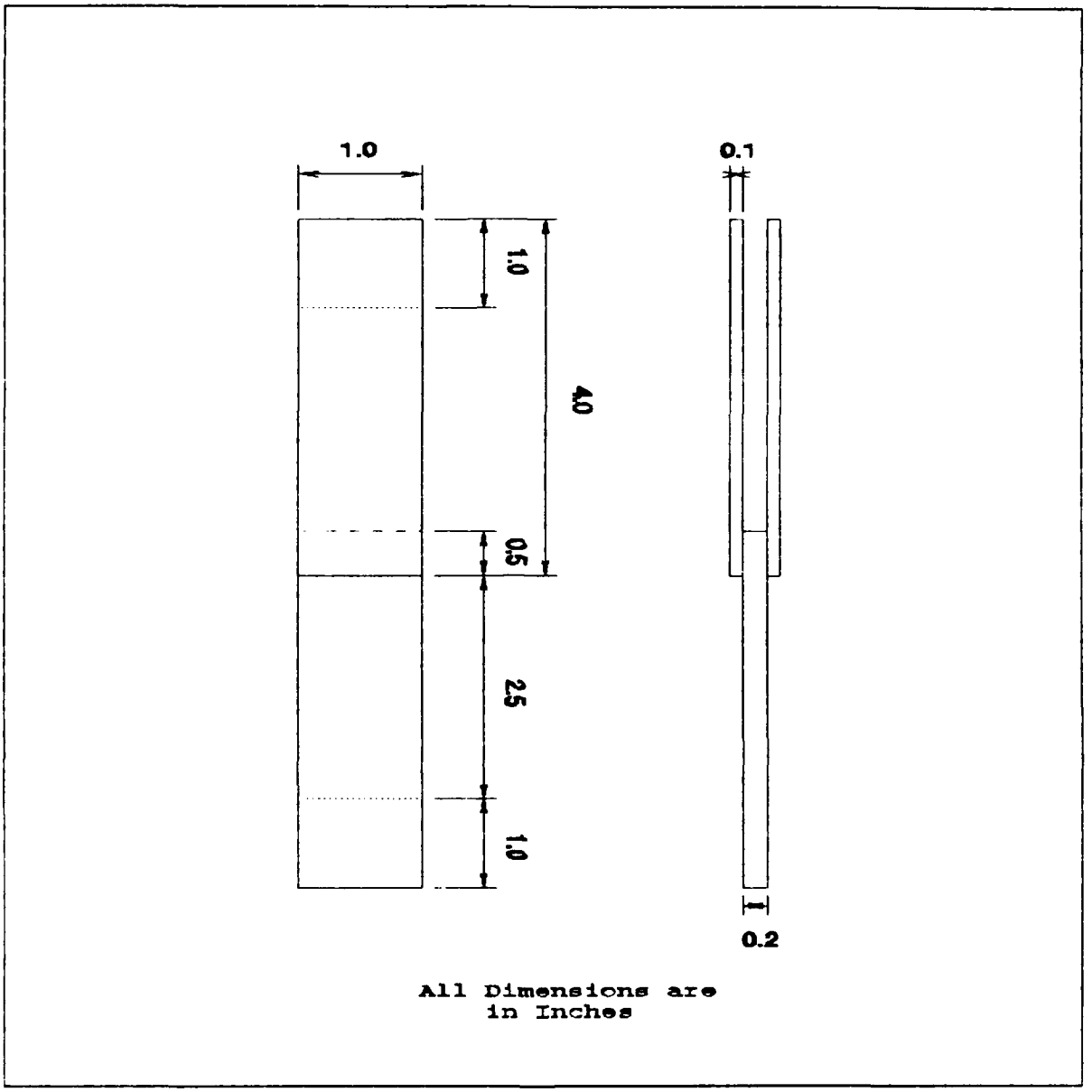

Figure 19. Form and Dimensions of Double Lap Shear Specimen

associated with the node in question. Thus, interior elements have a value of K for the spring stiffness, corner elements have 1/4 K and other boundary elements have 1/2 K.

The spring constant is defined using test data of the relative displacement of two points on the specimen. The points are at either end of the double lap, one on the thick

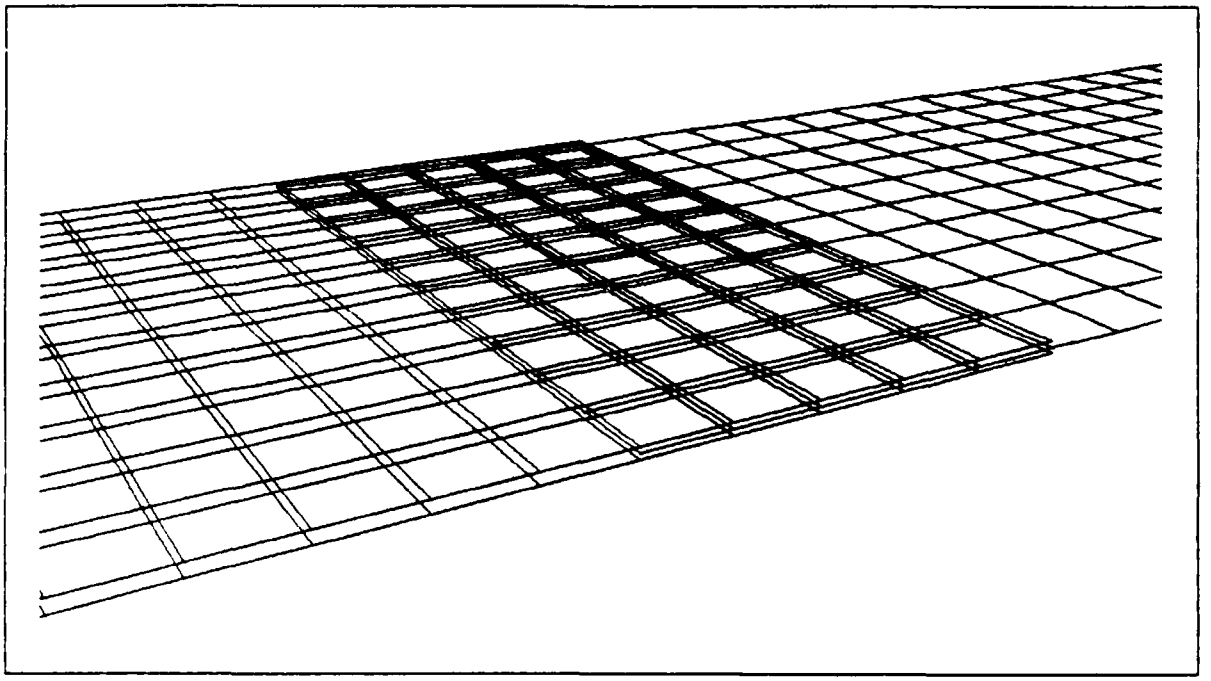

Figure 21. Magnification of FEM Double Lap Shear Specimen

adherend and the other on a thin adherend. The data received from the test are strain and load. The strain is converted to a displacement, utilizing the known reference length of the extensometer (which is the joint length). The model is loaded to the test load (using a consistent nodal approach and proper constraints and restraints) and the spring values of the model are adjusted until the displacement of the two points in the model matches those of the test specimen. Once the model and specimen agree, the in-plane spring value for interior nodes is calculated for one square inch of adhered area.

The spring stiffness value for one square inch of adhesive is then used to calculate stiffness values for all the modeled springs based on the bond area associated with a given pair of linked nodes. The bond area associated with the

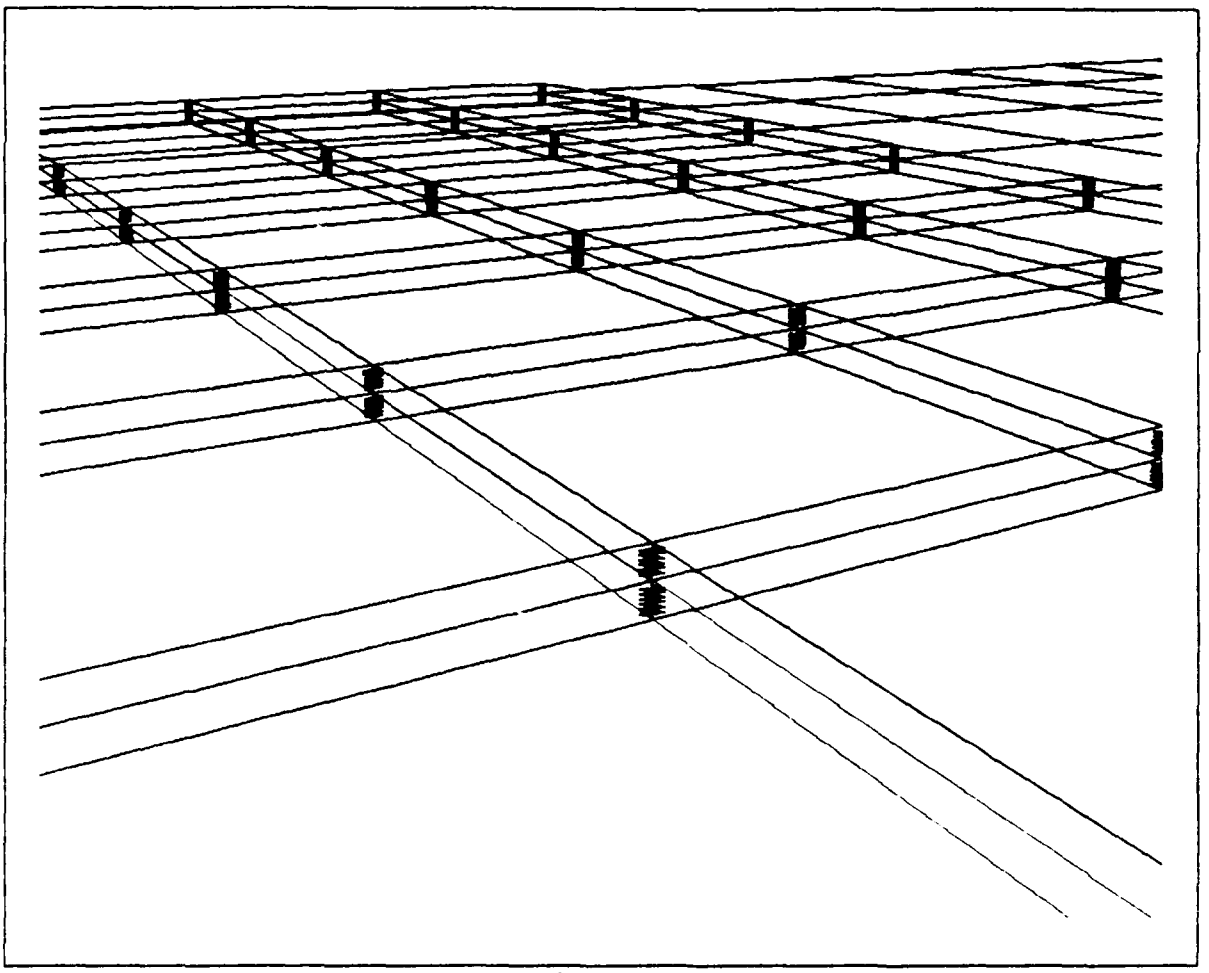

Figure 22. Spring Elements of Double Lap FEM

boundary nodes of the patch is the equivalent area of the actual patch and not the elements describing the patch. Thus, although the FEM patch is not round like the physical patch, the modeled adhesive is representative of the physical adhesive area.

V. Testing

The testing involved in this thesis is necessary to determine the characteristics of the epoxy film, which includes the linear or non-linear behavior of the adhesive. Also the testing will verify the panel and patch FEM using MSC/NASTRAN CELAS2 spring elements to model the bond between them.

Double Lap Shear Test. The CELAS2 elements must be "calibrated" before the modeling of the composite plate with patch can be finished. The shear test specimens are manufactured under the guidelines of the ASTM D 3528 test procedure as referred to earlier. The ASTM test calls for the use of 0.125 in. and 0.063 in. thick adherends for the specimens. For this thesis the coupons were made of 0.190 in. and 0.090 in. thick adherends. This was done because the shear strength of the adhesive was assumed to be about 6000 psi and a test under these parameters would have led to yielding of the adherends before failure of the adhesive. This would have blurred the data concerning the linear behavior of the adhesive.

The surface preparation was designed with a cohesive failure mode in mind. The adherends are 2024-T3 bare aluminum. The surface preparation consists of a phosphoric acid anodize followed by priming with BR-127 adhesive primer

of 0.0002 in. to 0.0003 in. dry film thickness. The criteria for a successful surface preparation was 100 percent cohesive failure in the coupons.

The adhesive used to bond the adherends is 3M's AF 377 film adhesive. The film weight is 0.03 lb/ft^2. The coupons are all cut from the same bonded plates to insure uniform cure conditions. The plates are cured under full vacuum (minimum 27 in. Hg) in an oven. The heat-up rate must be greater than 4°F per minute up to 205°F. The plates are held at that temperature for 120 minutes and then cooled at 10°F per minute. The temperature must be below 150°F before removing the vacuum.

The coupons are cut from the bonded plates using a sharp band saw. The edges of the panel are discarded. After the rough cuts are made the coupons are milled to the final dimensions. A total of seven coupons are cut from the bonded plates. The particulars of the coupons are noted in Table 3.

Specimen No.	Width (in)	LAP A (in)	LAP B (in)	GLT A (mils)	GLT B (mils)
4-1	0.9973	0.5045	0.4945	3.1	3.0
4-2	0.9986	0.5046	0.4971	3.0	2.9
4-3	1.0023	0.5057	0.4990	2.9	2.8
4-4	0.9986	0.5015	0.4980	3.5	3.1
4-5	1.0000	0.5018	0.5007	3.0	3.1
4-6	0.9987	0.5010	0.5035	3.0	2.9
4-7	0.9960	0.5005	0.5060	3.0	3.0

Table 3. Double Lap Shear Specimen Dimensions
GLT - Glue Line Thickness

Once the coupons are completed, the actual testing begins. The test stand is an Instron 4505 (Figures 23 and 24). An Instron Strain Gage Extensometer A515-11, with an initial gage length of one inch, is used to acquire the strain data about the lap joint. The extensometer spanned the entire joint. One knife edge rests on the thick adherend and the other edge rests on one of the thin adherends. The extensometer is held in place by elastic cord pulling the knife edges onto the specimen. The strain voltage, from the extensometer, runs through the Instron 4505 before being output to an HP 7090A X-Y Plotter. Other output from the Instron include, time of data acquisition, load, and grip extension. Only the load and strain data is used for evaluating the adhesive properties. The data is recorded on the X-Y plotter and also stored in an HP 9000 Series 300 computer which is connected to the plotter. After the test is completed the data stored in the computer is saved onto a floppy disk.

The first test run, 4-1, did not have the extensometer spanning the double lap shear joint. This test was run in order to find the approximate failure strength of the specimen and to verify the material properties of the aluminum comprising the coupons. The extensometer was attached to the thick adherend during this test. The load at failure is important because the extensometer can be damaged if it is engaged at the time of failure. During the remaining tests,

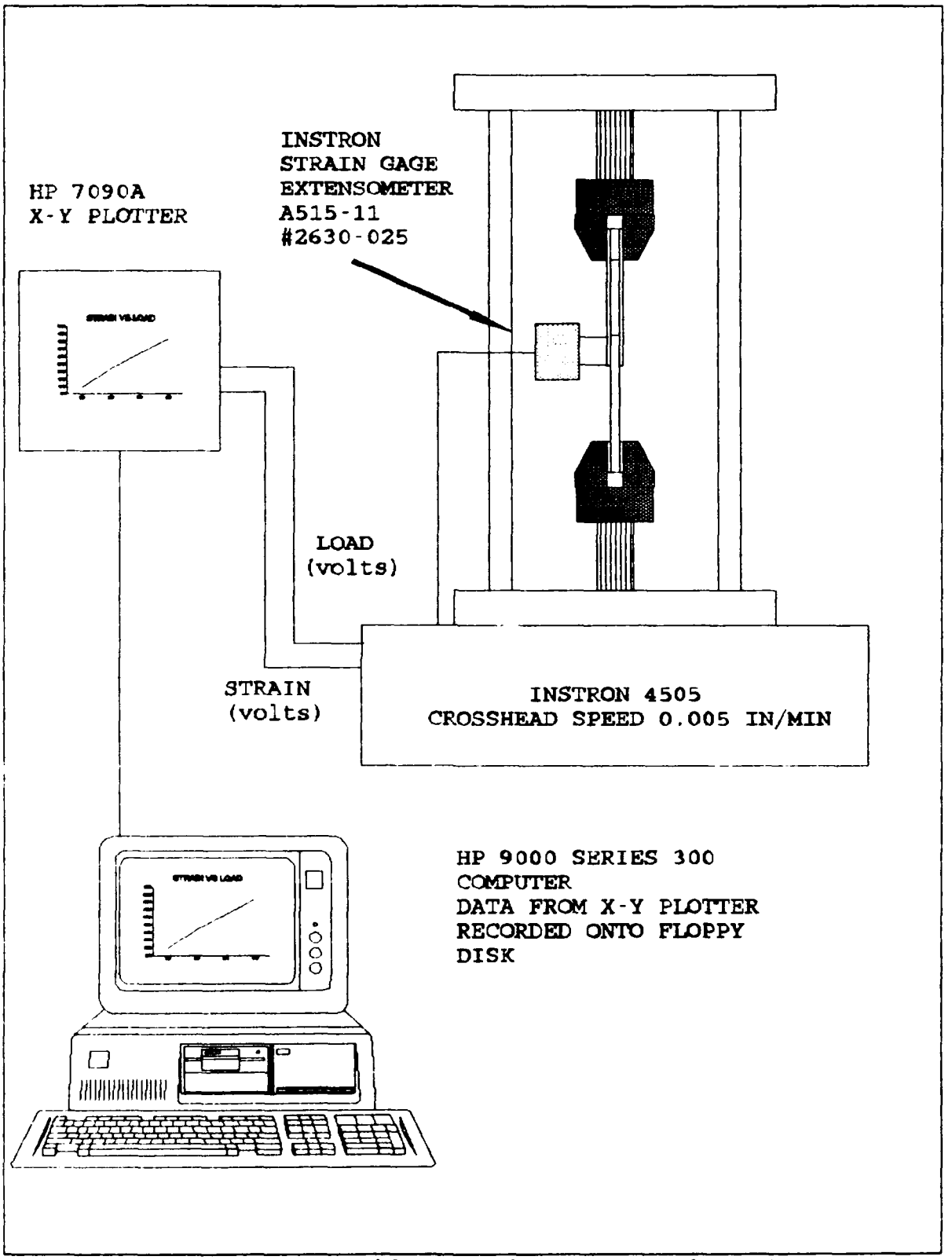

Figure 23. Double Lap Shear Test Schematic

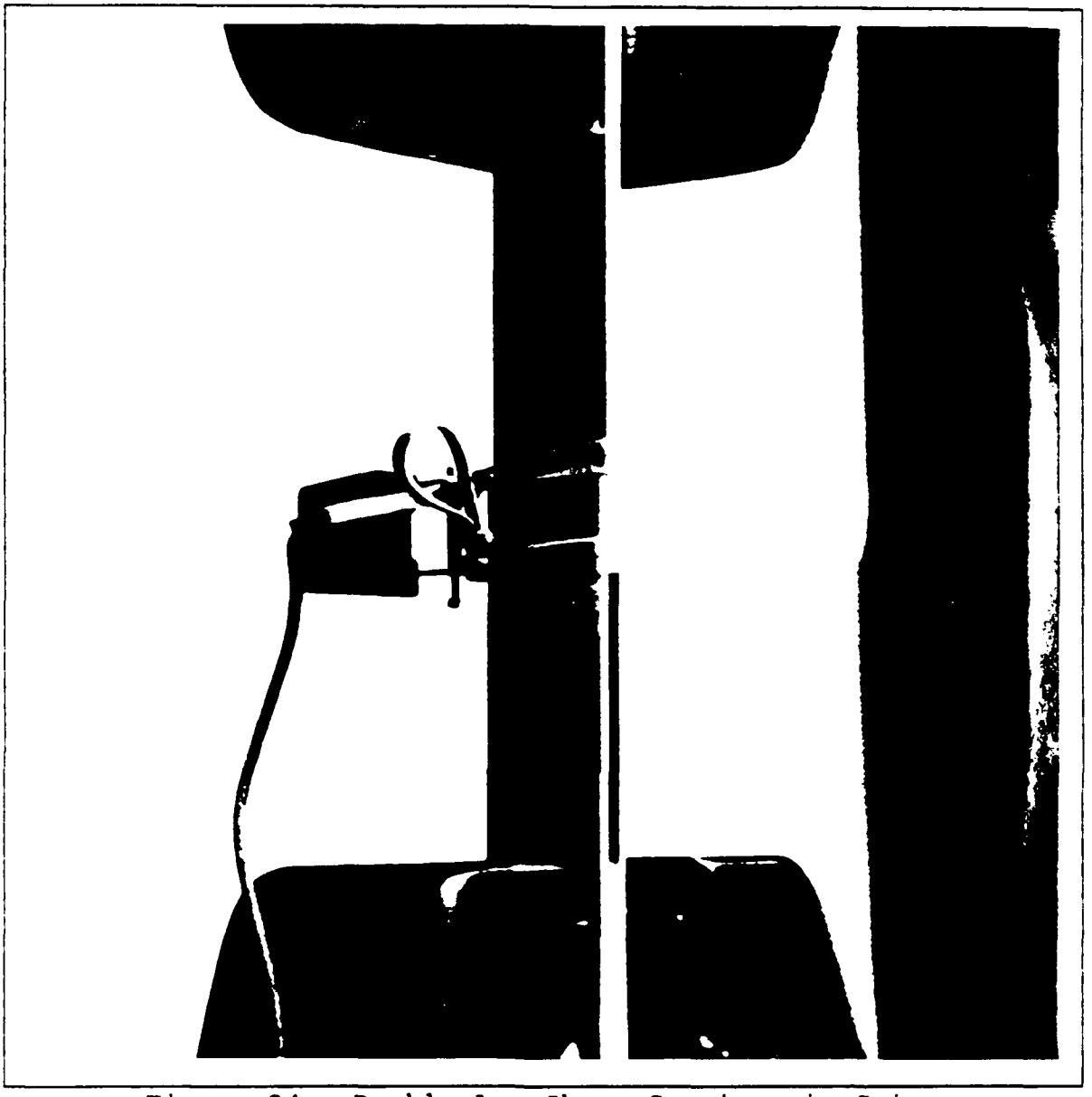

Figure 24. Double Lap Shear Specimen in Grips

the extensometer is removed before the specimen fails. As confidence is built through the tests, the extensometer is left on the specimen closer and closer to the failure load. The data acquired reflects this in that the data is complete for a percentage of the load spectrum. As an example, the first test recorded data until the load reached 84 percent of

the failure load, while the last test recorded data until the load reached 97 percent of the failure load. The data for the double lap shear tests is presented in Appendix A.

The data presented graphically is the lap stress versus lap strain; except for test 4-1, which is normal stress versus strain of the thick adherend. Lap strain is defined as the strain measured along the length of the lap joint. The gaged portion of the specimen is one inch long; this is L. The relative displacement of the ends of the lap joint is calculated below:

$$\Delta L = \varepsilon L \tag{20}$$

This relative displacement is for two points along the edge of the specimen. Once the relative displacement, for an average test under a given load, is determined, the CELAS2 elements can be "calibrated." The data used is the average of the linear portions of the stress-strain curves from the double lap shear tests. The spring element values are changed until the relative displacement of the two nodes, corresponding to the points that the extensometer knife edges rest on, matches the calculated extension.

Panel and Patch Test. Once the patches have been cured and bonded to the parent panel, as described earlier, the next step is the bonding of strain gages onto the specimen. The strain gages used are the Micro-Measurements Division CEA-06-

125UR-350. These gages are rectangular rosettes. The method of attaching the gages is as follows:

1. The areas where gages are to be attached are cleaned thoroughly with acetone.

2. The areas are then abraded to the point where the surface is smooth, i.e. free of fabric imprint.

3. Acetone is again used to clean the areas.

4. The strain gages are positioned with mylar tape to prevent inadvertent stretching of the gages.

5. M-Bond AE-10 Epoxy is mixed and applied to the underside of the gages and to the area where the gages will be attached.

6. The gages are taped back into place and pressure, in the form of weights, is applied to remove excess epoxy and provide clamp-up pressure.

7. After 48 hours the weights and tape are removed from the gages and the gages are cleaned with alcohol.

8. The strain gage leads are then soldered to the tabs of the gages.

For the panel and patch specimens, four strain gage rosettes are mounted on each specimen (for a total of 12 channels of strain). One in the center of the patch, two 2.25 inches from the edge of the cutout, and one far field gage, 12.5 inches away from the cutout edge (Figure 25). On the panels without a patch, there are three gages mounted. The rosettes are in the same locations except for the center one. On the one undamaged panel tested, two gages were mounted equally spaced longitudinally. All gauges were attached to one side of the panels, i.e. there was no averaging of strain from the two sides of the specimens.

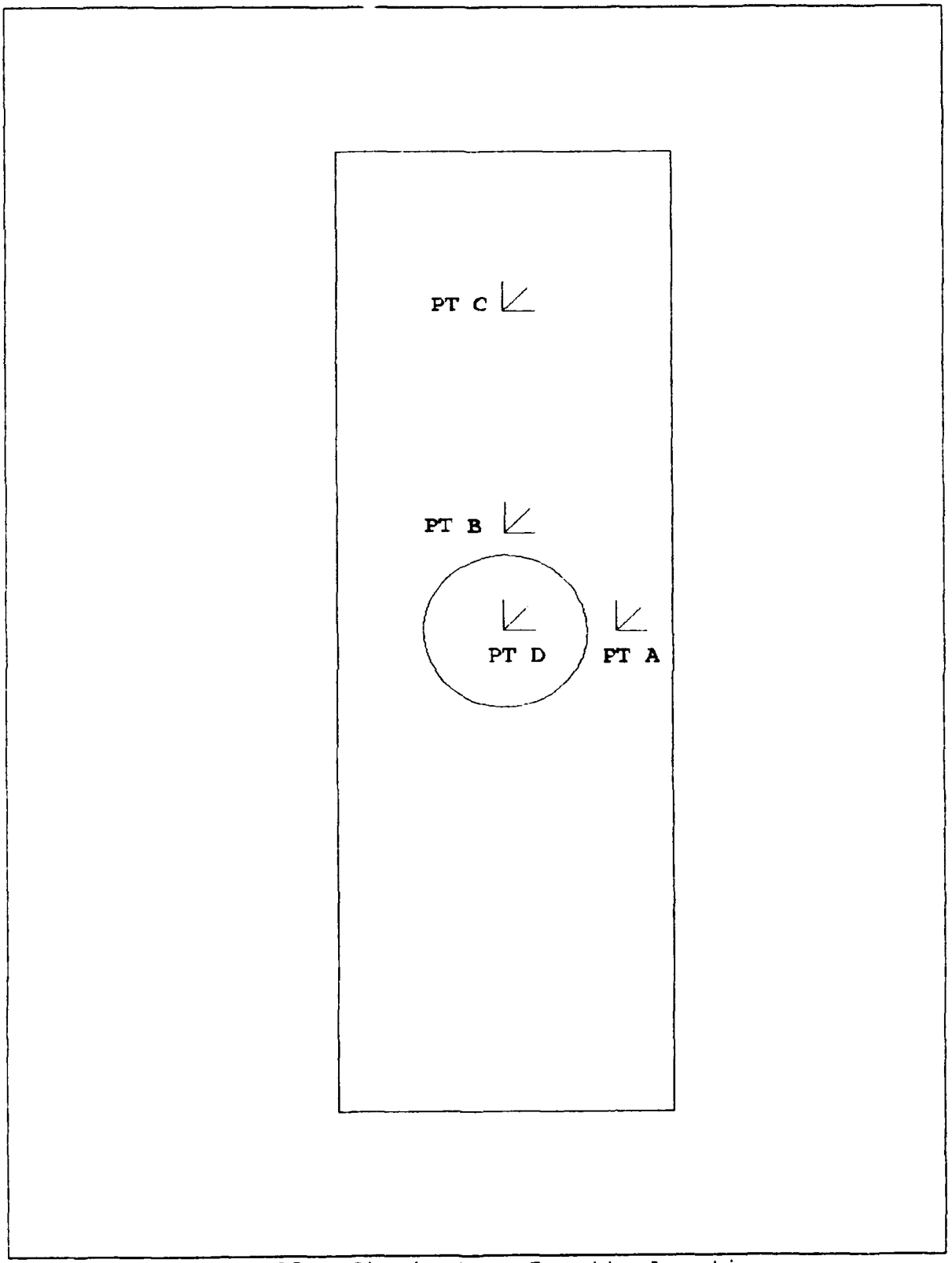

Figure 25. Strain Gage Rosette Locations

The actual dimensions of the panels tested is noted in Table 4. The column denoted as "DIM A" refers to the width of the portion of the panel where strain gage A (refer to Figure 25) was attached. "DIM B" refers to the width of the other portion of the panel across the cutout. Both of these dimensions where measured across the diameter of the cutout. If the panels had been cut perfectly the two dimensions would have been 2.500 inches.

Panel No.	DIM A (in)	DIM B (in)	HOLE DIA (in)
1-N	N/A	N/A	N/A
1-0	2.515	2.396	5.003
2-0	2.514	2.396	4.999
1-4	2.538	2.389	4.995
2-4	2.522	2.394	4.998
1-6	2.510	2.527	4.994
2-6	2.512	2.541	4.870
1-8	2.527	2.466	5.003
2-8	2.510	2.527	4.994

Table 4. Test Panel Dimensions

The test fixture is an MTS Testing System 976.01-58 with a Load Cell Model 661.31A-05 (Figures 26 and 27). The specimen is bolted into adapters for the hydraulic grips. The hydraulic grips are about three inches wide. The adapters allow the 10 inch wide panels to be secured in the load cell. The adapter was originally made to accept specimens up to 16

inches wide. The bolt pattern is staggered and requires nine 0.5 inch diameter bolts on each end to secure the specimen. The minimum thickness the adapter will allow for proper installation of a specimen is 0.75 inches. Since the panels are only 0.0832 inches thick, spacers are required to build up the apparent specimen thickness. Half-inch aluminum plates are used for this purpose. The plates are sandblasted and have a non-skid surface applied to the side in contact with the specimen. The idea behind the nonskid surface is to shear a portion of the grip load into the specimen rather than through the bolts. This way the bearing loads on the specimen can be reduced without using time consuming and costly tabs which must be bonded on.

The strain gage leads are run into an HP 3852A Data Acquisition/Control Unit (a multiplexer). From the multiplexer, the data is acquired from an HP 9000 Series 300 computer running the data acquisition software "MULT-STR." The data is displayed in real time on the computer monitor. The displayed data is load versus the various channels of strain. After the test is completed the data is saved onto a floppy disk for further evaluation. The data acquisition software is independent of the test cell controller and both are started simultaneously at the beginning of a test. The test cell controls the rate of grip extension and provides a load signal to the multiplexer which in turn is interrogated by the data acquisition software.

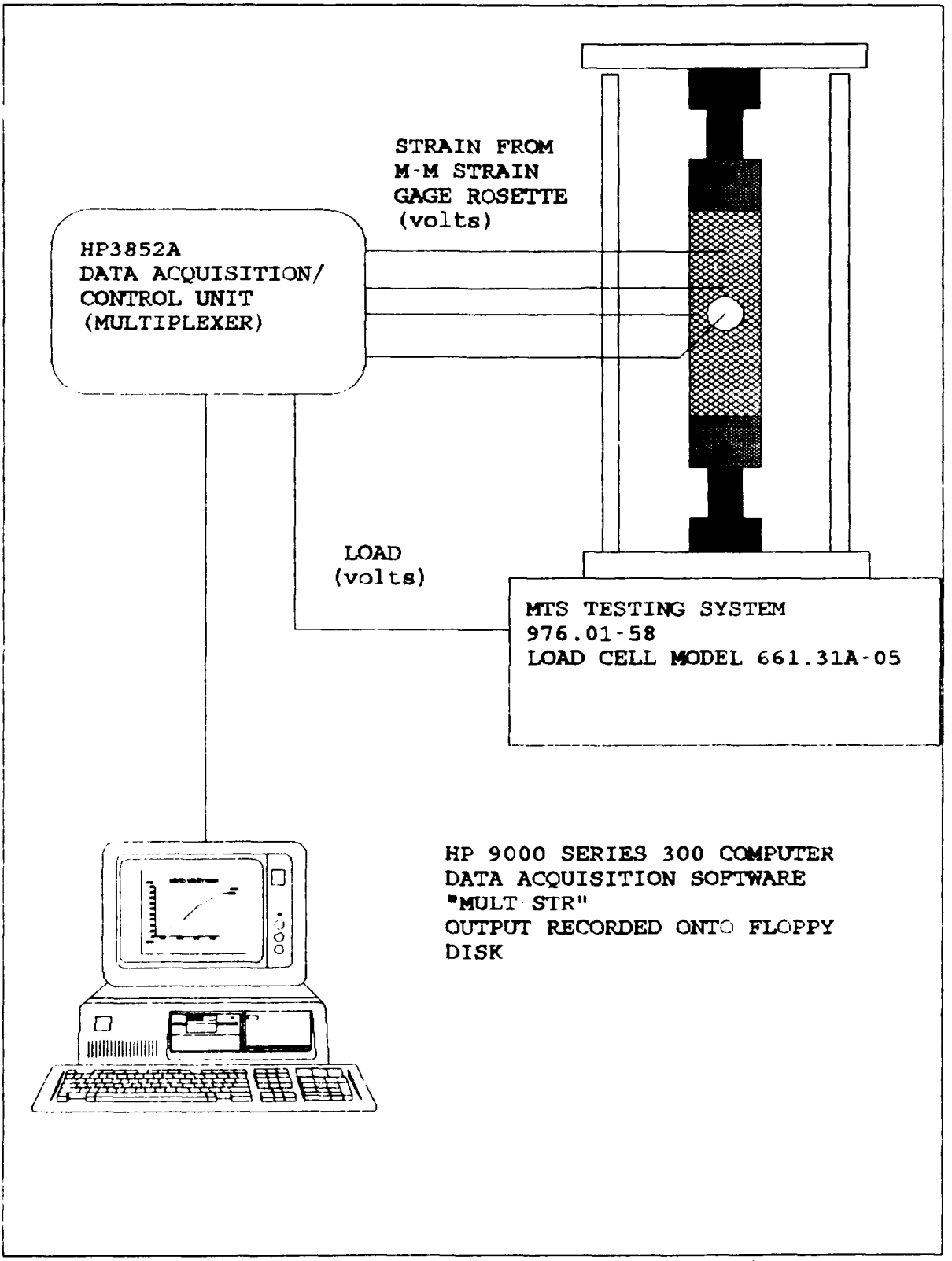

Figure 26. Panel and Patch Specimen Test Schematic

Figure 27. Panel and Patch Specimen in the Test Cell

The load cell is set to provide grip extension at 0.005 inches per minute. The scale of load voltage varies depending on the expected maximum load and is set before the test begins. The data acquisition software requires the following input before the test begins:

1. Test name.
2. Number of strain channels to be received.
3. Gage factor of the strain gages.
4. Level of load per 10 volts incoming signal.
5. Scale of the graphical display of load versus strain.

After the strain data that has been collected and saved onto a floppy disk, it is evaluated and reduced into a form comparable to the data output from the FEM. This involves resolving the strain gage rosette readings into Von Mises strain. Assuming the longitudinal strain gage in a rosette is number 1, the gage 45 degrees off from the longitudinal direction is number 2, and the transverse gage is number 3, the equations involving these recorded directions of strain and the principal strains are:

$$\varepsilon_1 = \frac{\varepsilon_{max}+\varepsilon_{min}}{2} + \frac{\varepsilon_{max}-\varepsilon_{min}}{2}\cos 2\theta \qquad (21)$$

$$\varepsilon_2 = \frac{\varepsilon_{max}+\varepsilon_{min}}{2} + \frac{\varepsilon_{max}-\varepsilon_{min}}{2}\cos 2\left(\theta+\frac{\pi}{4}\right) \qquad (22)$$

$$\varepsilon_3 = \frac{\varepsilon_{max}+\varepsilon_{min}}{2} + \frac{\varepsilon_{max}-\varepsilon_{min}}{2}\cos 2\left(\theta+\frac{\pi}{2}\right) \qquad (23)$$

Strains ϵ_1, ϵ_2, and ϵ_3 are measured by the strain gage rosettes. The principal strains are calculated after solving the above equations for ϵ_{max}, ϵ_{min}, and θ. The Von Mises strain is then obtained from the principal strains. It's the Von Mises strain from the experiments and FEM that are compared in the results section of this thesis. Von Mises strain was used for the strain field comparison since this comparison relates distortional energy which presents a more complete "picture" of the strain field behavior at a given point. All tests for this thesis were accomplished in the test facilities of the Wright Research and Development Center.

$$\varepsilon_{max,min} = \frac{\varepsilon_1+\varepsilon_3}{2} \pm \frac{1}{\sqrt{2}}\sqrt{(\varepsilon_1-\varepsilon_2)^2+(\varepsilon_2-\varepsilon_3)^2} \qquad (24)$$

$$\theta = \frac{1}{2}\tan^{-1}\left(\frac{\varepsilon_1-2\varepsilon_2+\varepsilon_3}{\varepsilon_1-\varepsilon_3}\right) \qquad (25)$$

$$\varepsilon_v = \sqrt{\frac{1}{2}\left\{(\varepsilon_{max}-\varepsilon_{min})^2+\varepsilon_{max}^2+\varepsilon_{min}^2\right\}} \qquad (26)$$

VI. Results

Finite Element Model. The results from the finite element model analysis make intuitive sense. Figures 28, 29, 30, and 31 illustrate the changing Von Mises strain field of the composite panel. The figures illustrate the strain field of the panel with the cutout under load and the same panel with different patches bonded to it. The patched panel figures show both surfaces of the panels, one side reveals the patch strain field entirely while the other side shows the strain field in the panel to the edge of the cutout.

The strain fields illustrated reveal how the load path changes from the unrepaired case to the repaired case. The 4-ply patch is highly stressed due to the adhesive shearing the load into it. As the patch laminate begins to match the original panel in the primary load direction, the strain fields become more closely matched. The 8-ply patched panel has only a slightly higher strain field than the far field areas of the panel. Most of this difference may be due to the Poisson contraction of the panel adjacent to the hole (since the patches are all unidirectional, the Poisson contraction is not countered in the "repaired" panels).

The maximum Von Mises strain in each of the four cases illustrated and the undamaged case are noted below:

1. Panel without repair. ϵ_v = 9.04 E-04
2. Panel with 4-ply patch. ϵ_v = 3.91 E-04
3. Panel with 6-ply patch. ϵ_v = 2.90 E-04
4. Panel with 8-ply patch. ϵ_v = 2.34 E-04
5. Undamaged panel. ϵ_v = 2.05 E-04

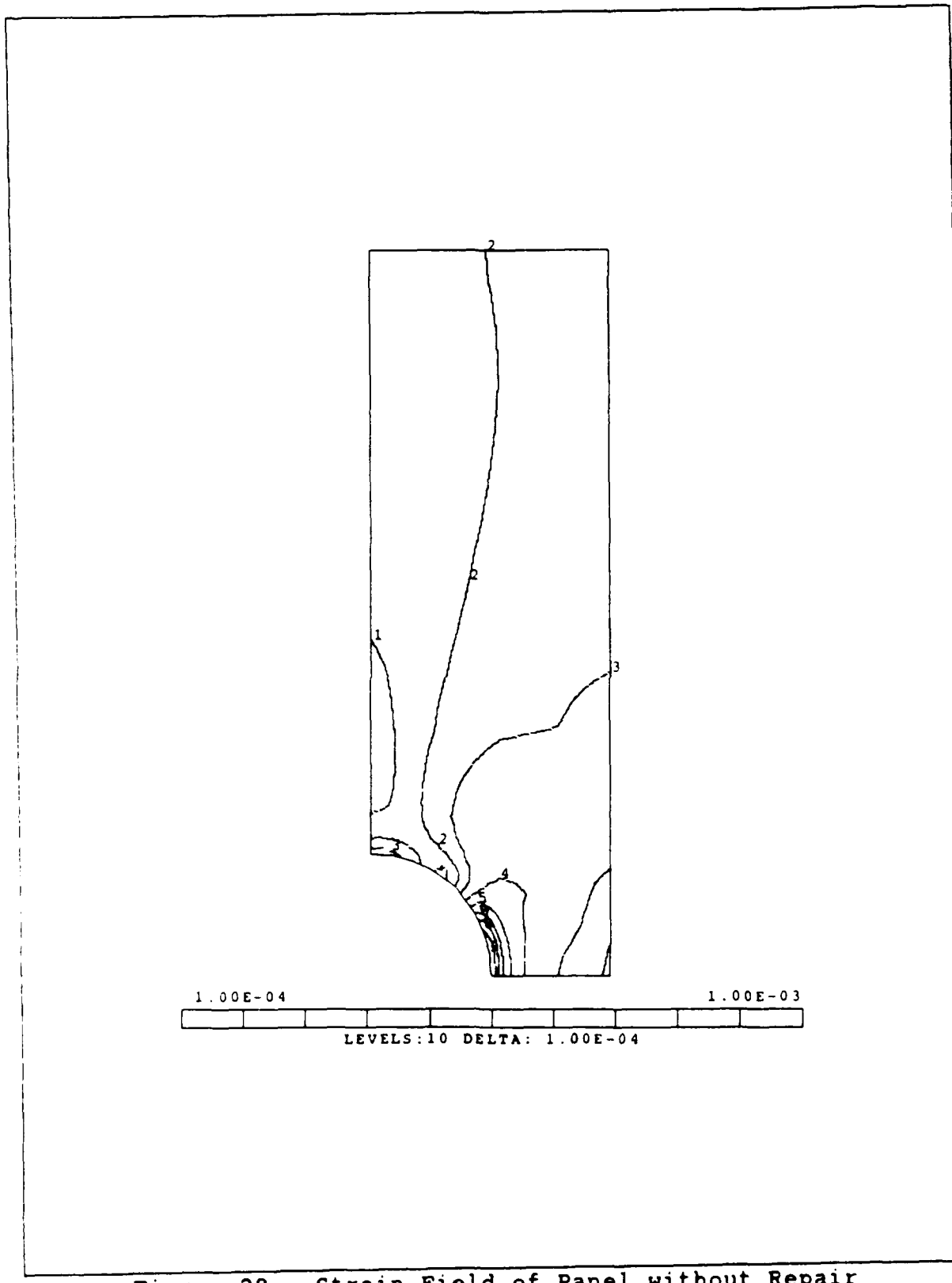

Figure 28. Strain Field of Panel without Repair

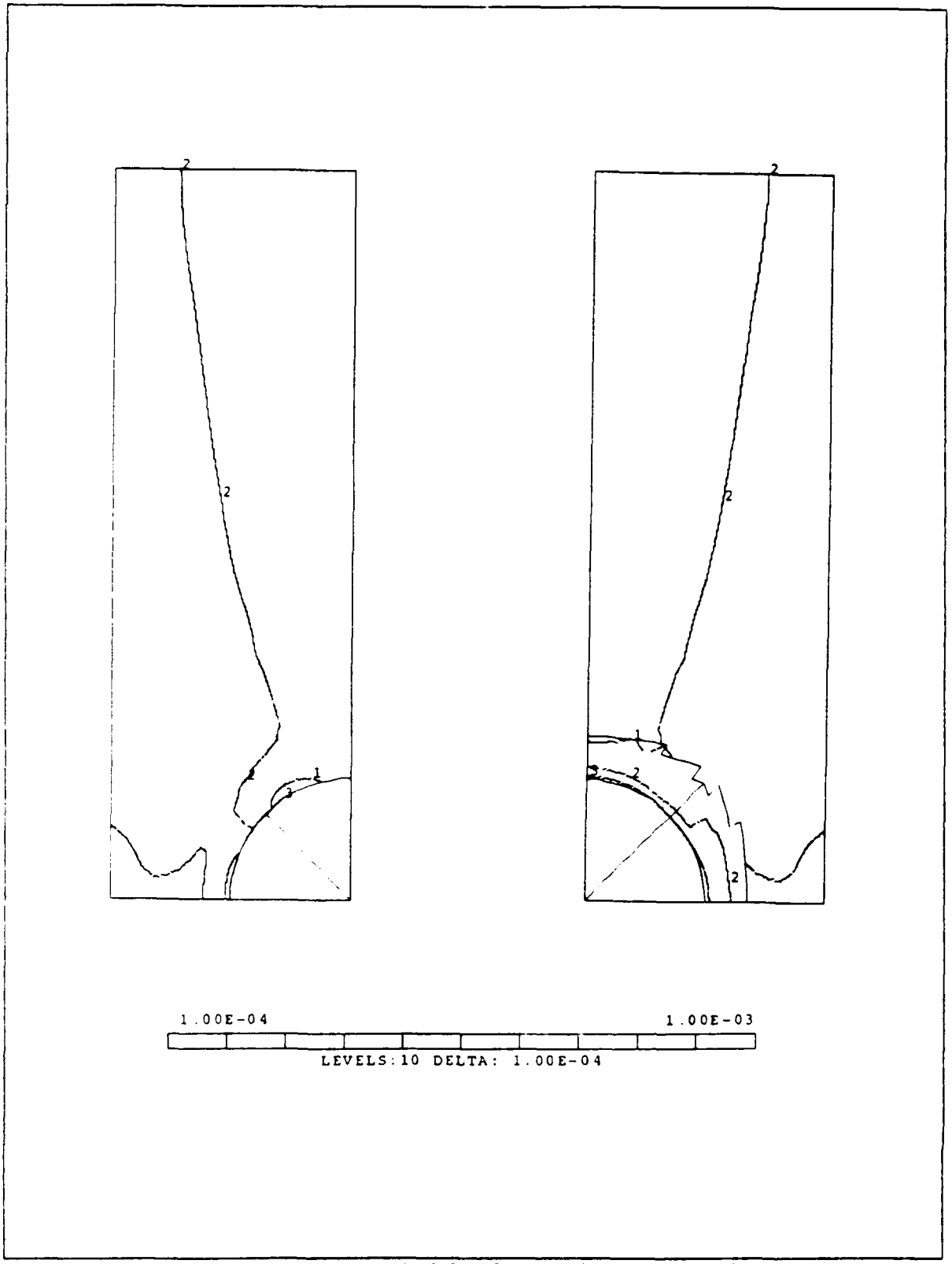

Figure 29. Strain Field of Panel with 4-Ply Patch

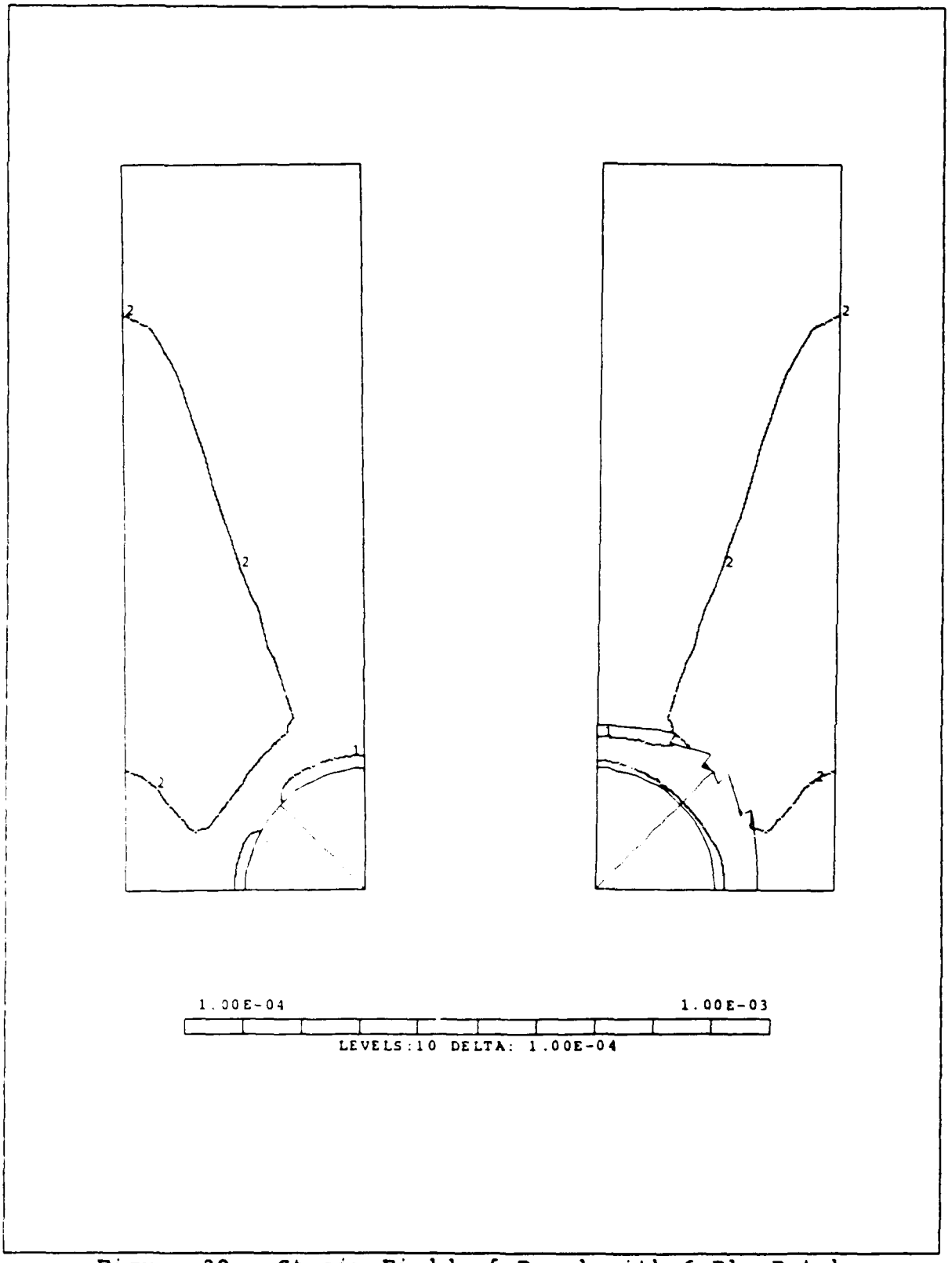

Figure 30. Strain Field of Panel with 6-Ply Patch

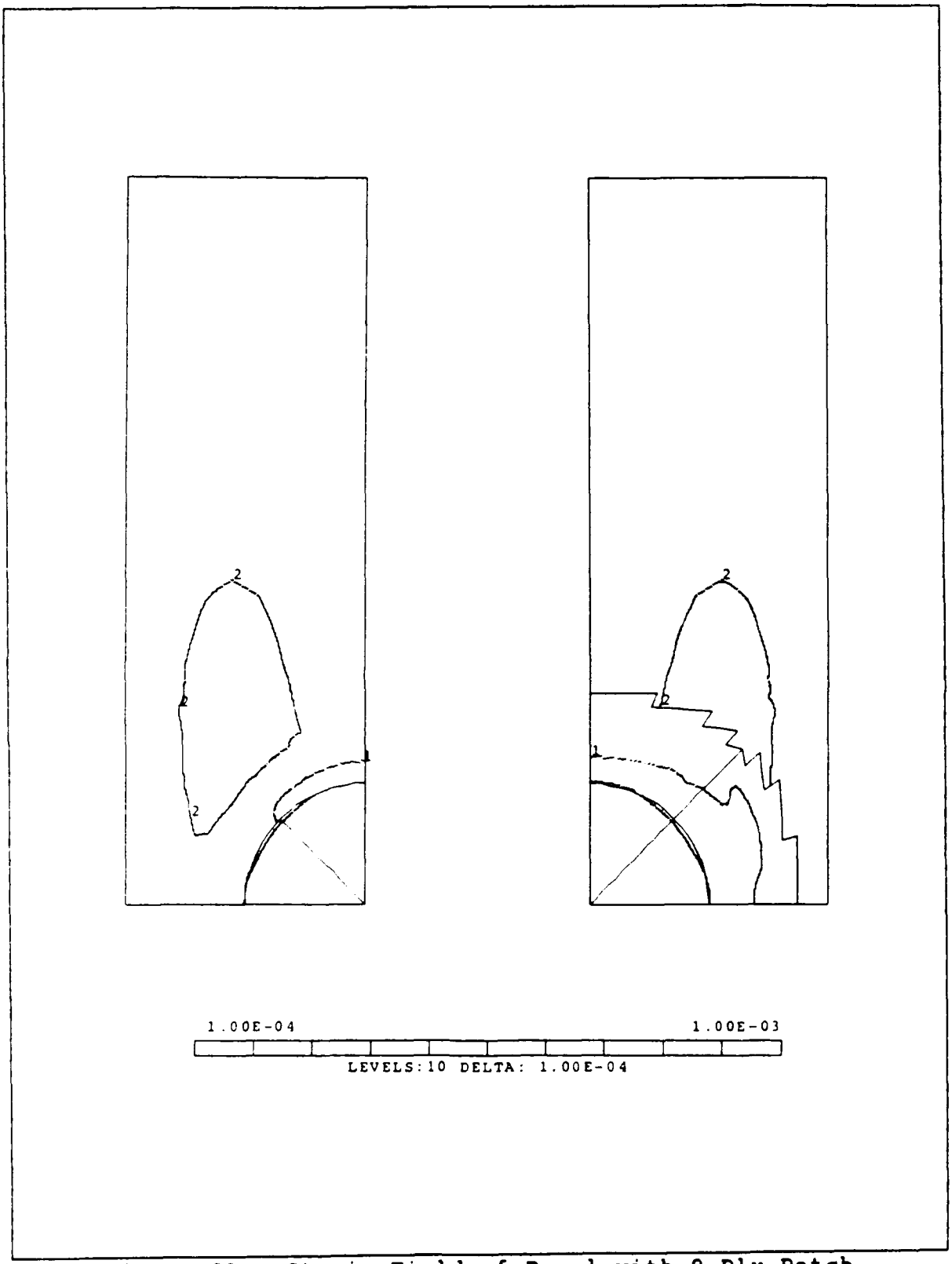

Figure 31. Strain Field of Panel with 8-Ply Patch

The areas adjacent to the cutout reveal the load tapering effect of the adhesive. The strain levels in the patch are raised incrementally from the edge of the patch toward the edge of the cutout. This agrees with intuitive reasoning.

Test Specimens. The physical tests were not as straight forward as the FEM. The first indication of problems was with the test of the "damaged" panel without repair. As the panel load was increased, but well below the tensile failure load, a portion of the panel near the cutout began to displace out-of-plane. The displacement was symmetric about the longitudinal axis. This behavior appears to be similar to a form of transverse buckling. C-Scans of one of the panels, before testing, revealed some delamination around the cutout. The delaminated areas extended into the panel no more than 1/8 inch. The delamination was probably caused in the machining of the cutout. Under the transverse compressive Poisson stress near the cutout, the delamination may have caused transverse shear which may have led to the transverse instability. This instability may also have been aggravated by the relatively thin panel and large cutout compared with the other panel dimensions. This is indicated in Figures 34 and 35. With the load between 8000 and 9000 pounds the strain at point B changed sharply (refer to Figure 25). This behavior was not modeled and it limited the acceptable data, of the test, to the moments before the out-of-plane behavior became the dominant strain mechanism. Generally, this limited

the useful data to end loads below 10,000 pounds. While the unrepaired panel was the most affected by this phenomenon, all the panels revealed signs of "transverse buckling" during the tests. The typical failure mode of the patched panels was one of transverse bending failure of the patches accompanied by delamination of the patch from the panel and then tensile failure, aggravated by out-of-plane displacement, of the parent panel. Since the patch fibers were all aligned with the load axis, the patch transverse strength was basically limited to that of the matrix. Figure 32 illustrates the patch transverse failure mode.

During the testing, all the patches underwent local bending near the edge of the cutout. The patches "sank" into the cutout after the load was applied to the panel. This bending did not appear to affect the centrally located strain gage rosette.

All the strain gage rosettes remained attached during the tests and acceptable data was generated through them. The Von Mises strain at the gages was measured and correlated with the predicted strain (Figures 33-41). The gages attached at points A and B (refer to Figure 25) on the patched panels did not correlate well with the predicted strain. This is probably due to the complex three-dimensional load interaction of the patch and panel at those locations, i.e. the local patch bending and load transfer. The data presented for the patched panels reflects that taken from gages centered on the

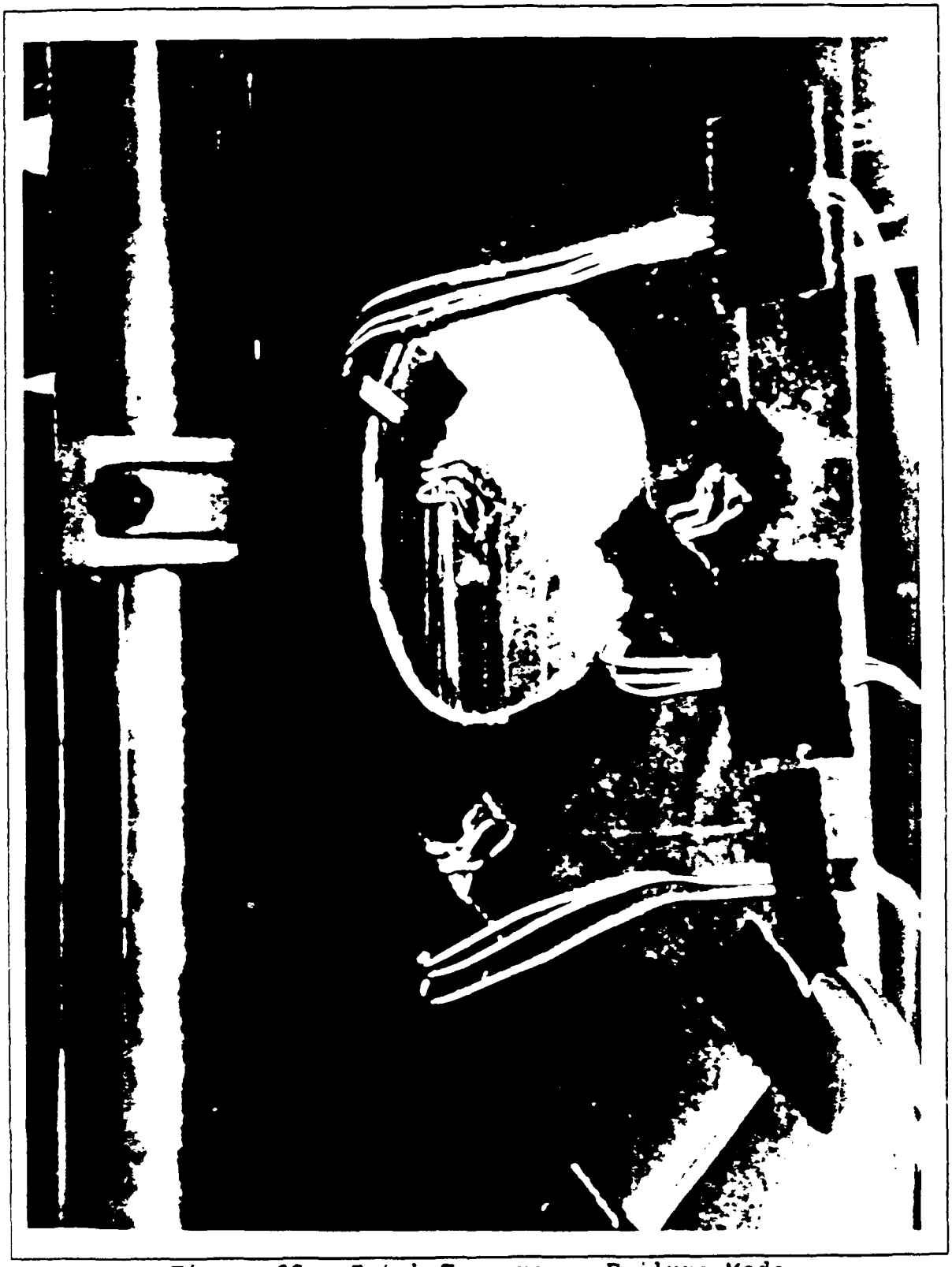

Figure 32. Patch Transverse Failure Mode

patch and far field, points D and C (refer to Figure 25).

Figures 36-41 show clearly the excellent correlation between the analytical model and experimental data. The use of the CELAS2 elements in this elastically loaded situation clearly modeled the elastic behavior of the panel-adhesive-patch load transfer mechanism successfully. The slight variation among the curves may be due to the imperfect test specimens as noted in Table 4.

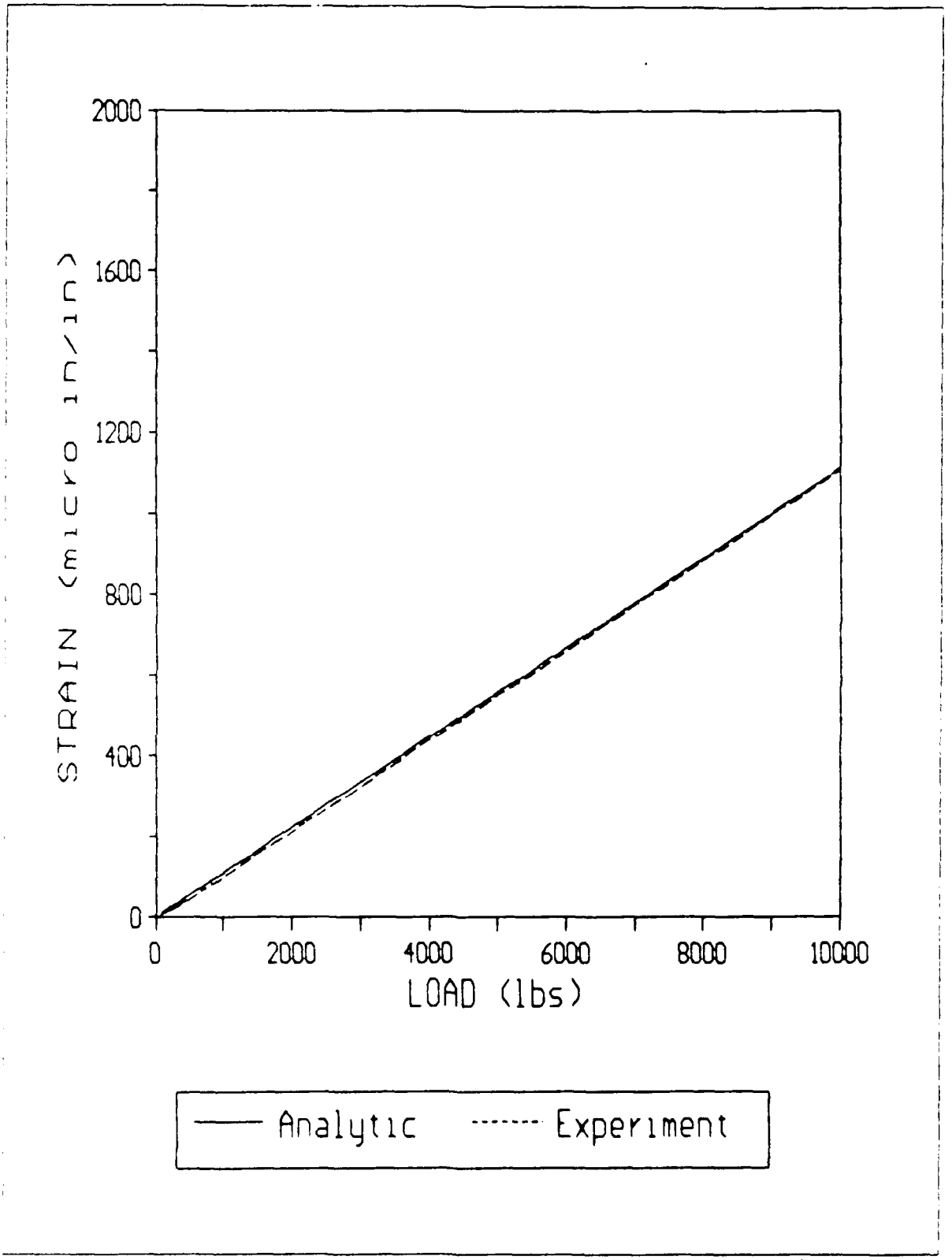

Figure 33. Von Mises Strain versus Load, Undamaged Panel

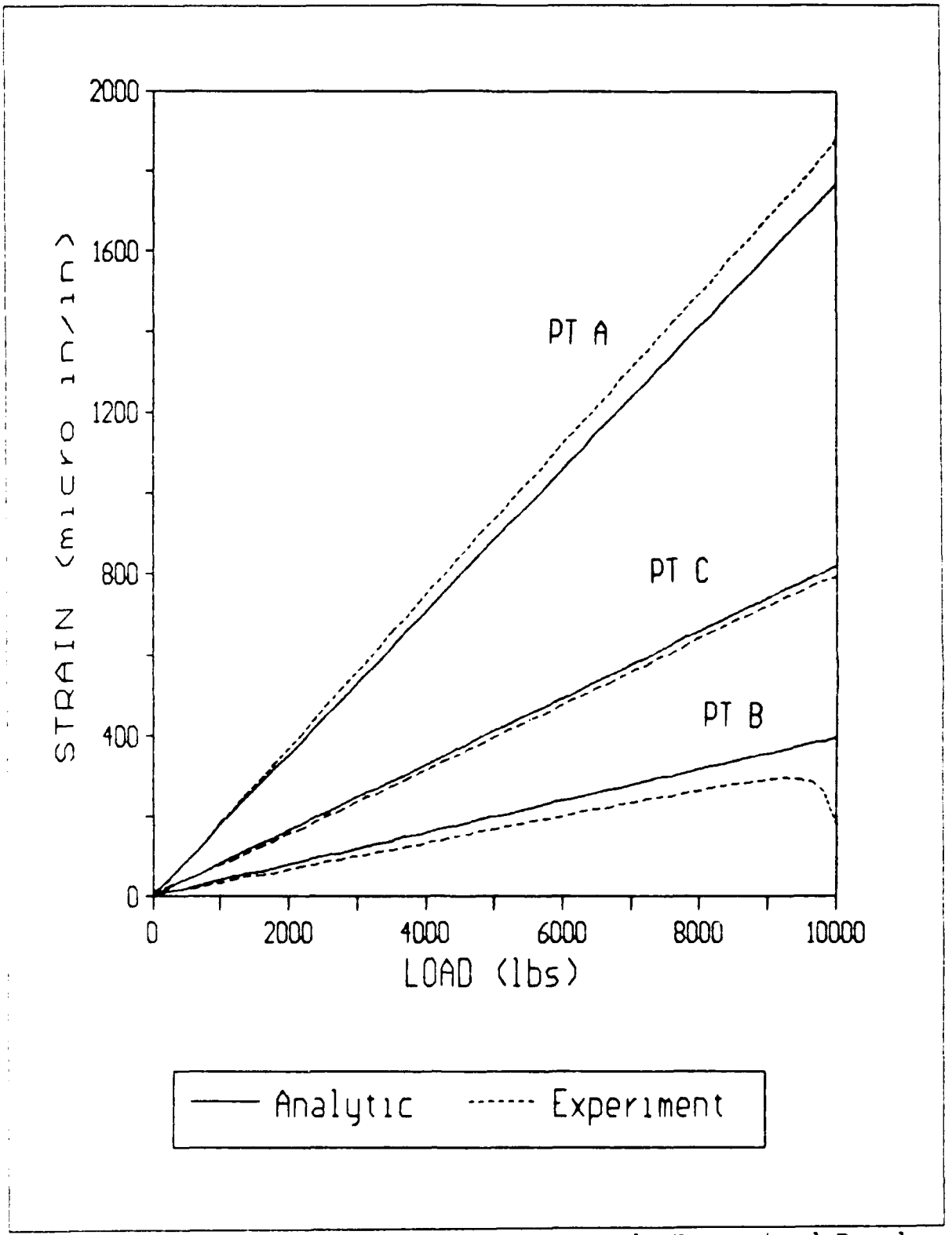

Figure 34. Von Mises Strain versus Load, Unrepaired Panel Number One

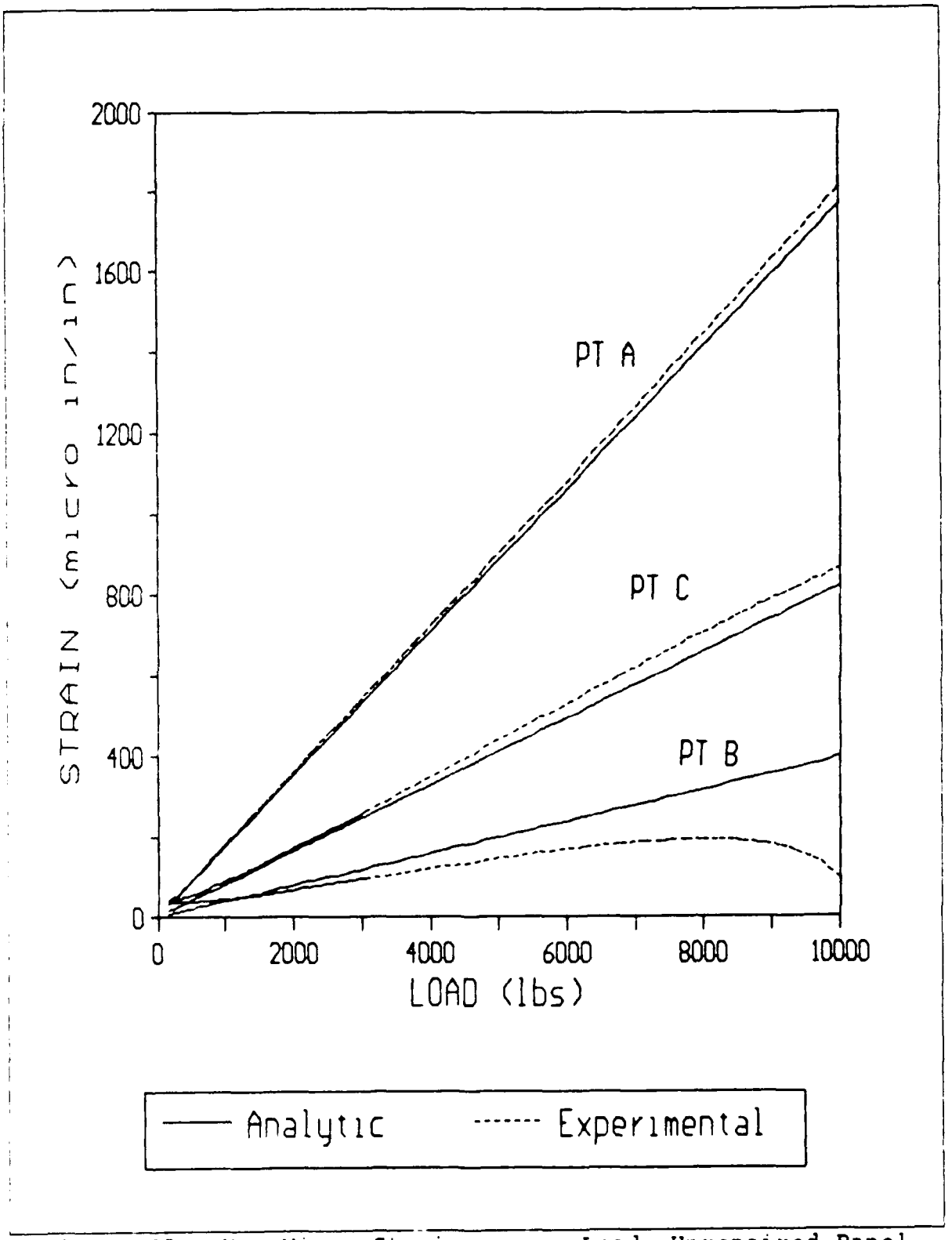

Figure 35. Von Mises Strain versus Load, Unrepaired Panel Number Two

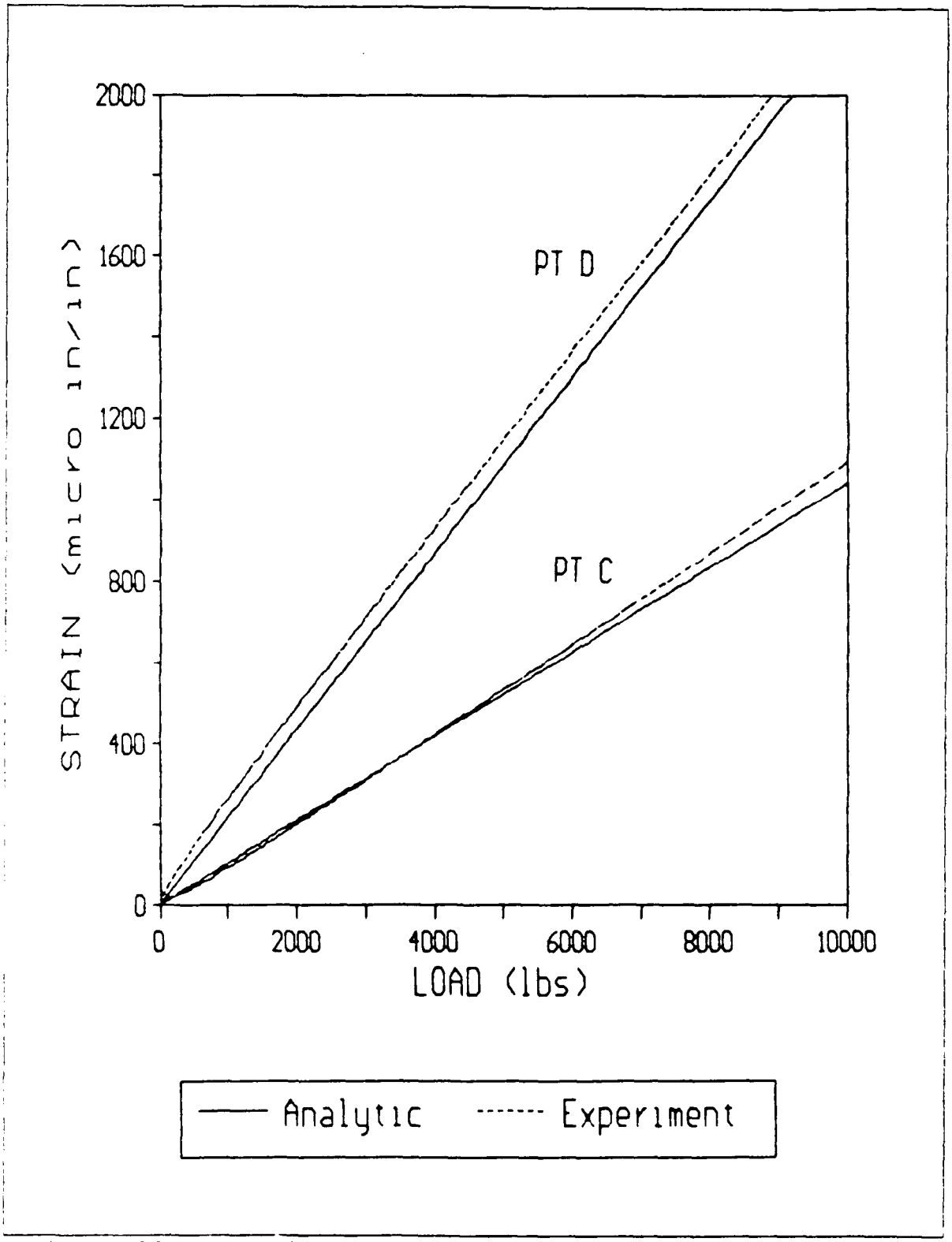

Figure 36. Von Mises Strain versus Load, 4-Ply Patch Panel Number One

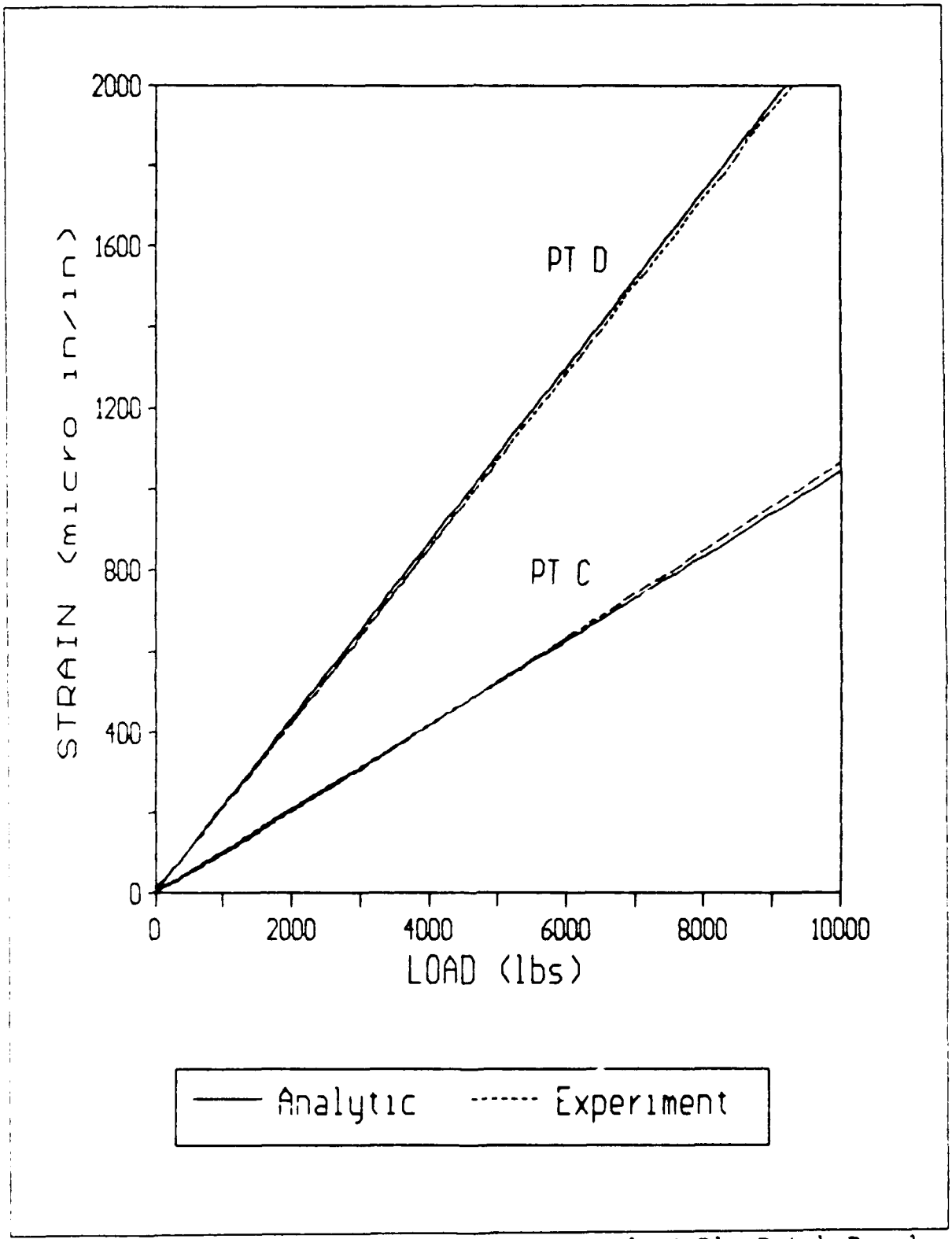

Figure 37. Von Mises Strain versus Load, 4-Ply Patch Panel Number Two

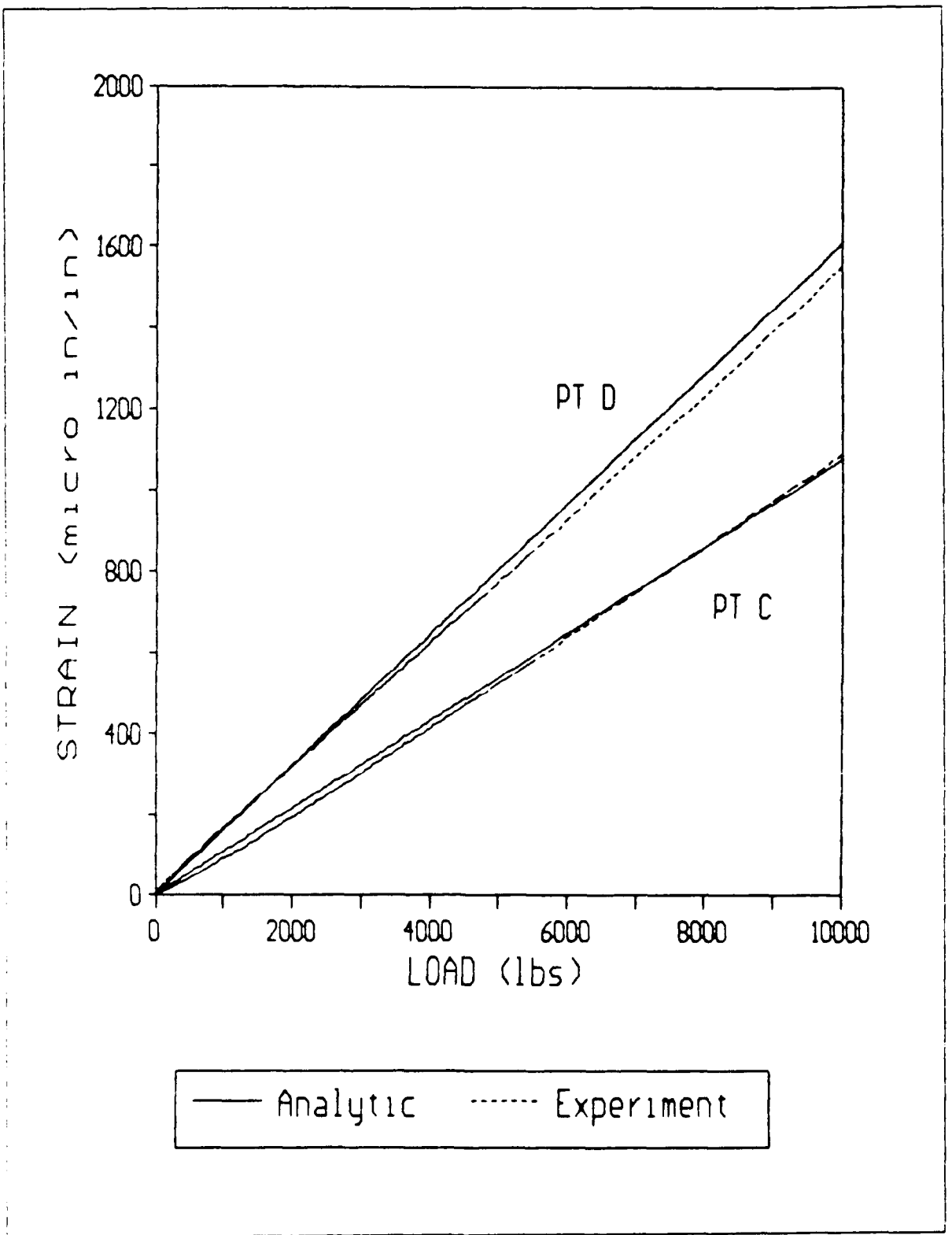

Figure 38. Von Mises Strain versus Load, 6-Ply Patch Panel Number One

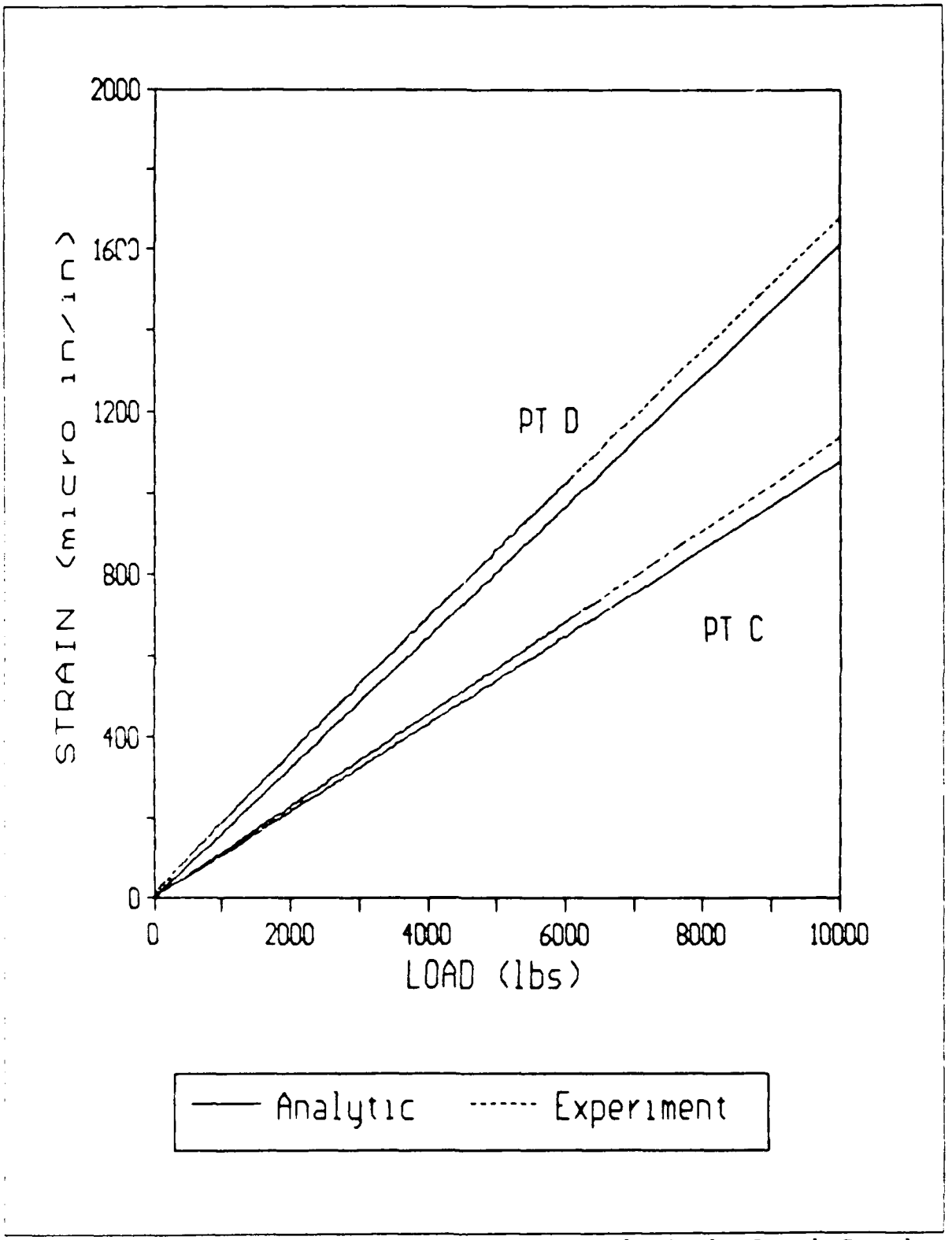

Figure 39. Von Mises Strain versus Load, 6-Ply Patch Panel Number Two

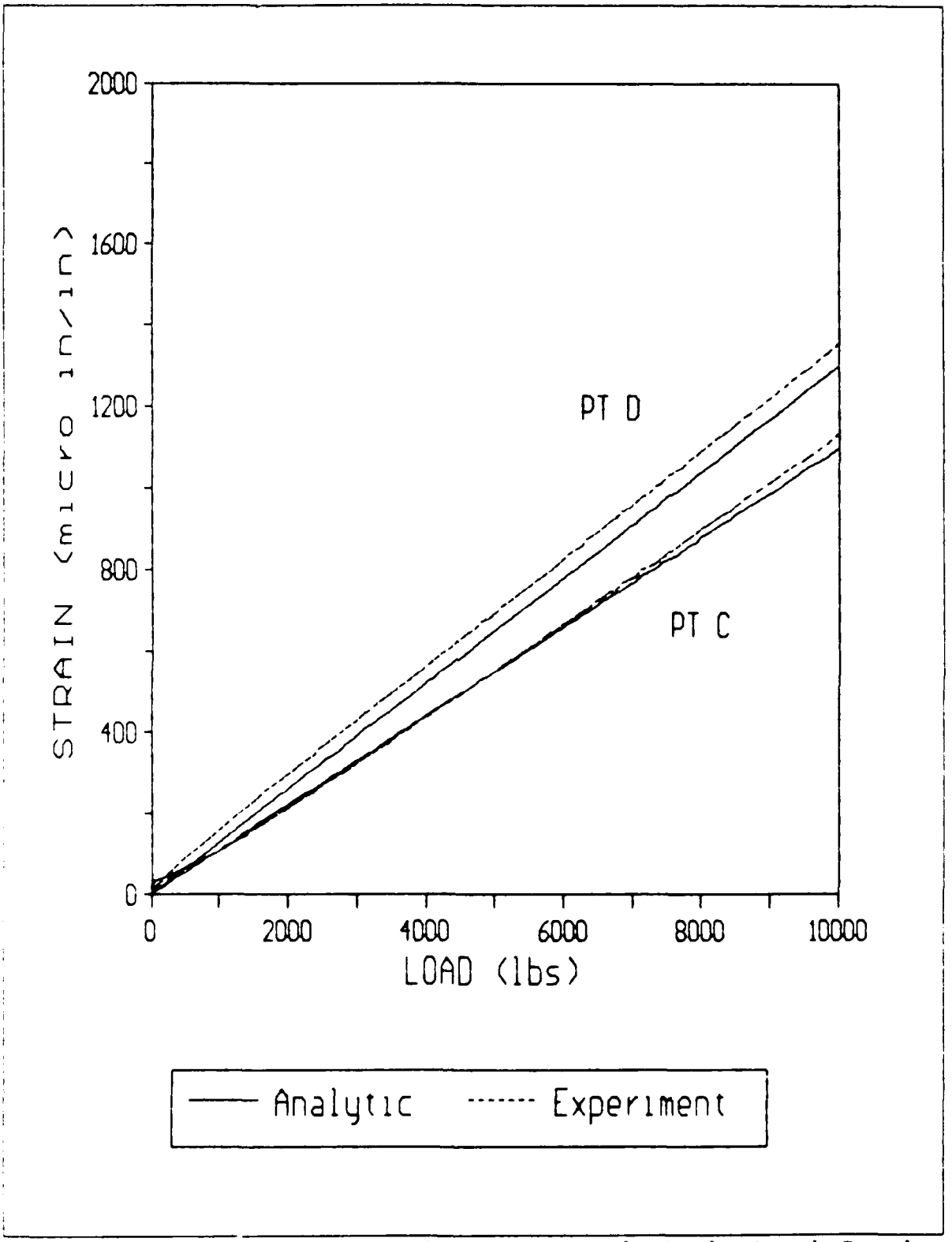

Figure 40. Von Mises Strain versus Load, 8-Ply Patch Panel Number One

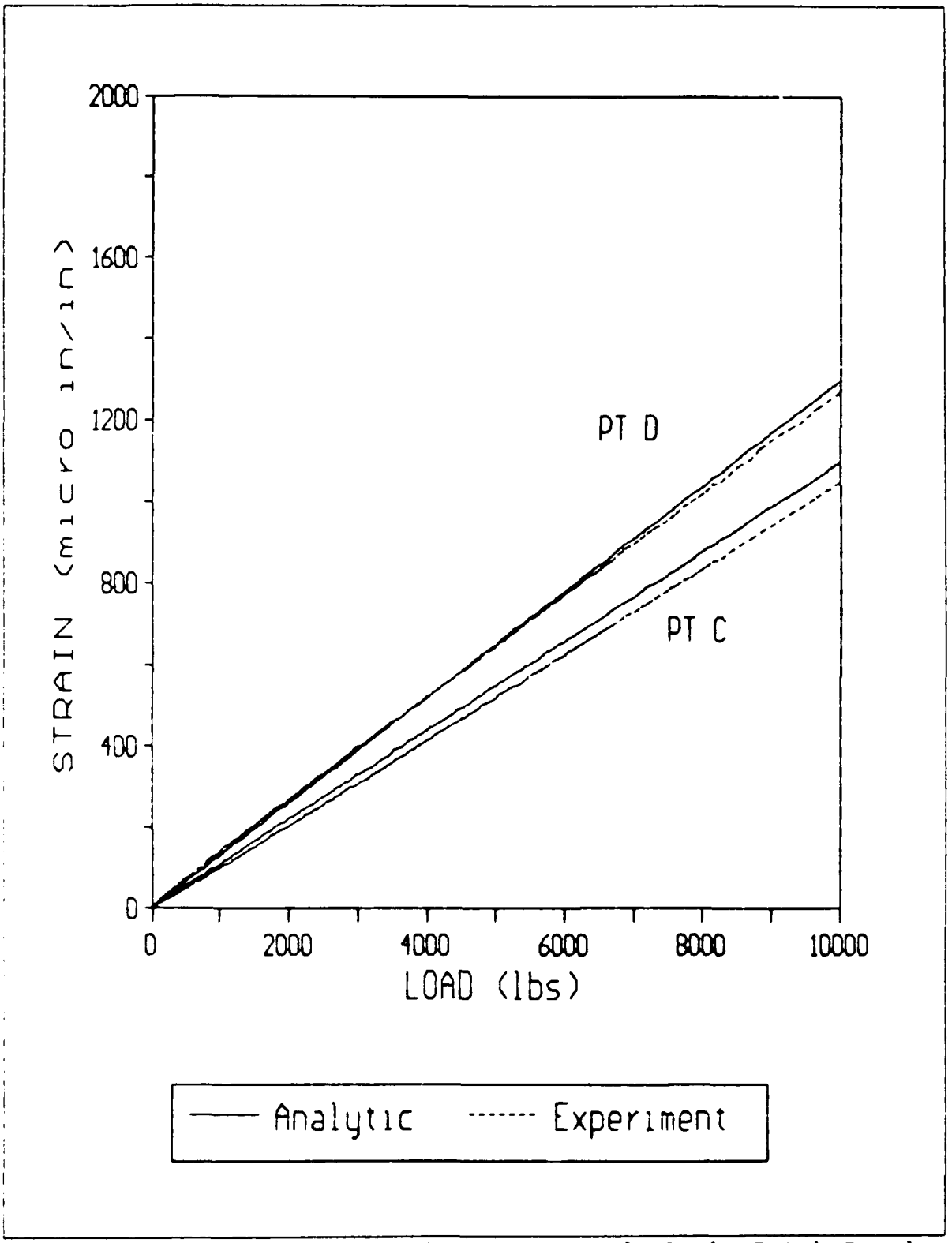

Figure 41. Von Mises Strain versus Load, 8-Ply Patch Panel Number Two

VII. Conclusions

The FEM. This thesis has shown conclusively that using CELAS2 spring elements to model an adhesively bonded joint can adequately predict a basically two-dimensional load transfer process. Both orthotropic and isotropic materials were used and modeled in this thesis. Use of the MSC/NASTRAN CELAS2 spring elements proved satisfactory in modeling the adhesive bond in both cases. The FEM accurately predicted the in-plane behavior of the damaged and repaired specimens. Good correlation was observed both in displacement and strain.

The effect of the bond was accurately modeled through the use of the linear spring elements. The use of linear spring elements, in an FEM, provides insight into the load transfer occurring in a bonded joint. This visualization should be extremely helpful is analyzing complex geometry bonded joints. The modeling method itself is not exceptionally difficult or time consuming and yet it provides realistic answers to complex problems.

This thesis did not explore the three-dimensional possibilities of the CELAS2 element. Since this element has three-dimensional capabilities, it may be feasible and realistic, to model such cases as a thin adherend single lap shear test specimen which undergoes shear and peel during the test. These specimens generally fail through the combined

action of in-plane and out-of-plane stress. Such a modeling and test analysis may be fairly straight forward.

MSC/NASTRAN is also equipped with rotational spring elements for modeling purposes. The spring force generated in the element is dependent on the rotation of the node it is associated with. The element does not function between elements but between particular nodes and the global coordinate system. The rotational spring applies a moment to the node. If the rotational spring element depended on the relative rotation of two associated nodes, then the shear modulus of the adhesive could have been used directly to model the bond.

The Materials. To be fair, nothing good or bad can be concluded about the low energy prepreg SP 377 CU1 material provided. At the time of this writing, 3M is still not sure how the defective roll of prepreg managed to leave their production facility. Other organizations, namely the U.S. Navy, have received and tested this material. The Navy reported some differences between the published SP 377 CU1 mechanical properties and what they observed in their tests. Further research into the applicability of this material for ABDR is necessary before any conclusions one way or the other may be made.

The AF 377 adhesive film worked well during the double lap shear specimen testing and the composite panel and patch fabrication and testing. The adhesive provided an easily

controlled and curable bonding agent. The adhesive shear strength data in Appendix A shows the impressive capabilities of this resin system.

The hot bonder concept was tried but no conclusive arguments can be made either way due to the defective raw materials involved.

Appendix A: Double Lap Shear Test Results Data

The plate thickness of the thick and thin adherends is 0.1965 in. and 0.0902 in. respectively.

Specimen No.	Failure Load (lbs)	Thick Adherend Stress (psi)	Thin Adherend Stress (psi)	Adhesive Shear Stress (psi)
4-1	6126	31260	34050	6149
4-2	6086	31020	33780	6084
4-3	6110	31020	33790	6067
4-4	6068	30920	33680	6080
4-5	6150	31300	34090	6135
4-6	6095	31060	33830	6076
4-7	6058	30950	33720	6043

Table 5. Double Lap Shear Failure Data

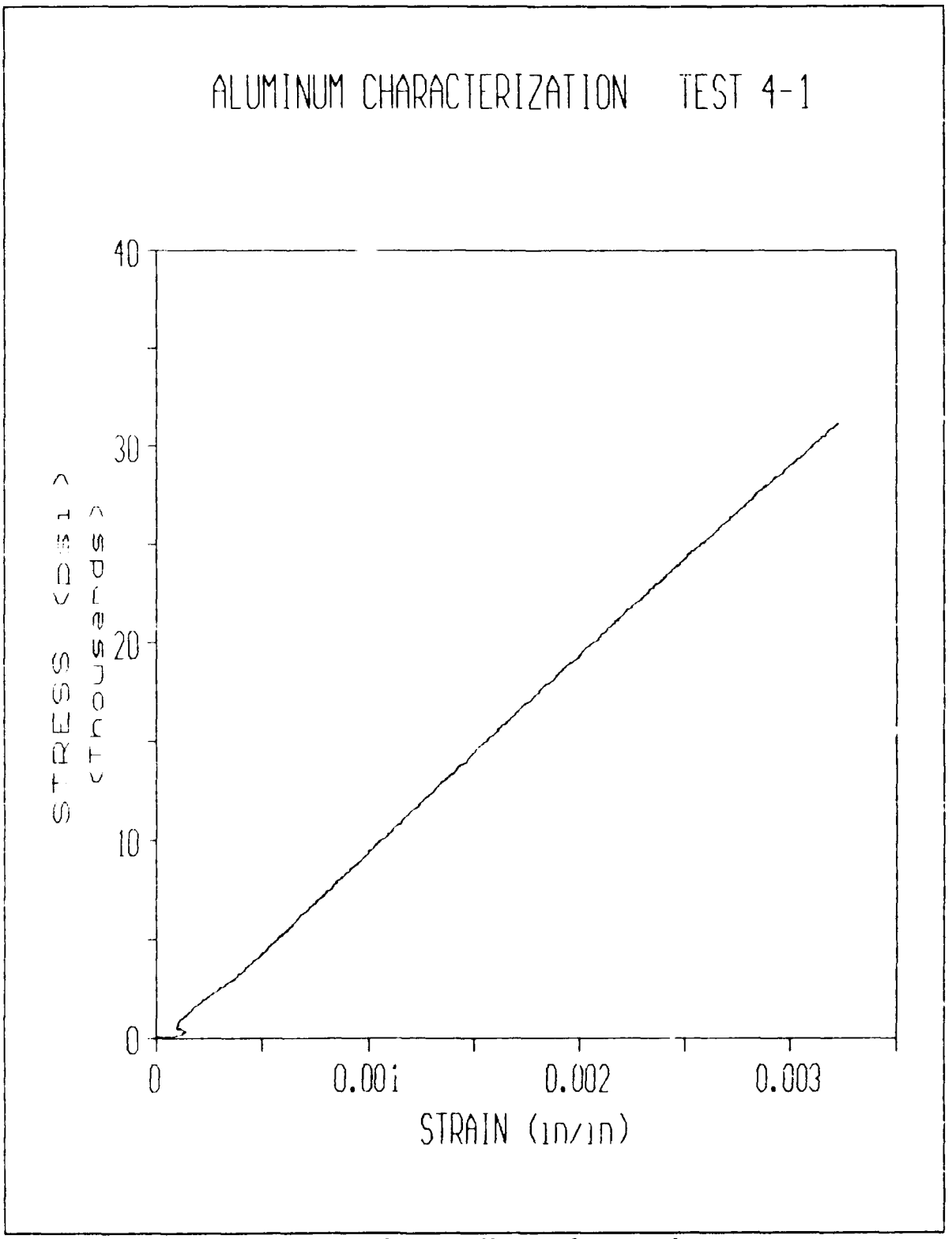

Figure 42. Test 4-1 Thick Adherend Normal Stress Versus Normal Strain

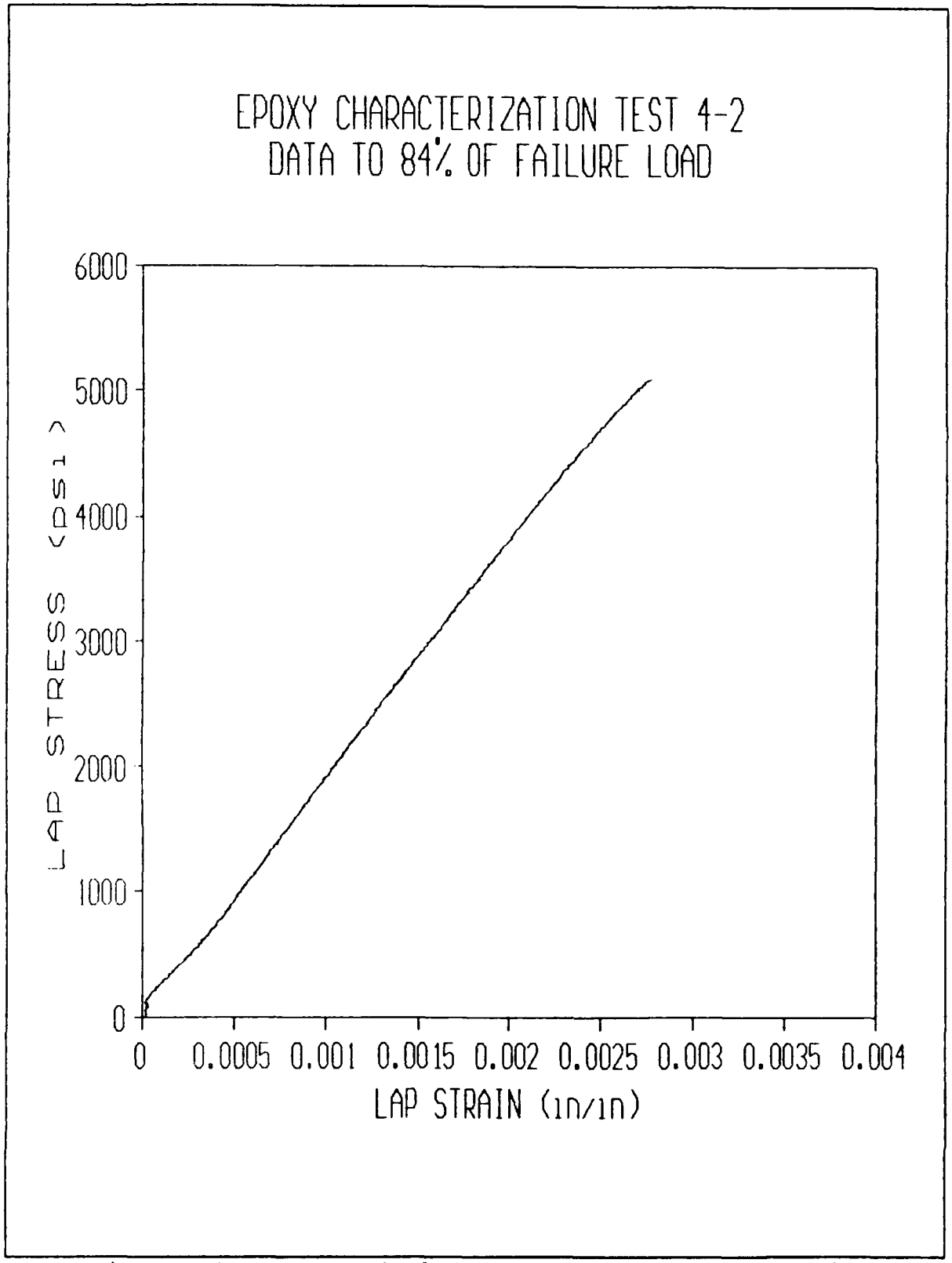

Figure 43. Test 4-2 Shear Stress Versus Lap Strain

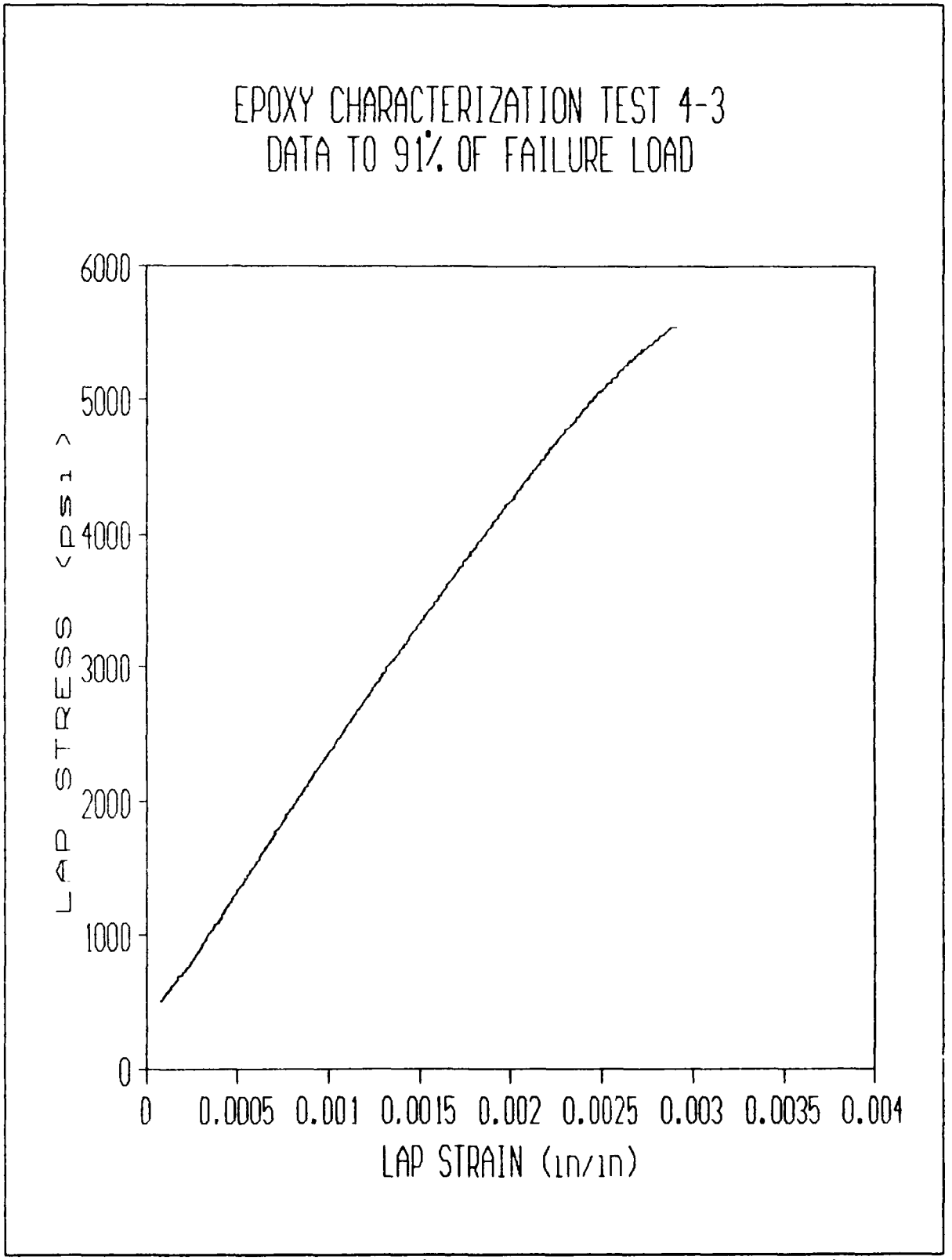

Figure 44. Test 4-3 Shear Stress Versus Lap Strain

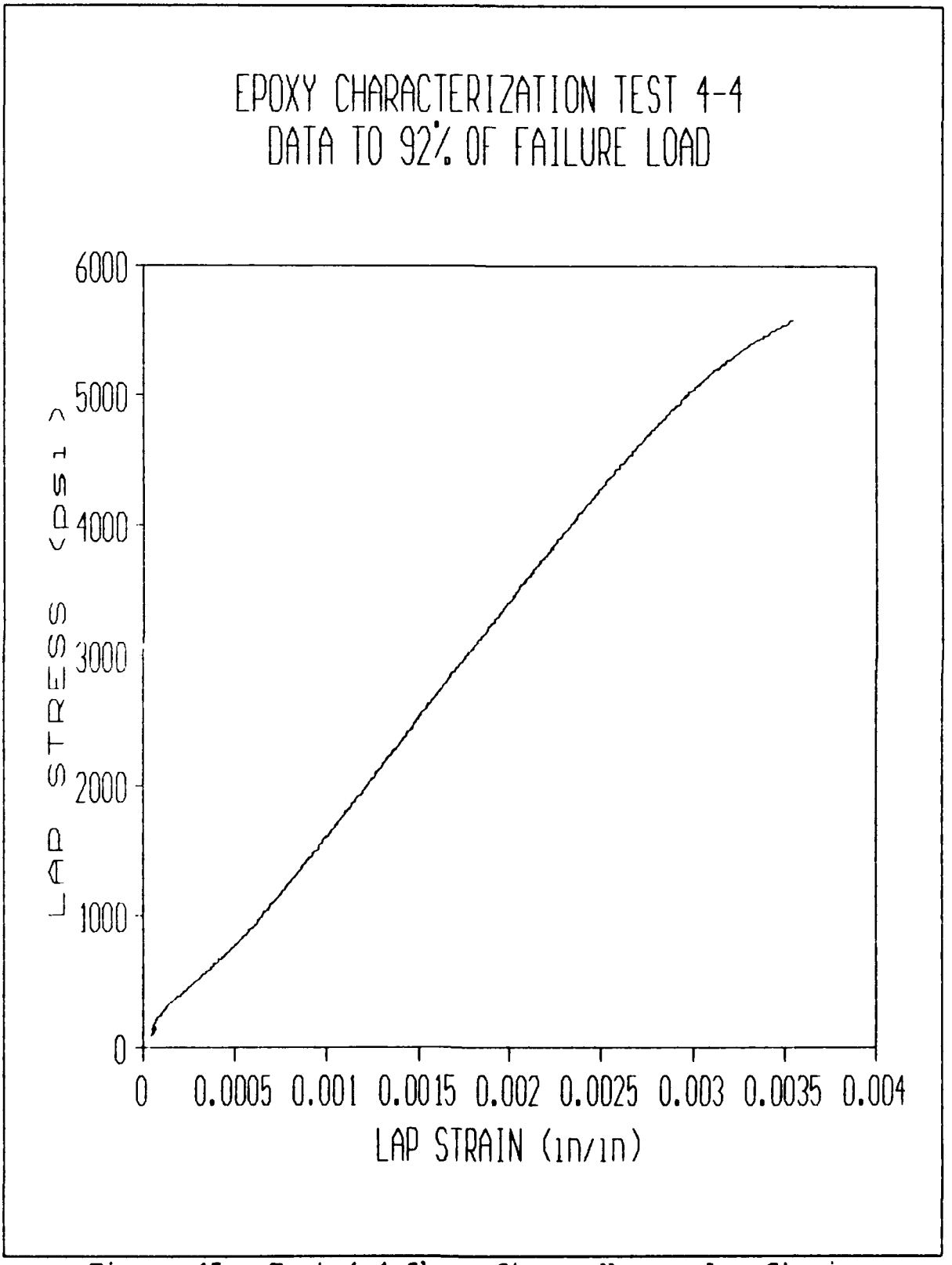

Figure 45. Test 4-4 Shear Stress Versus Lap Strain

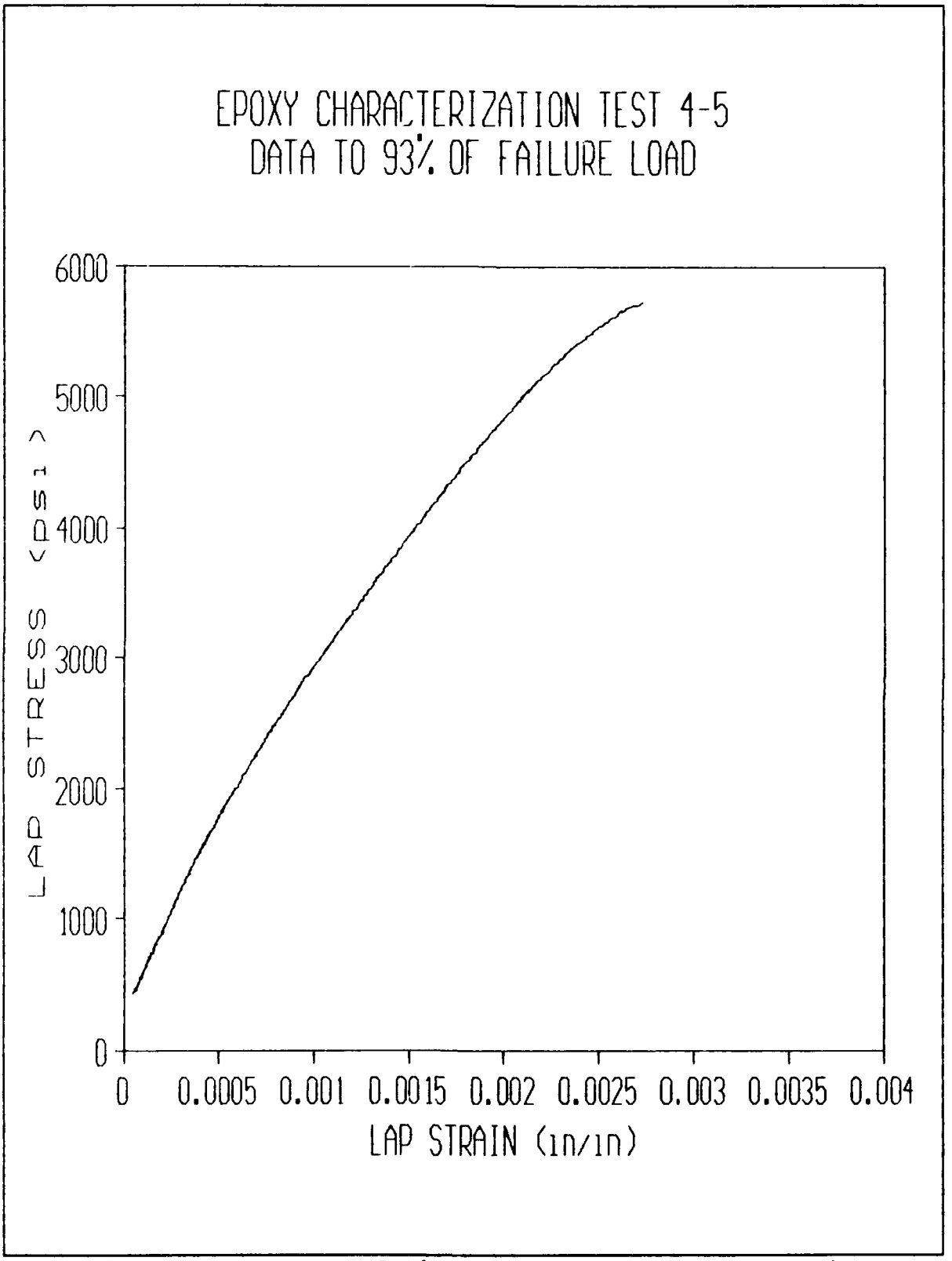

Figure 46. Test 4-5 Shear Stress Versus Lap Strain

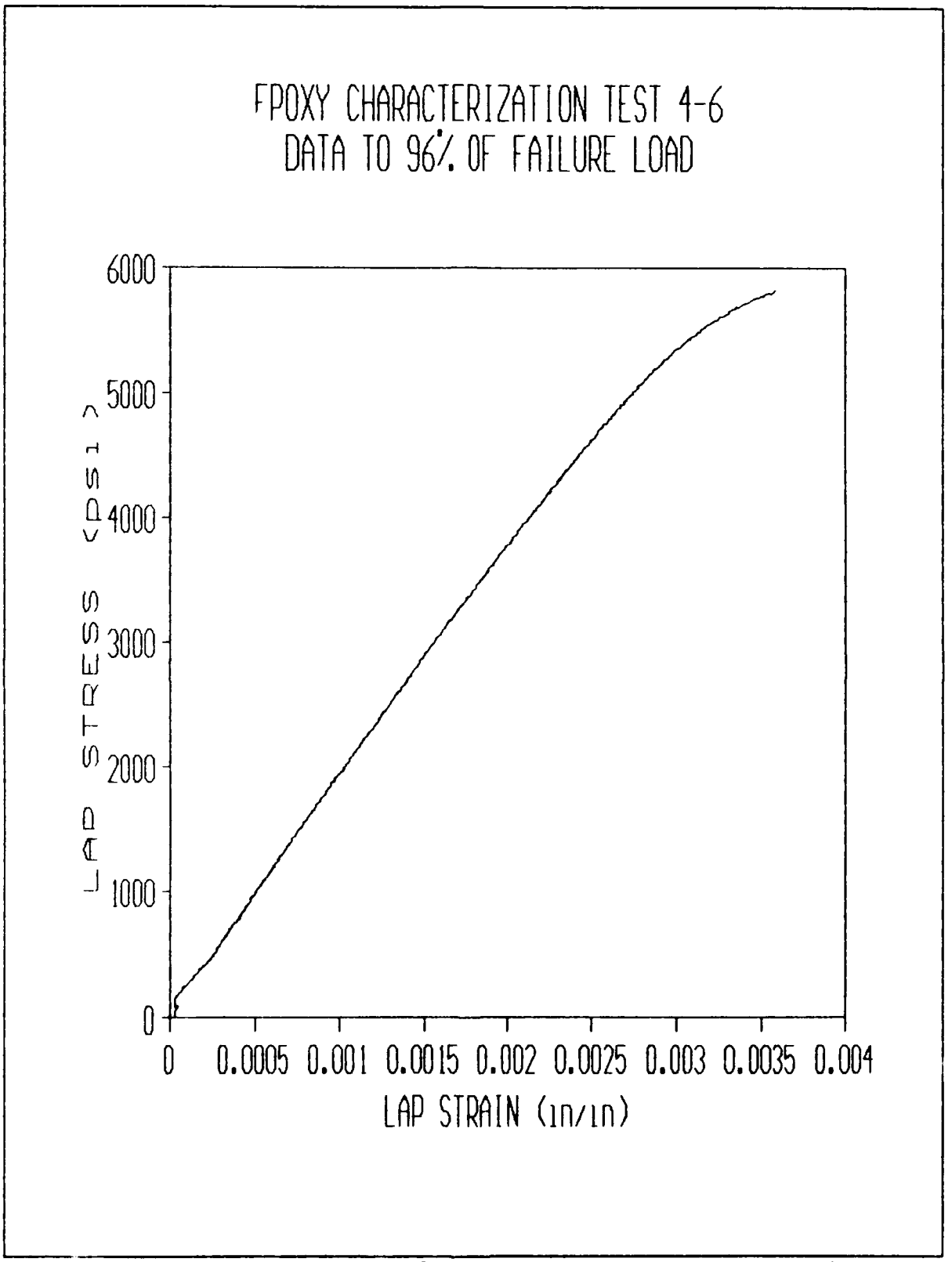

Figure 47. Test 4-6 Shear Stress Versus Lap Strain

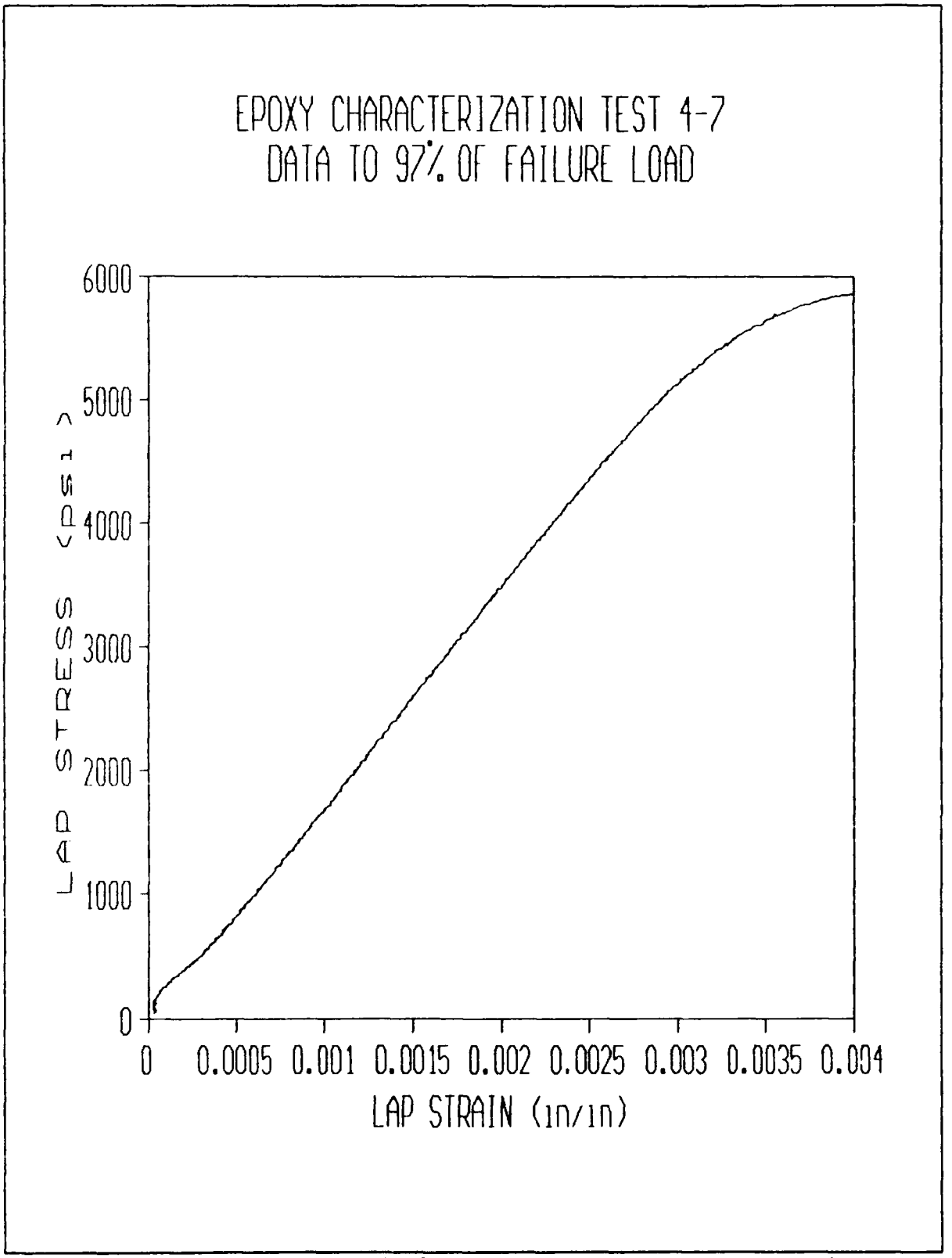

Figure 48. Test 4-7 Shear Stress Versus Lap Strain

1. Department of the Air Force, Technical Manual, General, Aircraft Battle Damage Repair, T O 1-1H-39, San Antonio: SA-ALC/MMEDT, 1 April 1984.

2. Hinkle, T. and Van Es, J. Battle Damage Repair of Composite Structures. AFWAL TR-87-3104. Air Force Wright Aeronautical Laboratories, Air Force Systems Command, Wright-Patterson AFB, OH 45433-6553, March 1988.

3. NATO Advisory Group for Aerospace Research and Development. The Repair of Aircraft Structures Involving Composite Materials. National Technical Information Service, Department of Commerce, Springfield, VA 22161, April 1986.

4. Jones, R. M. Mechanics of Composite Materials. Washington, D.C.: Scripta Book Company, 1975.

5. Franklin, B. Composites and Laminates, (First Edition). San Diego: D.A.T.A., Inc. and The International Plastics Selector, Inc., 1987.

6. I-DEAS Model Solution and Optimization Engineering Analysis User's Guide. Structural Dynamics Research Corporation, Milford OH, 1988.

7. Product Performance Guide. SP 377 Low Energy Cure Composite Prepreg Family. Issue No. 2. 3M Aerospace Materials Department, St Paul, MN, May 1989.

8. Smith, Lawrence R. Battle Damage Assessment Using Finite Element Analysis and Repair Techniques Using Composite Patches. MS Thesis. School of Science and Engineering, Naval Postgraduate School, Monterey, CA, December 1988 (AD-B131 668).

9. Cook, R. et al. Concepts and Applications of Finite Element Analysis. New York: John Wiley and Sons, 1989.

10. Reddy, J. An Introduction to the Finite Element Method. New York: McGraw-Hill Book Company, 1984.

11. Mall, S. Class handout distributed in MECH 541, Mechanics of Composite Materials. School of Engineering, Air Force Institute of Technology (AU), Wright-Patterson AFB OH, January 1990.

12. Handbook for Linear Analysis, MSC/NASTRAN Version 64. The MacNeal-Schwendler Corporation, Los Angeles, CA.

13. Beer, P. and Johnston, R., Jr. Mechanics of Materials. New York: McGraw-Hill Book Company, 1981.

14. Hughes, E. et al. "Mechanical Properties of Adhesives," Adhesive Bonding of Aluminum Alloys, edited by Thrall, E. New York: Marcel Dekker.

15. Annual Book of ASTM Standards, Volume 15.06, Adhesives. American Society for Testing and Materials, Philadelphia PA, 1985.

16. Grimes, G. "Adhesive-Honeycomb Relationship," Structural Adhesives Bonding, edited by Bodnar, M. New York: John Wiley & Sons, 1966.

Vita

Captain Mark W. Hunter [redacted] He graduated from Carmel High School in Carmel, California and attended Virginia Polytechnic Institute and State University, graduating with a Bachelor of Science in Aerospace Engineering in July 1985. During his senior year, he was chosen for the College Senior Engineering Program sponsored by the Air Force. Upon graduation, he attended Officer Training School at Lackland AFB, Texas. He graduated near the top of his class and was rewarded with a regular commission in the USAF. His first assignment was to Tinker AFB, Oklahoma. He served as the B-1B Reliability and Maintainability Engineer for the Oklahoma City Air Logistics Center. He tracked and analyzed the unreliable components on the B-1B. He also served as a field engineer for the B-1B Birdstrike Modification, where he provided on the spot engineering expertise to contractor personnel engaged in the modification, and he's a great windsurfer. He also served as a part-time ABDR engineer for the 507th Combat Logistics Support Squadron before entering the School of Engineering, Air Force Institute of Technology, in May 1989.

[redacted]

REPORT DOCUMENTATION PAGE

Form Approved
OMB No 0704 0188

1 AGENCY USE ONLY (Leave blank)	2 REPORT DATE	3 REPORT TYPE AND DATES COVERED
	December 1990	Master's Thesis

4 TITLE AND SUBTITLE
Modeling and Analysis of Orthotropic Plate with Circular Cutout and Adhesive Bonded Patch

5 FUNDING NUMBERS

6 AUTHOR(S)
Mark W. Hunter, Captain, USAF

7 PERFORMING ORGANIZATION NAME(S) AND ADDRESS(ES)
Air Force Institute of Technology, WPAFB OH 45433-6583

8 PERFORMING ORGANIZATION REPORT NUMBER
AFIT/GAE/ENY/90D-11

9 SPONSORING/MONITORING AGENCY NAME(S) AND ADDRESS(ES)
T. Reinhart
WRDC/MLSE
WPAFB, OH 45433-6533

10 SPONSORING/MONITORING AGENCY REPORT NUMBER

11 SUPPLEMENTARY NOTES

12a DISTRIBUTION/AVAILABILITY STATEMENT
Approved for public release; distribution unlimited

12b DISTRIBUTION CODE

13 ABSTRACT (Maximum 200 words)
To further advance aerospace battle damage repair techniques for composite repairs, a finite element model of an orthotropic plate with a cutout and patch was constructed to investigate the accuracy of such a model. The fundamental problem in this model is the development of a simple and accurate method of modeling the bond between the patch and plate. MSC/NASTRAN spring elements were used to this end. The spring elements provided an elastic method of load transfer between the plate and patch. MSC/NASTRAN was used for model solution while SDRC I-DEAS was used for Pre- and Post-Processing of the finite element model. Two-dimensional CQUAD4 elements were used to model the plate and patch. Physical test specimens were constructed to validate the model. The plate considered was a 16 ply AS4/3501-6 graphite/epoxy composite with dimensions 30" x 10" x 0.0832" with a five inch diameter hole centered in the plate. Three different patch concepts were modeled. The strain correlation between the finite element model and the test specimens was excellent for points far away from the hole and centered on the patch. Areas near the edge of the patch and hole were not as successful, probably due to changing strain fields near these areas.

14 SUBJECT TERMS
Aircraft Battle Damage Repair, Finite Element Model, Composite Repair, Bonded Repair, Adhesive Modeling, Adherend Modeling

15 NUMBER OF PAGES
104

16 PRICE CODE

17 SECURITY CLASSIFICATION OF REPORT	18 SECURITY CLASSIFICATION OF THIS PAGE	19 SECURITY CLASSIFICATION OF ABSTRACT	20 LIMITATION OF ABSTRACT
Unclassified	Unclassified	Unclassified	UL